Generation and Characterization of novel proteins for light-activated hyperpolarization of cell membranes

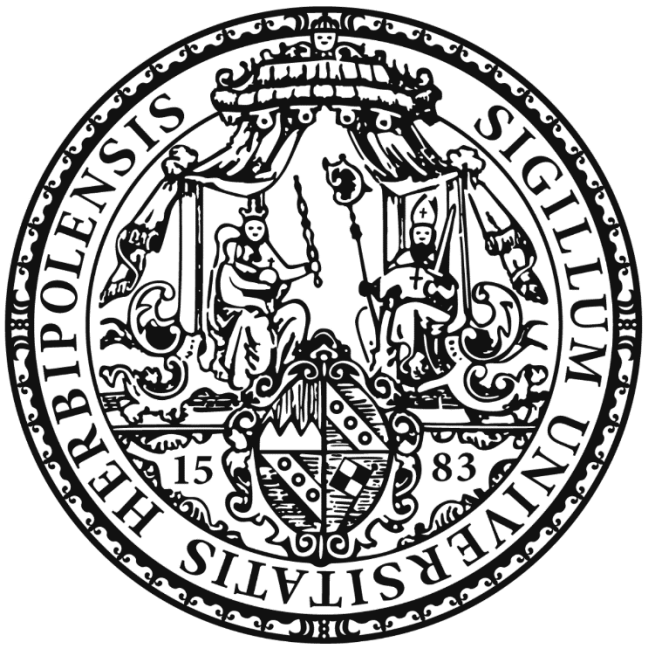

Dissertation zur Erlangung des
naturwissenschaftlichen Doktorgrades
der Julius-Maximilians-Universität Würzburg

vorgelegt von

Jing Yu-Strzelczyk

Jilin, China

Würzburg, 2022

Eingereicht am: ……..……..

Mitglieder der Promotionskommission:

Vorsitzender: ……..

Gutachter: ..Prof. Dr. Georg..Nagel…….....

Gutachter: ..Prof. Dr. Robert..Johannes..Kittel….....

Tag des Promotionskolloquiums: ……..…

Doktorurkunde ausgehändigt am: …….

Summary:

The light-gated cation channel Channelrhodopsin-2 was discovered and characterized in 2003. Already in 2005/2006 five independent groups demonstrated that heterologous expression of Channelrhodopsin-2 is a highly useful and simply applicable method for depolarizing and thereby activating nerve cells. The application of Channelrhodopsin-2 revolutionized neuroscience research and the method was then called optogenetics. In recent years more and more light-sensitive proteins were successfully introduced as "optogenetic tools", not only in neuroscience.

Optogenetic tools for neuronal excitation are well developed with many different cation-conducting wildtype and mutated channelrhodopsins, whereas for inhibition of neurons in the beginning (2007) only hyperpolarizing ion pumps were available. The later discovered light-activated anion channels (anion channelrhodopsins) can be useful hyperpolarizers, but only at low cytoplasmic anion concentration.

For this thesis, I optimized CsR, a proton-pumping rhodopsin from *Coccomyxa subellipsoidea*, which naturally shows a robust expression in *Xenopus laevis* oocytes and plant leaves. I improved the expression and therefore the photocurrent of CsR about two-fold by N-terminal modification to the improved version CsR2.0, without altering the proton pump function and the action spectrum. A light pulse hyperpolarised the mesophyll cells of CsR2.0-expressing transgenic tobacco plants (*N. tabacum*) by up to 20 mV from the resting membrane potential of -150 to -200 mV. The robust heterologous expression makes CsR2.0 a promising optogenetic tool for hyperpolarization in other organisms as well. A single R83H point-mutation converted CsR2.0 into a light-activated (passive) proton channel with a reversal potential close to the Nernst potential for intra-/extra-cellular H^+ concentration. This light-gated proton channel is expected to become a further useful optogenetic tool, e.g. for analysis of pH-regulation in cells or the intercellular space.

Ion pumps as optogenetic tools require high expression levels and high light intensity for efficient pump currents, whereas long-term illumination may cause unwanted heating effects. Although anion channelrhodopsins are effective hyperpolarizing tools in some cases, their effect on neuronal activity is dependent on the cytoplasmic chloride concentration which can vary among neurons. In nerve cells, increased conductance for potassium terminates the action potential and K^+ conductance underlies the resting membrane potential in excitable cells. Therefore, several groups attempted to synthesize artificial light-gated potassium channels but

all of these published innovations showed serious drawbacks, ranging from poor expression over lacking reversibility to poor temporal precision.

A highly potassium selective light-sensitive silencer of action potentials is needed. To achieve this, I engineered a light-activated potassium channel by the genetic fusion of a photoactivated adenylyl cyclase, bPAC, and a cAMP-gated potassium channel, SthK. Illumination activates bPAC to produce cAMP and the elevated cAMP level opens SthK. The slow diffusion and degradation of cAMP makes this construct a very light-sensitive, long-lasting inhibitor. I have successfully developed four variants with EC50 to cAMP ranging from 7 over 10, 21, to 29 μM. Together with the original fusion construct (EC50 to cAMP is 3 μm), there are five different light- (or cAMP-) sensitive potassium channels for researchers to choose, depending on their cell type and light intensity needs.

Generierung und Charakterisierung neuartiger Proteine für Licht-aktivierte Hyperpolarisation von Zellmembranen

Zusammenfassung:

Der lichtgesteuerte Kationenkanal Channelrhodopsin-2 wurde 2003 entdeckt und charakterisiert. Bereits 2005/2006 zeigten fünf unabhängige Gruppen, dass die heterologe Expression von Channelrhodopsin-2 eine sehr nützliche und einfach anwendbare Methode zur Depolarisation und damit Aktivierung von Nervenzellen ist. Die Anwendung von Channelrhodopsin-2 revolutionierte die neurowissenschaftliche Forschung und die Methode wurde dann Optogenetik genannt. In den letzten Jahren wurden immer mehr lichtempfindliche Proteine als „optogenetische Werkzeuge“ eingeführt, und nicht nur in den Neurowissenschaften erfolgreich angewandt.

Optogenetische Werkzeuge zur neuronalen Anregung sind mit vielen verschiedenen Kationen-leitenden Wildtyp- und mutierten Channelrhodopsinen gut entwickelt, während für die Hemmung von Neuronen zu Beginn (2007) nur hyperpolarisierende Ionenpumpen zur Verfügung standen. Die später entdeckten lichtaktivierten Anionenkanäle (Anionenkanalrhodopsine) können nützliche Hyperpolarisatoren sein, jedoch nur bei niedriger zytoplasmatischer Anionenkonzentration.

Für diese Arbeit habe ich CsR optimiert, ein Protonen pumpendes Rhodopsin aus Coccomyxa subellipsoidea, das von Natur aus eine robuste Expression in Oozyten von Xenopus laevis und in Pflanzenblättern zeigt. Ich habe die Expression und damit den Photostrom von CsR etwa um das Zweifache durch N-terminale Modifikation verbessert, ohne die Protonenpump-Funktion und das Aktionsspektrum bei der verbesserten Version von CsR2.0 zu verändern. Ein Lichtpuls hyperpolarisierte die Mesophyllzellen von CsR2.0-exprimierenden transgenen Tabakpflanzen (N. tabacum) um bis zu 20 mV gegenüber dem Ruhe-Membranpotential von -150 bis -200 mV. Die robuste heterologe Expression macht CsR2.0 zu einem vielversprechenden optogenetischen Werkzeug für die Hyperpolarisation auch in anderen Organismen. Eine einzelne R83H-Punktmutation wandelte CsR2.0 um in einen Licht-aktivierten (passiven) Protonenkanal mit einem Umkehrpotential nahe dem Nernst-Potential für intra-/extrazelluläre H+-Konzentration. Es wird erwartet, dass dieser Licht-gesteuerte Protonenkanal ein weiteres nützliches optogenetisches Werkzeug wird, z. zur Analyse der pH-Regulation in Zellen oder dem Interzellularraum.

Ionenpumpen als optogenetische Werkzeuge erfordern hohe Expressionsraten und eine hohe Lichtintensität für effiziente Pumpströme, wobei eine Langzeitbeleuchtung unerwünschte Erwärmungseffekte verursachen kann. Obwohl Anionen-Channelrhodopsine in einigen Fällen wirksame hyperpolarisierende Werkzeuge sind, hängt ihre Wirkung auf die neuronale Aktivität von der zytoplasmatischen Chloridkonzentration ab, die zwischen den Neuronen variieren kann. In Nervenzellen beendet eine erhöhte Leitfähigkeit für Kalium das Aktionspotential und die K+-Leitfähigkeit liegt dem Ruhe-Membranpotential in erregbaren Zellen zugrunde. Daher versuchten mehrere Gruppen, künstliche lichtgesteuerte Kaliumkanäle zu synthetisieren, aber alle diese veröffentlichten Innovationen zeigten schwerwiegende Nachteile, die von schlechter Expression über fehlende Reversibilität bis hin zu geringer zeitlicher Präzision reichten.

Ein hoch Kalium-selektiver Licht-empfindlicher Inhibitor der Aktionspotentiale ist von hohem Wert für die Neurowissenschaft. Um dies zu erreichen, habe ich einen Licht-aktivierten Kaliumkanal durch genetische Fusion einer photoaktivierten Adenylylcyclase, bPAC, und eines cAMP-gesteuerten Kaliumkanals, SthK, konstruiert. Beleuchtung aktiviert bPAC zur Produktion von cAMP und der erhöhte cAMP-Spiegel öffnet SthK. Die langsame Diffusion und Degradation von cAMP macht dieses Konstrukt zu einem sehr Licht-empfindlichen, lang anhaltenden Inhibitor. Ich habe darüber hinaus erfolgreich vier Varianten mit EC50 für cAMP im Bereich von 7 über 10, 21 bis 29 µM entwickelt. Zusammen mit dem ursprünglichen Fusionskonstrukt (EC50 zu cAMP beträgt 3 µM) gibt es damit nun fünf verschiedene Licht-empfindliche Kaliumkanäle, die je nach Zelltyp und Lichtintensitätsbedarf für optogenetische Experimente ausgewählt werden können.

Contents

Chapter 1 Introduction 8

1.1 Optogenetics 8

1.1.1 Optogenetics 8

1.1.2 Pioneering efforts 9

1.1.2 Optogenetic tool box 10

1.2 Photoreceptors 11

1.2.1 Rhodopsins 11

1.2.1.1 CsR 13

1.2.1.2 BeCyclOP 15

1.2.2 Photoactivated Adenylyl Cyclase 15

1.2.2.1 bPAC 16

1.2.2.3 Photoactivation Mechanism of bPAC 18

1.3 Optogenetic silencing tools 19

1.3.1 rhodopsin-based ion pumps 20

1.3.2 rhodopsin-based anion channels 20

1.3.3 Synthesized Light-activated potassium channels. 21

1.3.3.1 PTL channels 21

1.3.3.2 PIRK using Uaa 22

1.3.3.3 Lumitoxin 23

1.3.3.4 Blink 24

1.3.4 Presynaptic vesicular release inhibition 24

1.3.5 Vertebrate rhodopsins 25

1.4 Cyclic nucleotide-gated channels 25

1.4.1 SthK 27

1.5 Phosphodiesterase 30

1.6 Motivation of the study 31

Chapter 2 Method 32

2.1 Chemicals and reagents 32

2.2 Molecular biology 32

2.2.1 DNA cloning 32

2.2.2 Site-directed mutagenesis 33

2.2.3 E. coli transformation 33
2.2.4 Cracking of *E. coli* cells 34
2.3.6 Plasmids extraction and verification 34
2.2.7 In vitro transcription 35
2.3 Oocytes preparation 35
2.3.1 Surgical oocytes excision 36
2.3.2 Microinjection and maintenance of oocytes 36
2.4 Electrophysiology recording 36
2.4.1 Two-electrode voltage-clamp 36
2.4.1.2 Solution used for oocytes TEVC 37
2.4.1.3 Electrodes and capillaries for TEVC 38
2.4.2 Inside-out patch clamp 38
2.4.2.1 Removing the vitelline membrane 40
2.4.2.2 Patch clamp electrode fabrication 40
2.4.2.3 “Gigaseal” formation 40
2.4.2.4 Inside-out patch excision 41
2.4.3 Impalement 41
2.4.3.1 Leaf discs preparation 41
2.4.3.2 Impalement electrode fabrication 42
2.4.3.3 Membrane potential recording 42
2.4.4 Data analysis 42
2.4.4.1Software for electrophysiology recordings 42
2.4.4.2Mathematical fitting of the electrophysiology data 42
2.5 cAMP/cGMP ELISA assay from whole oocyte lysates 43
2.6 Light source 43
2.7 Fluorescence imaging 43
2.8 Experimental design and statistical analysis 44
2.9 Bioinformatics 44
Chapter 3 RESULTS 45
3.1 Improving CsR membrane targeting and converting it into a proton channel 45
3.1.1 Impoving the membrane targeting of CsR with LR sequence 45
3.1.2 one-point mutation converts CsR2.0 from a proton pump to a proton channel 47
3.1.3 An additional Y58A mutation enhanced the proton channel photocurrent 48
3.1.4 A slow triple mutation mutant 50

3.1.5 Comparison of two channel mutants 51
3.1.6 CsR2.0 hyperpolarizes mesophyll cells 51
3.2 Assemble a light activated-potassium channel 54
3.2.1 The potassium conductance and cAMP Cyclase function of SthK-bPAC 54
3.2.2 SthK-bPAC is activated by cAMP and inhibited by cGMP 56
3.2.3 Channel characterization 57
3.2.4 PDE helps to reduce closing time 57
3.2.5 Screening for low light sensitivity SthK-bPAC variant 58
3.2.6 Determine the sensitivities of SthK-bPAC variants to cAMP 61
3.2.7 Optimising the targeting of desired location 63
Chapter 4 Discussion 65
4.1 Improve the membrane targeting of CsR and convert it into a proton channel 65
4.1.1 Robust heterologous expression 65
4.1.2 Rhodopsin proton channel 65
4.2 Design of a Light-gated potassium channel 67
4.2.1 SthK-bPAC functions as a long lasting light-activated potassium channel 67
4.2.2 Application SthK-bPAC in hippocampal neurons and larve motoneuron 67
4.2.3 Strategy to reduce SthK sensitivity to cAMP and optimize the targeting 68
4.2.4 SthK(TV418)-bPAC outperforms GtACR2 in low light condition in blocking hippocampal neuron action potential 70
4.2.6 SthK(TV418)-bPAC VS KCRs 70
5. references 74
6. Appendix 84
6.1 List of primers used for Sthk and CsR clonings. 84
6.2 Abbreviation 86
7. Acknowledgement 88
Curriculum Vitae ..... **Error! Bookmark not defined.**

Chapter 1 Introduction

1.1 Optogenetics

1.1.1 Optogenetics

Optogenetics is non-invasive manipulation of intercellular processes by genetically encoded light-activated proteins (1). Optogenetics has revolutionized neuroscience research by using light to control membrane potential in neurons, especially the studies of brain function (2, 3). Although optogenetics is originally from seeking approach for precise spatial and temporal photocontrol of neuronal action potentials, it also facilitated cardiac function, cellular signaling studies, visual and hearing restoration (4-8).

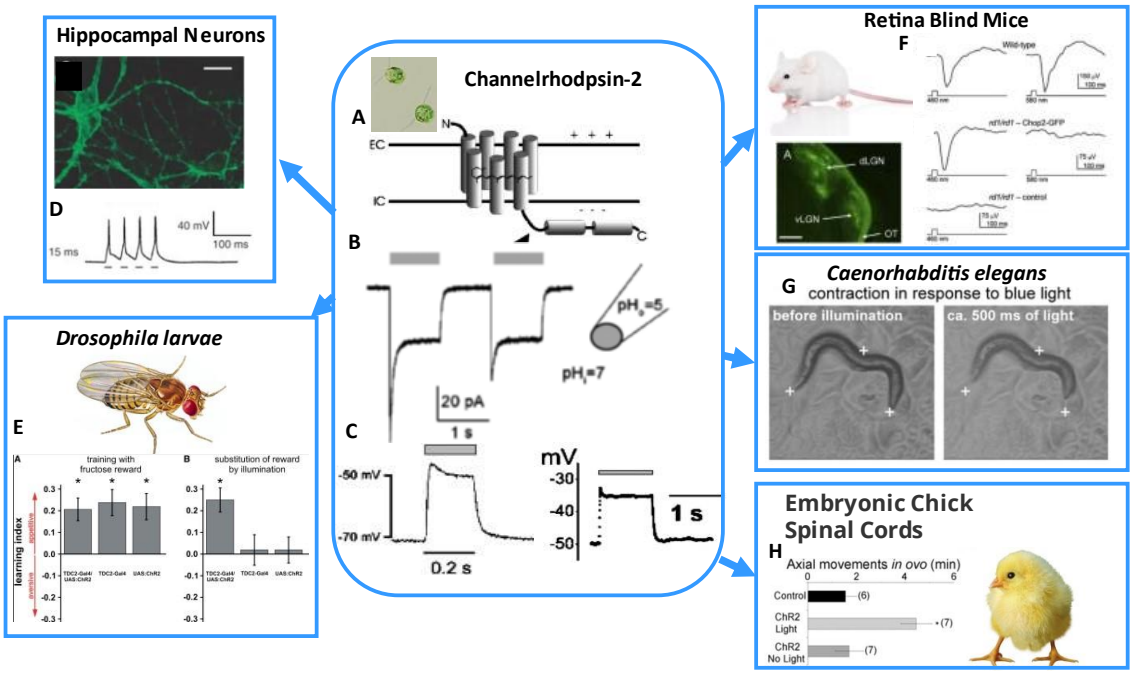

Figure 1.1 Functional discovery of Channelrhodopsin-2 and its applications. A, Scheme of the predicted structure of ChR2. B, Activation of inward photocurrents by light pulses of 442 nm (gray bars). C, Blue light-induced depolarization of ChR2 expressing *Xenopus* oocyte (left) and HEK293 cell (right). D, ChR2 enables light-driven neuron spiking in hippocampal neurons. E, Light-Induced Activation of modulatory neurons substitutes for reinforcing stimuli during olfactory learning. F, Central projections of ChR2-Expressing retinal ganglion cells and visual-evoked potentials in retinal blind Mice. G, ChR2 Expression in *C. elegans* body muscles permits light-evoked contractions. H, ChR2 is used to regulate the frequency of spontaneous rhythmic activity in isolated embryonic chick spinal cords and living embryos. Taken from (9-15).

The discovery of channelrhodopsins (ChRs) is the milestone of the development of optogenetics. In 2002, Nagel et al demonstrated a heterologously expressed light-gated proton

channel, channelrhodopsin-1 (ChR1), in *Xenopus* oocytes. ChR1 is originally from *Chlamydomonas reinhardtii* and involved in the phototaxis of green algae (16). In 2003, Nagel *et al* published a light-activated non-selective cation channel from the same organism, channelrhodopsin-2 (ChR2), which triggers the strong light-induced depolarization of oocytes and human embryonic kidney (HEK293) cells (9), and proposed that ChR2 would be a powerful tool to depolarize the cell membrane by illumination. As a dream tool that many neurologists were seeking for decades, 6 laboratories, including Zhou Pan, Karl Deisseroth, Stefan Herlitze, Hiromu Yawo, Alexander Gottschalk and Andre´ Fiala functionally applied ChR2 in retina blind mice (14), hippocampal neurons (10), intact vertebrate spinal cords (12), PC12 cells (11), living animals *Caenorhabditis elegans* (13) and *Drosophila* larvae (15), respectively in 2005 and 2006 (Fig. 1.1).

"We did not expect that research on the molecular mechanism of algal phototaxis and archaeal light-driven ion transport might interest readers of a medical journal…" wrote Peter Hegemann and Georg Nagel in EMBO molecule medicine perspective in 2013. It is worthy of note that the development of optogenetics is a beautiful example of revolutionary biotechnology growing out of purely basic research, in this case research primarily on the chemical mechanisms of phototaxis reception by microorganisms.

1.1.2 Pioneering efforts

The term "optogenetics" appears on the scene in 2006 (17). However, before the discovery of ChR, neurologists already made endeavour to achieve photo-stimulation of neuron. In 2002, Miesenböck group selectively elicits action potentials of genetically modified neurons by co-expression of three genes (the *Drosophila* photoreceptor genes encoding arrestin-2, rhodopsin, and the alpha subunit of the cognate heterotrimeric G protein, which they term "chARGe") in hippocampal neurons. (18) In 2004, Kramer, R. H. group has synthesized photoisomerizable azobenzene-regulated K^+ (SPARK), which is turned on by 380 nm and turned off by 500 nm. Exogenous expression of these channels in rat hippocampal neurons, followed by chemical modification with the photoswitchable gate, enabled different wavelengths of light to switch action potential firing on and off (39). In 2005, Miesenböck group remotely controlled the behavior of *Drosophila larvae* through genetically targeted photostimulation of neurons by photoreleasing of the active compounds from the respective "caged" precursors (19).

1.1.2 Optogenetic tool box

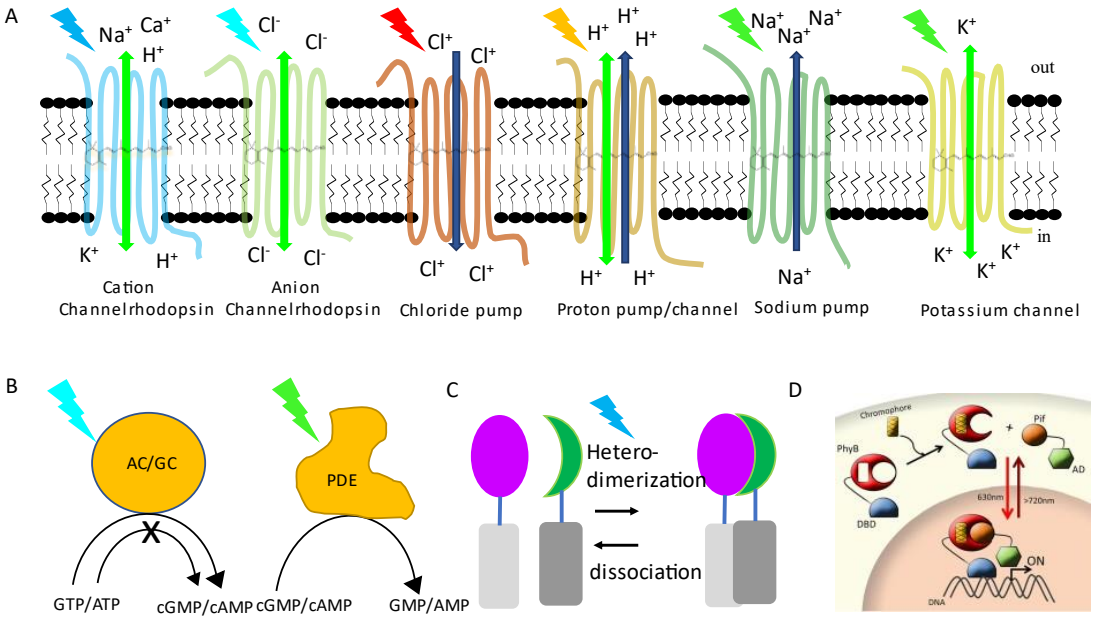

Figure 1.2 The optogenetic tool box. A, light-activated ion channels and pumps. B, light-regulated enzymes. C, light-induced dimerization tool. D, light inducible gene expression system. Modified from (20, 21).

It is almost 20 years, since the discovery of ChRs. The demand of light controlled cellular process is beyond the original function of light-controlled ion flow. The optogenetic tool box kept expanding with natural photoreceptors and artificial photoreceptors with customized light-gated function. To date, besides light-activated ion channels, the optogenetic tool box processes also light-activated ion pumps, light-activated enzymes, Photocontrol of protein-protein interaction and gene expression regulation. After the discovery of ChRs, anion channel rhodopsins (GtACRs, iChloC etc.), Kalium channel rhodopsin (HsKCRs, preprint reported in September, 2021) are also discovered or engineered, and facilitated in cell depolarization or hyperpolarization. Light-activated ion pumps include proton pumps (BR, Arch, CsR etc.) and chloride pumps (NpHR, Jaws etc.), which are used in depolarization and pH value regulation (22, 23). Light-regulated enzymes include photoactivated adenylyl cyclase (EuPAC, mPAC, bPAC etc.), light-activated guanylyl cyclase (BeCyclOP), light-inhibited guanylyl cyclase (Cr2C-cyclop1 and Vc2C-cyclop1) and a phosphodiesterase with light-enhanced substrate affinity (SrRhoPDE), which regulate important second/massanger, cAMP or cGMP level (24-27). Light-induced protein dimerization systems (Cry2/CIB1 pair, PhyB/PIF, iLID etc.) are also

developed for optogenetic manipulation of protein dimerization or protein localization to specific subcellular domains and protein purification (28). Optogenetic systems were also adapted to regulate gene expression (21) (Fig. 1.2).

1.2 Photoreceptors

Organisms of all domains of life harvest light, either for energy generation or for approaching suitable environments. Photoreceptor proteins are employed to sense and respond to light. The light-sensitivity of photoreceptor proteins arises from bound chromophores, such as retinal in retinylidene proteins, bilin in biliproteins, and flavin in flavoproteins. I will introduce rhodopsins and flavins, since I was working with some of them during my doctoral research.

1.2.1 Rhodopsins

Rhodopsin was originally a synonym for "visual purple". In 1876, German physiologist Franz Christian Boll first discovered rhodopsin by noticing that the light-sensitive pigment in the rods of the retina tended to fade in the presence of illumination. Not only in the animal visual system, evolutionary homologous proteins, which consist of opsin apoproteins and a covalently linked retinal, are also found in prokaryotes, algae, and fungi, and termed microbial rhodopsins (type I) (29). While sharing practically no sequence similarity, microbial (type-I) and animal rhodopsins (type-II) rhodopsins, share a common architecture of seven transmembrane (TM) (eight TM rhodopsin was also found, e.g. BeCyclop, introduced in 1.2.1.2) α-helices with the N- and C-terminus facing out- and inside of the cell, respectively (Figure 1.3). The retinal molecule is covalently fixed in the binding pocket within the 7-TM helices and forms a protonated retinal Schiff base ($RSBH^+$) with a conserved lysine residue located on TM helix seven (TM7) (Fig. 1.3) (30, 31). Retinal, the aldehyde of vitamin A, is derived from β-carotene. Upon absorption of a photon, the retinal chromophore isomerizes and triggers a series of structural changes leading to ion transport, channel opening, or interaction with signaling transducer proteins (29). lower organisms utilize the type I rhodopsins for surviving and to adapt to the environment. Animals use type II, a subset of G-protein-coupled receptors (GPCRs), for visual and nonvisual phototransduction, circadian rhythm and pigment regulation (32).

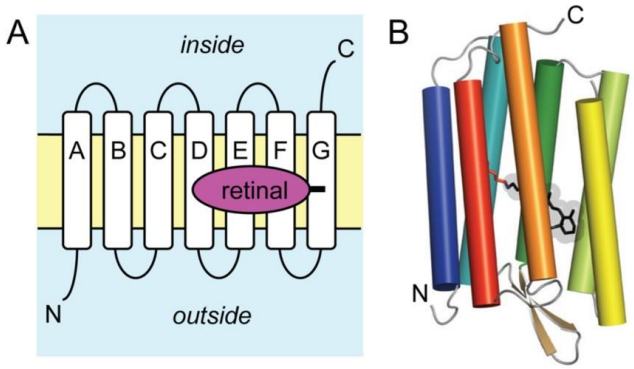

Figure 1.3 Topology of the retinal proteins. (A) These membrane proteins contain seven α-helices spanning the lipid bilayer. The N-terminus faces the outside of the cell and the C-terminus the inside. Retinal is covalently attached to a lysine side chain on TM7. (B) Cartoon representation of the helical arrangement of a microbial rhodopsin with attached all-trans-retinal (bacteriorhodopsin, PDB ID: 1C3W). Taken from (33).

The microbial rhosopsins are appreciated tools for optogenetic applications, on account of their fast kinetics (34). In microbial rhodopsins, an *all-trans* retinal isomerizes to the 13-*cis* configuration upon photon absorption. The activated retinal molecule remains associated with its opsin protein partner and thermally reverts to the all-trans state while maintaining a covalent bond to its protein partner (35). What is more, microbial rhodopsins consist of light-driven ion pumps, light-gated ion channels, which have immediate effect. Unlike the situation in type I microbial rhodopsins, in Type II animal rhodopsins the retinal dissociates from its apoprotein after isomerization into the *all-trans* configuration, and a new 11-*cis* retinal must be recruited. The activated type II GPCRs are capable of transducing the activation signal by catalyzing GDP/GTP exchange on membrane-bound heterotrimeric G proteins within the cell, thus initiating G protein mediated signaling cascade (36). Due to these chromophore turnover reactions and the requirement for interaction with downstream biochemical signal transduction partners, type II opsins affect cellular changes with slower kinetics compared to type I opsins.

Bacteriorhodopsin (BR) from *Halobacterium salinarum* is the best-studied microbial rhodopsin. This light-driven proton pump generates an electrochemical gradient across the membrane that is used by the cells for adenosine triphosphate synthesis and other vital energy-requiring functions (37-39). The proton pathway is spectroscopically well characterized. It is stepwise but spatially noncontinuous and unidirectional. The photocycle shows the isomeric and protonation state of the retinal. Near the RSB, microbial rhodopsin contains protein-bound water molecules for stabilization of the $RSBH^+$ in the hydrophobic protein interior. The photocycle, exemplified by bacteriorhodopsin (BR), contains the spectrally distinguishable

quasi-stable states K, L, M, N, and O. Upon photon absorption, retinal twists as the primary red-shifted K state. Right after is the blue-shifted L state, which serves as the precursor of the proton transfer reaction from the $RSBH^+$ to its primary carboxylic proton acceptor. The strongly blue-shifted M state can divide into M formation and M decay. The $RSBH^+$ deprotonated upon M formation and the RSB reprotonated from the cytoplasmic side upon M decay. In the case of chloride pumps, the RSBH+ does not deprotonate during the photocycle and the L state converts directly to the N state. Largest changes in the protein backbone conformation appears at the N state, mostly outward tilts of the cytoplasmic end of helix F. The last red-shifted O resets the original un-photolyzed conformation (Figure 1.4) (33, 40).

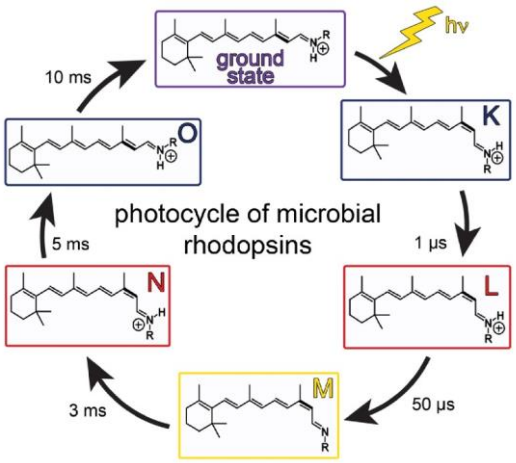

Figure 1.4 Typical photocycle of microbial rhodopsins. Taken from (33).

1.2.1.1 CsR

CsR was named as CvRh, a proton-pumping rhodopsin from *Chlorella vulgaris* (41). However, according to the present sequence data, the green alga is reclassified into the *Coccomyxa* genus with a species name of *C. subellipsoidae*. *Coccomyxa subellipsoidea* is a small elongated non-motile unicellular arctic alga and is psychrotolerant that resides in temperatures ranging from − 50 °C to + 25 °C (42). The same proton pump rhodopsin now is abbreviated as CsR (43).

CsR expresses well and produces large photocurrents in *Xenopus* oocytes with action spectrum maximum at 545nm (43). In 2019, the crystal structure of CsR is solved, and displayed a homotrimeric arrangement with an overall structural topology similar to that of other light-driven pumps: consisting of seven transmembrane α-helices with the N- and C-terminus facing

out- and inside of the cell (Fig. 1.5). *All-trans* retinal chromophore bound to Lys215 of TM7 via a RSBH+, which is stabilized by a negatively charged counterion complex Asp86 and Asp211. Arg83 and six water molecules forms hydrogen-bonding network at the extracellular side. The highly conserved Arg83, previously described as a key proton shuttle residue in BR, forms a hydrogen bond with the hydroxyl group of a non-conserved Tyr14 at the TM1(Fig. 1.5) (44).

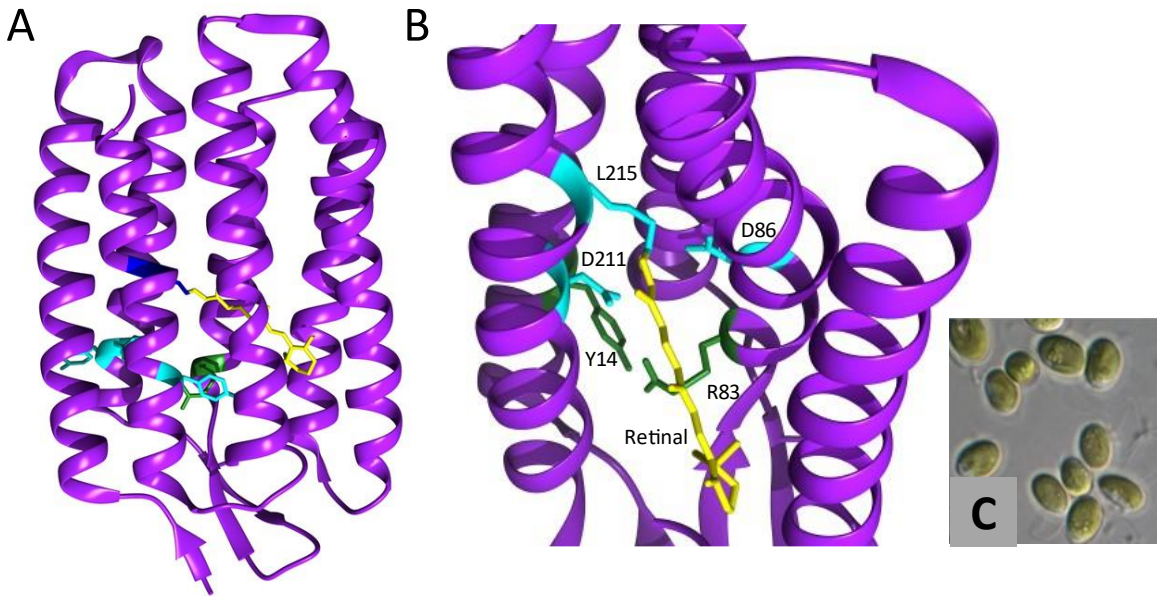

Figure 1.5 Structrue of CsR (Rhodopsin from *Coccomyxa subellipsoidea*). A, overall structure of CsR. B, enlarged picture of retinal binding region. The retinal molecular is shown in yellow, and binds to Lys215 (in cyan) of TM7 via a $RSBH^+$. The negatively charged counterion complex Asp86 and Asp211 (in cyan) stabilize the retinal. Arg83 forms a hydrogen bond with the hydroxyl group of a non-conserved Tyr14 and prevent proton release (PBD 6GYH). C, Image of *Coccomyxa subellipsoidea* (a small elongated non-motile unicellular arctic alga and is psychrotolerant that resides in temperatures ranging from − 50 °C to + 25 °C)(45).

Structural changes enable successive proton release to the extracellular medium and delayed proton uptake from the intracellular side. Upon photon absorption, (1) the proton of RSBH+ is transferred to primary proton acceptor Asp86 (L to M formation). (2) Protonated Arg86 makes Arg83 switched outward towards the proton-releasing complex Glu193 and Glu203, resulting in proton release into the extracellular medium (M formation to M decay). In the second part of the photocycle, (3) the deprotonated RSB reprotonates from proton donor (M to N state). (4) This is followed by Asp97 reprotonates from the cytoplasmic bulk phase (N to O state). At the end of the photocycle, during the transition from O-state to the dark-state, (5) the proton is

transferred from Asp86 to the proton release group, passing or bypassing Arg83 and Tyr57 (43, 44).

1.2.1.2 BeCyclOP

BeCyclOP (for guanylyl cyclase opsin from *Blastocladiella emersonii*) is a Light-activated Cyclase Opsin, has eight transmembrane helixes, which is not like other rhodopsins. It converts guanosine triphosphate (GTP) to cyclic guanosine monophosphate (cGMP) and pyrophosphate (Fig. 1.6). Co-expression of BeCyclOp and CNG channel (comprising TAX-2 and TAX-4 subunits from *C. elegans*) in *C. elegans* muscle cells, demonstrates light-driven depolarization. The photoactivation of BeCyclOp triggers rapid tactic behavioural responses in O^2/CO^2 sensory neurons of C. elegans s via intrinsical cGMP signalling. BeCyclOp is a potent optogenetic tool for modulation of CNG channels and cGMP signalling in cells and animal.

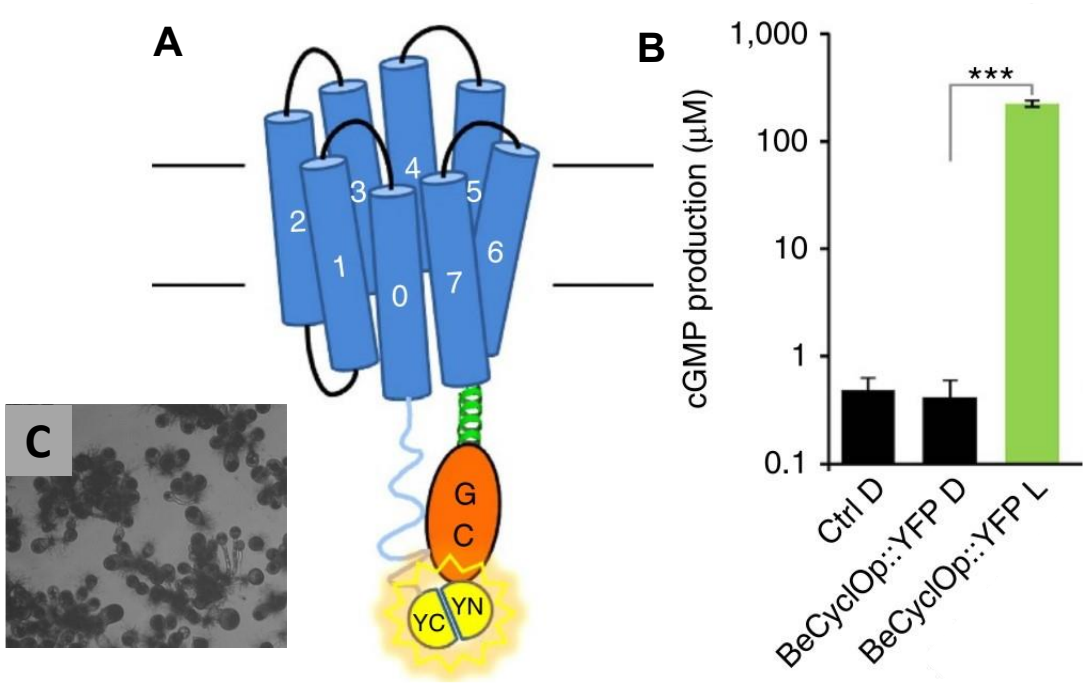

Figure 1.6 A, Illustration of BeCyclOp with eight transmembrane helices and Guanylyl Cyclase at the C terminal. B, cGMP production in *Xenopus* oocyte expressing BeCyclOp in dark (D) and after illumination (L; 532 nm, 0.2 $mWmm^{-2}$, 2 min). Taken from (27). C, image of *Blastocladiella emersonii* (a saprobic aquatic fungus)(46).

1.2.2 Photoactivated Adenylyl Cyclase

As optogenetic tools, ChR, BR, and HR are so well appreciated because they modulate the membrane potential as a universal parameter relevant for basically all neuronal cells. This

success stimulated the demand for optogenetic tools that modulate other general cellular parameters such as the second messengers Ca^{2+}, cAMP, cGMP, or inositol triphosphate.

In 2007, Nagel's lab firstly successfully control the intracellular cAMP level by light, by heterologously and functionally expressing euPAC in *Xenopus* laevis oocytes, HEK293 cells and *Drosophila melanogaster* flies (47).

EuPAC is from *Euglene gracilis,* a unicellulat flagellate. It changes its swimming direction upon sudden blue light intensity change. A sudden increase in blue light intensity causess step-up its photophobic responses, resulting in photoavoidance, *vice versa*(48). To find out the photoreceptor molecules that mediating its photomovement, in 2002 Iseki, M. et al isolated paraflagellar body from Euglena, and found out that a flavoprotein, which is an adenylyl cyclase, is the major constituent of the paraflagellar body and acts as the photoreceptor for the step-up photophobic response. The flavoprotein is designated as photoactivated adenylyl cyclase (PAC)(49). EuPAC forms heterotetramer in the flagellate and is composed of two subunits PACα and PACβ: Each subunit harbors two BLUF-type photoreceptor domains, binding flavin adenine dinucleotide (FAD) and two catalytic domains that are homologous to class III adenylyl cyclases (49).

PACα alone was used for photomanipulation of cAMP level (47, 50). Neuroscientists employed PACα in Aplyisa neurons where a light pulse can increase the spike width (51), and in *Caenorhabditis elegans* cholinergic neurons where it manipulates neurotransmitter release (52). However, large molecular mass (>1000 aa), low solubility, significant dark activity, and only moderate light activation prevent PACα from wide application.

To date, a variety of other PACs including bPAC(53), nPAC (54), TpPAC (55), mPAC (56), OaPAC (57), cPAC (58) DdPAC (59) were identified or engineered to be introduced as the optogenetic tools for cAMP manipulation. Among them, bPAC is the most popular one, because of its small size, low dark activity and high light activaty (53, 60).

1.2.2.1 bPAC

Beggiatoa is a sulfide oxidizing bacterium that colonizes large areas of sea ground in the form of widely extended microbial mats (8). As a chemolithoautotroph, *Beggiatoa* utilizes oxygen or nitrate as electron acceptors during sulfide oxidation (61, 62) (Fig. 1.7A). In the genome of *Beggiatoa*, a gene, putatively encoding a 350-aminoacid protein, consisting of a blue

light-sensing BLUF domain linked C-terminally to a typeIII adenylyl cyclase, was found (53, 60).

This gene encodes a photoactivated adenylyl cyclase, terms bPAC. The purified bPAC has the absorption spectrum of BLUF-bound flavin with a maximum at 440 nm (18) and 15 nm right-shift upon blue light illumination (Fig. 1.7B). Heterologously expression of bPAC in *Xenopus* oocytes, with either CFTR or olfactory cyclic nucleotide-gated ion channel (CNG-channel), is able to produce light-induced inward current. A half-saturated intensity of 4 $\mu W/mm^2$ and 300-fold light to dark enzymic activity is determined with the purified protein from *E. coli* (Fig. 1.7C)(53).

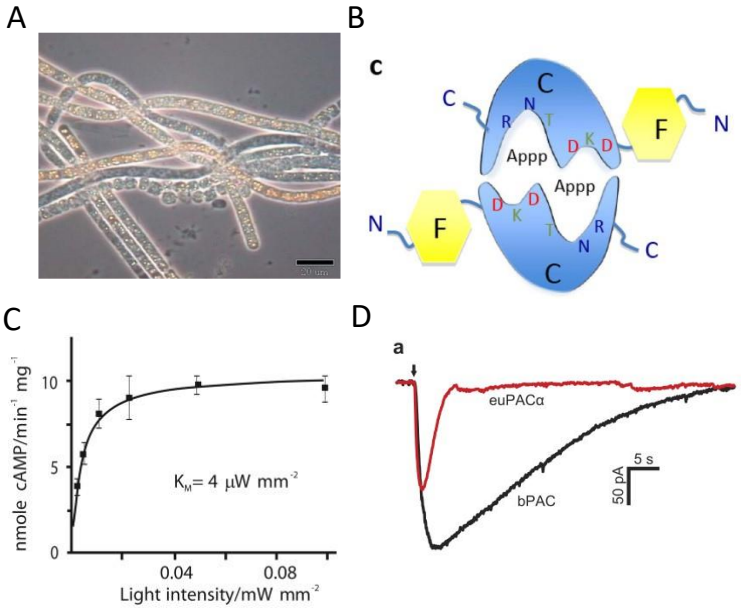

Figure 1.7 A, Filaments of *Beggiatoa*. Image from Microbial Diversity 1997 (Rolf Schauder). B, model of the dimeric bPAC with flavin-binding BLUF domain (F) in yellow and the catalytic domain (C)in blue. C, light intensity dependence of cAMP production by purified bPAC. D, Comparing bPAC-and euPAC -induced currents in neuron. Taken from (53).

bPAC is also employed in neuronal cells to precisely control intracellular cAMP level. Expression of bPAC in conjunction with CNG channels in CA1 pyramidal cells induces rapid and highly reproducible photocurrent when applying blue light irradiation. More importantly, bPAC outperformed EuPACα in evoking CNG currents (Fig. 1.7D). In the *Drosophila* central nervous system, bPAC mediates light-dependent cAMP increase and behavioural changes in freely moving animals (53). Besides neural application, bPAC was further introduced in various studies including sperm fertilization (63), neuronal repair (64), neurotransmission (65),

mechanosensitive GPCR (66) and insulin secretion (67). Low dark activity, high light-induced activity and high light sensitivity make bPAC a powerful tool for optogenetic application. My colleagues further studied on bPAC and found that, membrane binding can further decrease the dark activity (24), which gave us a hint that fusing bPAC with a CNG channel may eliminate the dark conductance.

1.2.2.3 Photoactivation Mechanism of bPAC

In 2017, a series states (isolated AC domain, dark, illumination, and *pseudo*-lit) of bPAC structures were solved and provided a photoactivation mechanism of light-regulated adenylyl cyclase. As a Type III Cyclase, bPAC forms a homodimer within two domains: an N-terminal BLUF domain and a C-terminal AC domain. A central coiled-coil ($\alpha3_{BLUF}$) and a handle like platform ($\alpha4_{BLUF}$ -$\beta1_{AC}$) connect between BLUF and AC. The AC domain contains a tongue-like extrusion ($\beta4_{AC}$- $\beta5_{AC}$) that reaches over into the other monomer (Fig. 1.8). The affinity to ATP of bPAC is not changed by light with similar Km values of about 50-100 μM and the isolated AC domain is constitutively inactive, which indicate that the ATPs are "parked" in binding sites of AC even in dark, and that the interplay between BLUF and AC domains is required for catalysis (68).

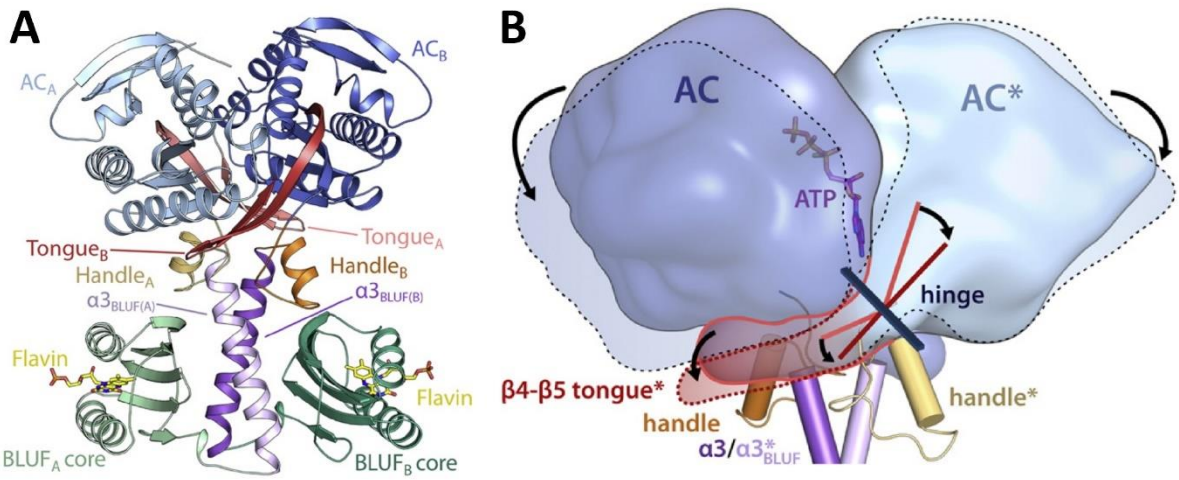

Figure 1.8 Structure and photoactivation mechanism of bPAC. A, The overall structure of bPAC. B, The clamshell-like movement of the AC domains. Taken from (68).

Upon absorption of a blue light photon, the FAD chromophore triggers structural changes in the BLUF domain: the conformation changes of Tyr7 ($\beta1_{BLUF}$) transmit to the kink (Leu77 and Lys 78) in $\beta4_{BLUF}$. The side chains of residues Leu75 and Lue 77 are in van der Waals contact with the side chains of Glu124 and His120 ($\alpha3_{BLUF}$). By this way, light induced changes

relay from $\beta1_{BLUF}$ to $\beta4_{BLUF}$, and $\alpha3_{BLUF}$, and the C-terminal capping of BLUF domain. Through the interaction between Lys125 and Tyr126 in $\alpha3_{BLUF}$ and Met264 and Asn257 in $\beta4_{AC}$- $\beta5_{AC}$, structure changes in $\alpha3_{BLUF}$ propagate to the AC domain. The $\beta4_{AC}$- $\beta5_{AC}$ moves towards the BLUF domain, which opens the active site cleft for accommodation of ATP and repositions of catalytic residues (68).

1.3 Optogenetic silencing tools

Reversible silencing of neuronal activity is a nice approach to isolate the roles of specific neuronal populations in circuit dynamics and behaviour (69). Unlike the abundant optogenetic tool kit for neuronal excitation, which possesses ChRs and variants with diverse kinetics, ion selectivity as well as light absorption, the neuronal silencing tools are limited, especially for long term inhibition.

The neuron silencing tool box includes ion pump rhodopsins, anion conducting rhodopsins (ACRs), synthesized light-activated potassium channels, presynaptic vesicular release inhibition methods and vertebrate rhodopsins (Fig. 1.9).

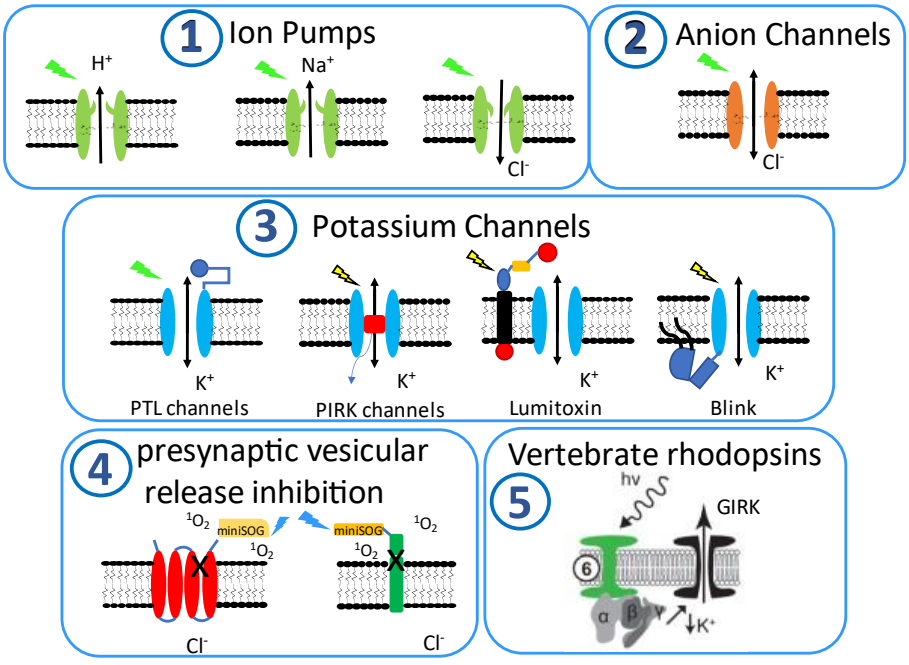

Figure 1.9 light-activated silencing tools. 1, Rhodopsin ion pumps comprises outward proton or sodium pumps (e.g. ArCh), inward chloride pumps (e.g. NpHR). 2, anion channelrhodopsins (e.g. iC++, iChoC, *Gt*ACRs). 3, Synthesised light-activated potassium channels include PTL (for photoswitched tethered ligands) channels, PIRK (for photoinducible inwardly rectifying potassium using unnature

amino acids) channels, Lumitoxin (is a fusion protein containing a peptide toxin as the ion channel ligand and a LOV domain photoswitch tethered to the cell membrane,), BLINK (for a blue-light–induced K^+ channel). 4, InSynC (for Inhibition of Synapses with CALI), which is achieved via singlet-oxygen generation through miniSOG. 5. vRh (for Vertebrate rhodopsins) couples to other Gi/o family, and activates G-protein-coupled inwardly rectifying K^+ (GIRK) channels. Detailed mechanisms of each tool are described below.

1.3.1 rhodopsin-based ion pumps

Rhodopsin-based outward proton or sodium pumps, inward chloride pumps are used for neuronal silencing. A proton pump, archaerhodopsin-3 (Arch) from *Halorubrum sodomense*, are reported to be able to silence neurons in the awake mouse brain with yellow light illumination (70). A chloride pump, NpHR from *Natronomonas pharaonic*, allows either eliminating single action potentials or sustained suppression of spiking (71). a red-shifted chloride pump, Jaws, derived from *Haloarcula salinarum*, are engineered to be activated by red light, and can mediate transcranial optical inhibition of neurons deep in the brains of awake mice (72).

However, ion pumps can only pump one ion per photon, which makes them low light sensitive. And the tools exhibit a decline in photocurrent amplitudes when illuminated for prolonged periods (A 60-s illumination can cause a reduction of 50%–90% of peak activity), which is so called inactivation, and need several seconds to recover from the inactivation to the initial photocurrent. The strong inward chloride pump activities can also alter the intracellular chloride concentrations.

1.3.2 rhodopsin-based anion channels

While rhodopsin-based pumps induce hyperpolarization in neuron, Anion conducting rhodopsins (ACRs) induce shunting effects, which is more efficient. Two mutated ChR variants, iC++ and iChoC, are highly anion-selective. iC++ is reported to control free moving animal (73). iChloC enables inhibition of spiking activity evoked by visual stimulation in the primary visual cortex of anesthetized mice (74). The soma-targeted *Gt*ACR2, which is a natural light-gated anion channel from *Guillardia theta* strictly conducted anion, produce several-fold larger photocurrents in mammalian cells than any of the anion conducting ChR mutants(75, 76). Even so, whether ACRs will inhibit or excite the neuron activity, depends on the reversal potential of chloride, which can vary among neurons (77-80).

1.3.3 Synthesized Light-activated potassium channels.

Potassium channels are universal native channels to terminate action potentials and underlie the resting membrane potential in excitable cells. A light-activated K^+ channel would overcome ion gradients and reversal potential limitations. Over the last 10 years, scientists have put extensive efforts to mutate existing ChR to more potassium conducting channels and explored new ChRs that have high potassium conductance. On the other hand, scientists attempted to snythesize light-activated potassium channels.

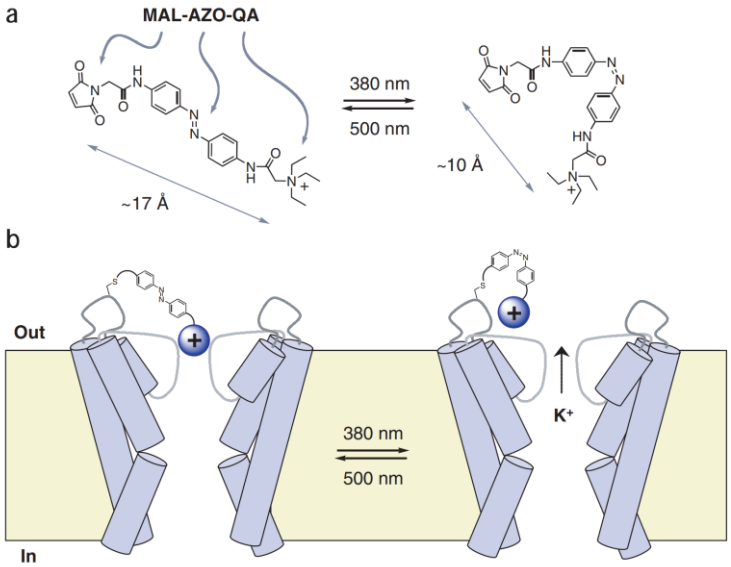

Figure 1.10 Photoisomerization of MAL-AZO-QA gates ionic currents through modified Shaker channels (an example of PTL channel). (a) The rigid core of MAL-AZO-QA (between the α carbons flanking the azo moiety) changes by about 7 Å upon photoisomerization. (b) MAL-AZO-QA blocks ion flow in the *trans* configuration but is too short to block effectively after photoisomerization to the *cis* configuration. Diagram shows a model of the inner helices of the Shaker K^+ channel with the dimensions of MAL-AZO-QA drawn roughly to scale. Taken from (81).

1.3.3.1 PTL channels

PTL channels are photoswitched tethered ligands-based channels. As early as 2004, Kramer, R. H. group has developed a chemical gate that confers light sensitivity to modified shaker channels. The gate, termed MAL-AZO-QA (MAQ), consists of a maleimide (M), which selectively conjugate to an engineered K^+ channel, a photoisomerizable azobenzene (A), and a quaternary ammonium (Q) group that blocks the pore of the channel. Cyan light (500 nm) drives

the azobenzene moiety into its extended *trans* configuration, allowing the blocker (Q) to reach the pore. UV light (380 nm) generates the shorter *cis* configuration, retracting the blocker and allowing conduction (Fig. 1.10). The synthesized photoisomerizable azobenzene-regulated K^+ (SPARK) enabled remotely control of neuronal firing (81). With a similar concept, in 2010 and 2011, their group published HyLighter and several PTL potassium channels (82, 83). The requirement of sufficient concentration of additional synthetic photoswitch, constant illumination with cyan light to block the pore, and UV light to active the channel, have limited their wide application.

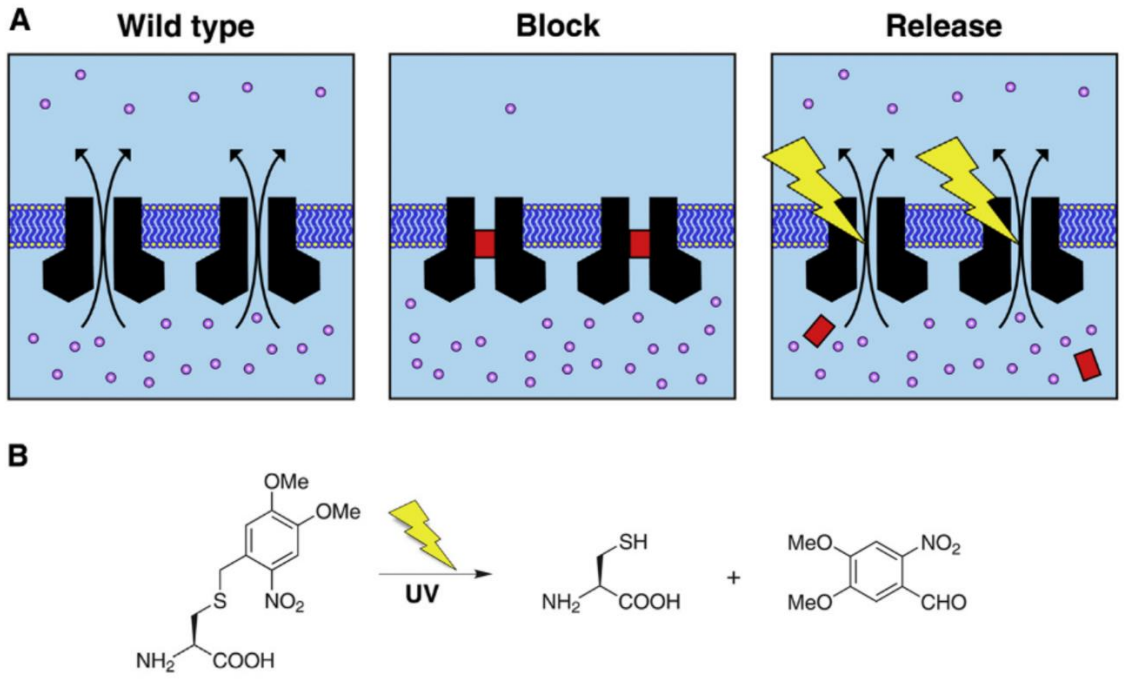

Figure 1.11 PIRK channel using genetic incorporation of photocaged unnatural amino acids. A, A model illustrating photoactivation of PIRK channels expressed on the plasma membrane. Left: wild-type Kir2.1 channels (black) conduct K^+ (in purple) current in physiological conditions. Middle: incorporating the Uaa Cmn (in red) in the pore of Kir2.1 channels renders the channel nonconducting (PIRK channels). Right: UV light exposure irreversibly removes the dimethoxyni-trobenzyl group to allow permeation through theKir2.1 channel, restoring outward K^+ (in purple) current and reducing membrane excitability. B, Chemical pathway for photolysis of Cmn. UVlight cleaves the S-C bond, releasing the dime-thoxynitrobenzyl group from Cys. Cys would remain on the protein. Taken from (84).

1.3.3.2 PIRK using Uaa

In 2014, Kang, J. Y. et al designed photoinducible inwardly rectifying potassium (PIRK) by genetic incorporation of a photoreactive unnatural amino acid (Uaa) into the pore of Kir2.1.

Before light illumination, the channel was blocked by Uaa and nonconductive. Upon light illumination, the Uaa was released from the pore and the channel was opened, and efflux of K^+ (Fig. 1.11). Expression of PIRK allowed light-activatable suppression of neuronal firing in rat hippocampal neurons. However, the light activation is single-use and irreversible (84).

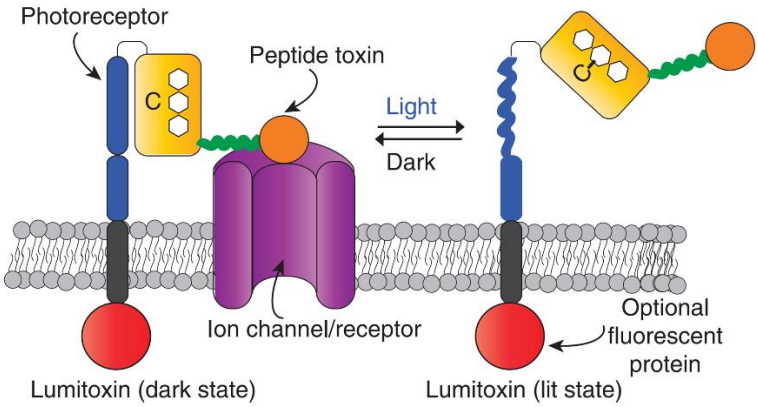

Figure 1.12 Lumitoxin. Architecture of fusion protein containing a membrane-anchored (PDGF-R, black) photoreceptor AsLOV2 (yellow; 'C' indicates the location of key cysteine, and molecular structure schematically represents flavin)/Ja (blue) connected to a peptide toxin (orange) via a flexible linker (green wiggly line), optionally equipped with a fluorophore (red sphere). Taken from (85).

1.3.3.3 Lumitoxin

The same year, Edward Boyden group presented a fully genetically encoded modular protein architecture for optical control of peptide ligand concentration, and subsequently control of ion channels. Lumitoxin, which is a fusion protein containing a peptide toxin as the ion channel ligand and a light-oxygen-voltage (LOV) domain photoswitch tethered to the cell membrane, can actuate endogenous voltage-gated K^+ (Kv) channels with light (Fig. 1.12). On a brief light illumination changes conformation of the LOV domain, and lowers the local concentration of the peptide toxin near the cell surface, and thus enabling the ion channel target's functionality in response to light (85).

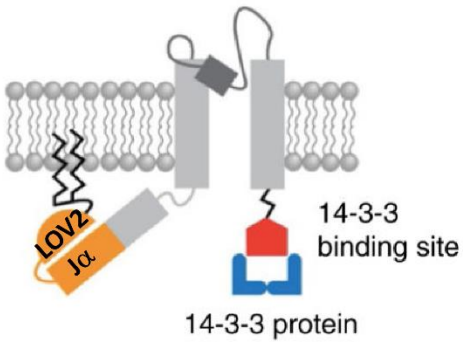

Figure 1.13 Cartoon representation of BLINK2 showing the Kcv_{PBCV1}channel (gray), LOV2 domain (orange), N-terminal myristoylation and palmitoylation sites (zigzagging black lines) and a fragment of *Arabidopsis thaliana* KAT1 protein (red) for binding of 14-3-3 proteins (blue). Taken from (86).

1.3.3.4 Blink

In 2015, Cosentino, C. et al published a blue-light–induced K^+ channel 1 (BLINK1) by fusing a small viral potassium channel to the photosensitive LOV2-Jα domain of the plant blue-light receptor, with several additional modifications to reduce dark activity (Fig.1.13). The poor mammalian cell surface expression level hampers its wider use (87). In 2018, a C-terminal signal sequence modified version, BLINK2, showed good expression in neurons in three species, but the 2.7 min open time makes it difficult to control (86).

1.3.4 Presynaptic vesicular release inhibition

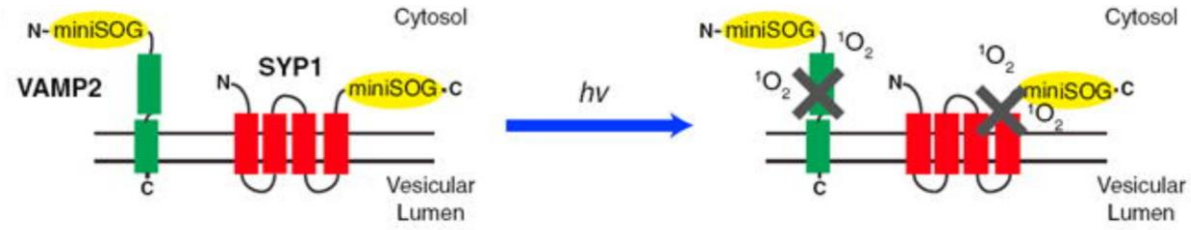

Figure 1.14 Two designs of InSynC with miniSOG fused to Vesicular Associated Membrane Protein 2 (VAMP2) or Synaptophysin (SYP1). In the design with VAMP2, miniSOG is fused to the N terminus of VAMP2 facing the cytosolic space. With the SYP1 design, miniSOG is fused to the C terminus of the SYP1 also facing the cytosol. After light illumination, singlet oxygen ($^1O_2$) is generated by miniSOG leading to the inactivation of fusion protein. Taken from (88).

In 2011, Roger Y. Tsien group engineered miniSOG (for mini Singlet Oxygen Generator), which is a fluorescent flavoprotein and originally from *Arabidopsis* phototropin, for introducing

contrast in electron microscopy of fixed tissue (89). In 2013, they published InSynC (for Inhibition of Synapses with CALI) by fusing miniSOG to VAMP2 (Vesicle Associated Membrane Protein 2) or synaptophysin (Fig. 1.14). InSynC enabled disruption of presynaptic vesicular release upon illumination with blue light (88).

1.3.5 Vertebrate rhodopsins

Vertebrate rhodopsins are photoreceptive proteins present in vertebrate rod photoreceptor cells, which are responsible for scotopic vision and are orders of magnitude more light-sensitive than channelrhodopsins. vRh inhibite neuronal activity via coupling to Gi/o family members activates endogenous G-protein-coupled inwardly rectifying K^+ (GIRK) channels (90-92).

1.4 Cyclic nucleotide-gated channels

Cyclic nucleotide-gated ion channels are nonselective cation channels, which are activated by second messengers, adenosine 3, 5-cyclic monophosphate (cAMP) and (or) guanosine 3,5-cyclic monophosphate (cGMP) (93). When scientists were investigating the intracellular messenger that mediates the photo response in retinal photoreceptors, they found cGMP could directly activate the light-dependent channel in the rod outer segment (94). Similar channels were also found in cone photoreceptors, olfactory sensory neurons and other neuronal and nonneuronal cell types (95-97). CNG channels are significant in signal transduction in vision and olfaction, as well as in hormone release and chemotaxis (98). Numerous inherited retinal degenerative disorders, achromatopsia, and anosmia are reported to be related to mutations in human CNG channel genes (99).

The voltage-gated potassium channel superfamily includes 4 types of channels: the ether-a-gogo (EAG) and human eag-related gene (HERG) family of voltage-activated potassium channels, several plant potassium channels commonly referred to as KAT, AKT, and KST channels, hyperpolarization-activated and cyclic nucleotide-gated (HCN) pacemaker channels which is also highly potassium permeable, and cyclic nucleotide-gated channels. Although they are not potassium selective and are voltage independent, CNG channels belong to this superfamily. Like other superfamily members, CNG channels form a tetramer, have six transmembrane segments (S1-S6), a positive charged S4, a pore forming region between S5

and S6, and a cytoplasmic C-terminal (93). the C-linker and cyclic nucleotide-binding domain (CNBD) of CNG channels are thought to be responsible for gating (Fig. 1.15). Upon cNMP binding, CNBD makes a conformation change, drags the C-linker, and further opens the channel.

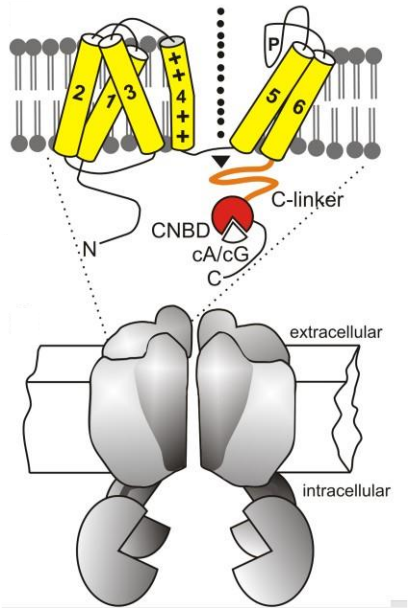

Figure 1. 15 Domain structure of CNG and HCN channel subunits. 1-6, transmembrane helices; P, pore-loop harboring the ion selectivity filter; C-linker (C-terminal linker domain); CNBD, cyclic nucleotide binding domain. The dotted arrow indicates the flow of cations through the pore. C, channel tetramer. Taken from (139).

More and more prokaryotic CNG channels are also identified as eukaryotic CNG channel ortholog, when scientists tried to investigate the gating mechanism of the CNG channel family. Because one productive avenue toward high-resolution ion channel structure is currently provided by bacterial homologues, which in some cases allow overexpression in *Escherichia coli* of properly assembled proteins amenable to purification and crystallization study. MlotiK1, SthK, and LliK are among these prokaryotic CNG channel homologs, three of them are all highly potassium selected and are more sensitive to cAMP over cGMP (100-102). MlotiK1 is first identified in 2004 from *Mesorhizobium loti*, which is the most structure studied prokaryotic CNG channel, with a cAMP K_D of 150 nM and cGMP of 1.7 μM(100, 103). SthK is described in 2014 from *Spirochaeta thermophila* with a cAMP EC_{50} of 3.7 μM, its C-terminal structure is available. A nonnegligible character of SthK is that cGMP acts as an antagonist or agonist with higher affinity and very low efficiency, which is the exclusive CNG channel that cGMP binding could not active it(101, 104, 105). The intact structure of LliK is reported in 2017, it is from *Leptospira licerasiae* with a binding affinity for cAMP of 2.4μM (102).

1.4.1 SthK

SthK is a prokaryotic cyclic nucleotide-gated K^+ channel from *Spirochaeta thermophila*, which is identified by Brams M and Kusch J. cAMP act as an agonist to SthK with EC_{50} value of 3.7 μM, while cGMP act as an antagonist or agonist with higher affinity and very low efficiency (Fig. 1.16 A, B and C)(105). Albeit the single channel current amplitudes and the single-channel open probabilities of recombinant SthK in lipid bilayers are reported to be voltage-dependent, the macropatch current is voltage insensitive (101, 105). For avoiding the channel activated by other factor than light, the unique effective agonist and voltage insensitive is favourable for light control. With K^+ filter signature sequence T-V-GYG, SthK allows K^+ but not Na+ to permeate with a single channel conductance of 71 pS, which shares the similar character with native K^+ channels responsible for repolarization (Fig. 1.16 D). In the presence of cAMP, the channel shows no inactivation or desensitization. The simple kinetics of SthK, make it a good candidate for engineering a light-activated K^+ channel.

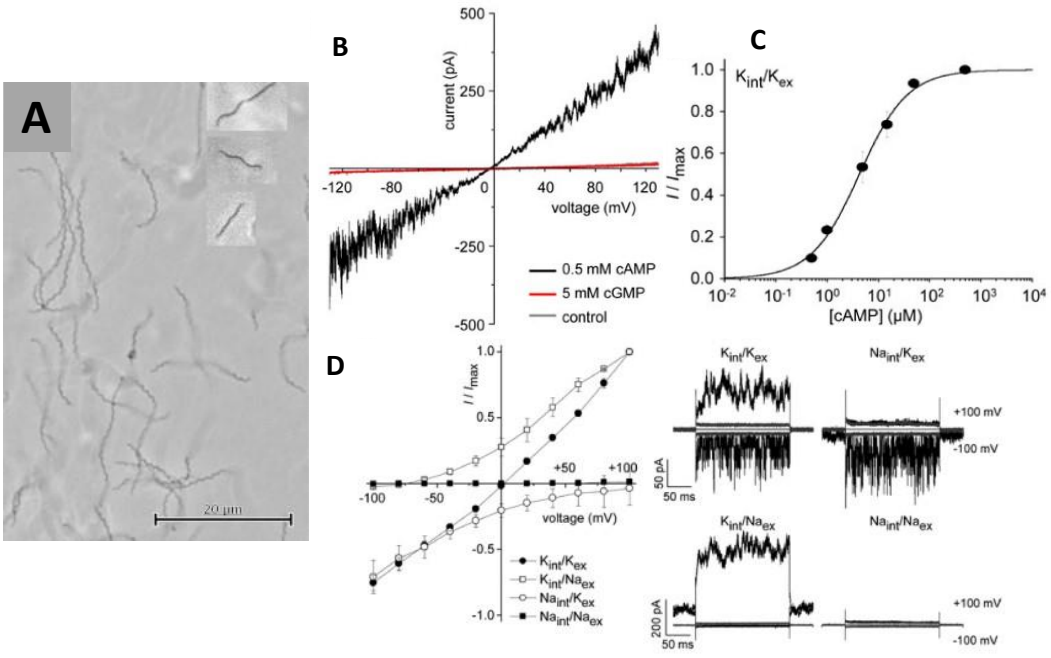

Figure 1.16 A, Image of *S. thermophila* (a member of the phylum *Spirochaetes*, and has optimal growth temperatures of 48–52°C and 66–68°C). B, A voltage ramp ranging from −130 to +130 mV in 4.5 s was applied to an inside-out macropatch excised from a SthK-GFP–expressing *Xenopus laevis* oocyte. The black trace represents the current response after applying 500 μM cAMP at symmetrical potassium. There was no current response after removal of cAMP or applying 5 mM cGMP to the same patch, shown as gray and red traces, respectively. C, The concentration–activation relationship for cAMP. D,

Current–voltage relationship as measured under four different ionic conditions. Bath solution and pipette solution contained either K^+ or Na^+ ions, respectively. The bath solution additionally contained a saturating cAMP concentration of 500 μM. (Right) Representative currents (black traces: at 500 μM cAMP; gray traces: no cAMP) for each of the four ionic conditions. Taken from (101, 106).

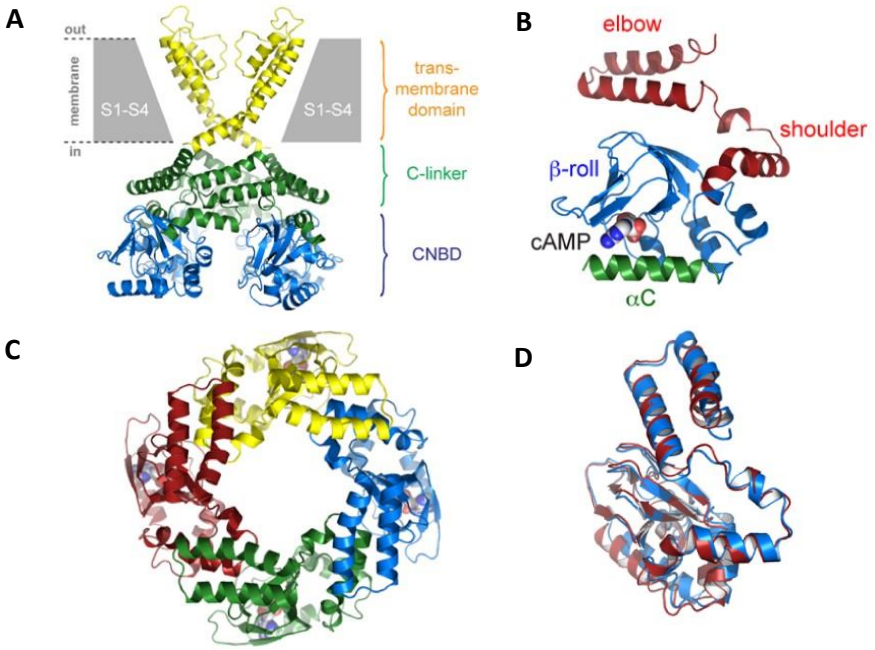

Figure 1.17 Molecular architecture of the SthK C-terminal domain. A, Superposition of the SthK-C-term tetramer onto the open gate structure of the Kv1.2 channel. The CNBD is shown in blue, the C-linker in green and the transmembrane domain in yellow. Only two transmembrane subunits are shown for clarity. B, Cartoon representation of a single SthK-Cterm monomer. The C-linker is shown in red, the β-roll in blue and the C-helix in green. The cAMP molecule is shown in sphere representation. Blue atoms are nitrogen, white atoms are carbon and red atoms are oxygen. C, Top down cartoon view of the SthK-Cterm tetramer along the fourfold symmetry axis. Each of the four subunits is shown in a different color. D, Differences in monomer conformation after superposition of the cAMP-bound tetramer onto the cGMP-bound tetramer. Blue is cGMP-bound, red is cAMP bound. Taken from (107).

Alignment data indicate that the structure motif of SthK is among members of the superfamily of voltage-gated potassium channels. It has six transmembrane segments (S1-S6) with cytoplasmic N- and C-terminals. As a CNG channel, the C-terminal of SthK contains a C-linker and a CNBD (Fig. 1.17A). The structure of SthK C-terminal is available and shows a tetramer, which radially assembles along a four-fold symmetry axis that extends to the ion channel pore of the transmembrane domain (Fig. 1.17C). The C-linker domain of cAMP-bound SthK has six α-helices (αA' to αF'). The A'-and B'-helices form an antiparallel helix-turn-helix motif (Fig. 1.17B). The tetramer interface of C-terminal is mainly formed by the C-linker

domain, with the 'elbow' (αA' and αB') of one subunit resting on the 'shoulder' (αD' and αE') of its neighboring subunit (Fig. 1.17C). The C-linker domain is followed by the CNBD, which contains four helices (αA, αB, αP, αC) and eight β-strands. The β-strands arranged in a so-called β-roll, which is flanked by the A- and B-helices (Fig. 1.17B).

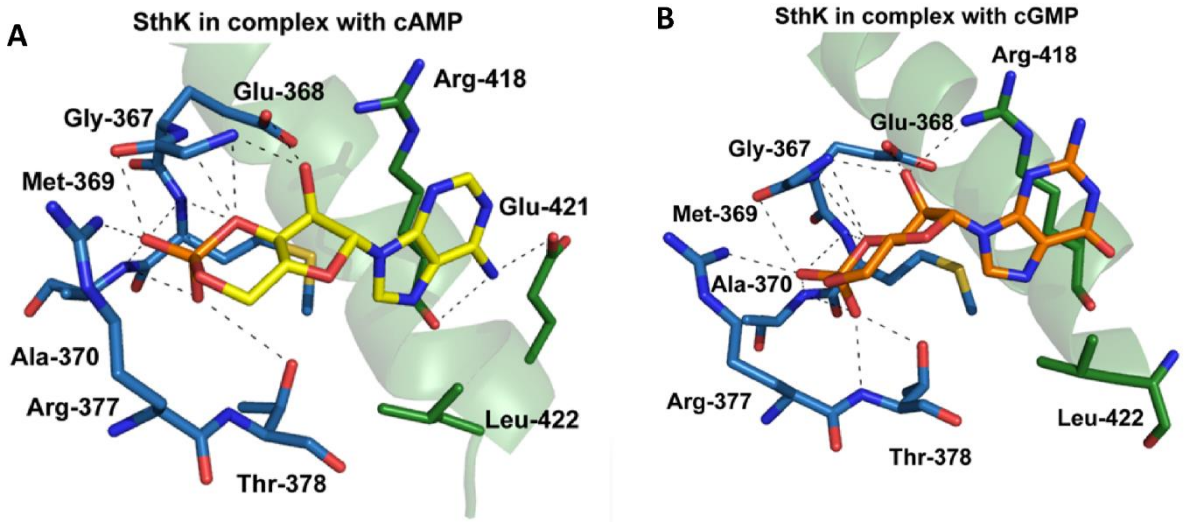

Figure 1.18 Molecular determinants of ligand recognition in the SthK-Cterm in complex with cAMP or cGMP. A and B, Comparison of the amino acids in the ligand binding site involved in recognition of cAMP or cGMP in SthK. Amino acids of the β-roll are shown in blue sticks, residues of the C-helix in green sticks. The C-helix is shown in cartoon representation. The cAMP molecule is shown in yellow or orange. Dashed lines represent hydrogen bonds or salt bridges. Taken from (104).

As cAMP act as an agonist to SthK and cGMP act as an antagonist, the conformational changes between SthK C-terminal in complex with cGMP and cAMP reveal a gating mechanism. Upon cAMP binding, the CNBD makes an outward swinging movement, this causes a significant widening of the SthK tetramer pore near the CNBD. In the C-linker domain, the C'-helix makes an outward motion and the A'-helix undergoes an upward (i.e. toward the membrane side) and outward bending (Fig. 1.18A).

In the CNBD of SthK C-terminal, the β-roll and C-helix form a binding cavity for cAMP and cGMP. The cAMP molecule is bound in an anti-conformation, whereas the phosphoribose group from cAMP is buried into this binding cavity, and the adenosine ring is pointing towards the opening of the binding cavity. The phosphoribose from cAMP interacts with residues Gly-367, Glu-368, Met-369, Ala-370 Arg-377and Thr-378. The purine ring from cAMP also interacted with residues in binding cavity: Arg-418 and Glu-421 form hydrogen bounds with N6. cGMP is also bound with SthK in its anti-conformation, while the phosphoribose group from cGMP establishesthe same interactions with residues in the binding cavity as cAMP (Fig.

1.18A&B). However, previously published agonist cGMP-bound CNBD structures showed the cGMP molecule bound in its syn conformation. Replacement of a conserved residue Asp with Leu-422 may prevent cGMP to bind in an anti-conformation.

The structure information of SthK provides theoretical basis for further modification and engineering.

1.5 Phosphodiesterase

The cyclic nucleotide cyclases and phosphodiesterases underline the tight regulation of the spatial and temporal residence of cyclic nucleotides concentrations, which enable the ubiquitous intracellular signalling messengers, cyclic nucleotides cAMP and cGMP, to mediate various responses in diverse organisms, including apoptosis, smooth muscle relaxation, and vision(34, 108-110). There are11PDE gene families, and they have diverse specificity and affinity for cAMP and cGMP. The PDEs encompasses a relatively conserved C-terminal catalytic domain and a more variable N-terminal domain, through which their activity is regulated by parallel or feedback signalling pathways, such as calcium/calmodulin, protein kinase A (PKA) or cGMP(111, 112). In PDE2, PDE5, PDE6, PDE10, andPDE11, the PDE activity is mediated by binding cGMP to N-terminal cGMP PDE/adenylyl cyclase/FhlA (GAF) domains (113).

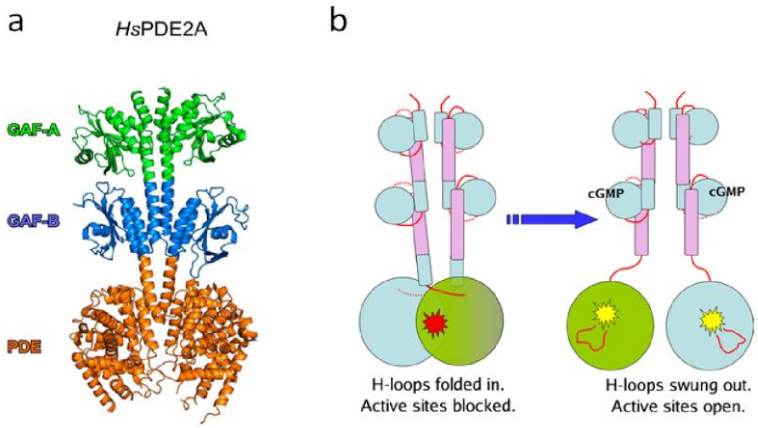

Figure 1.19 (a) Structure of hPDE2A (215–900 aa)**. (b) mechanism of activation.** Taken from (113).

The Homo sapiens PDE2A (*Hs*PDE2A) hydrolyses both cAMP and cGMP. It forms a parallel homodimer and each subunit consists of a N-terminal regulatory GAF-A and GAF-B and a C-terminal catalytic domain connected by long α -helices (Fig. 1.19)(114). Upon cGMP

binding to GAF-B, the structure changes propagate to the catalytic domains through the GAF-B/catalytic domain linker, and such that the H-loops swing out to allow substrate access (113). The catalytic domain of *Hs*PDE is used to engineer a red-light-activated PDE with a trio of Per-ARNT-Sim (PAS), GAF, and phytochrome (PHY)-specific domains from bacterial phytochrome Pseudomonas aeruginosa (PaBPhy) (115-117).

To eliminate potential cAMP accumulation caused by long term SthK-bPAC channel activating, we wonder if we can take advantage of PDE to mimic the subcellular cyclic nucleotide-PDE system. In this thesis, I try to fuse PDE2A to the C-terminal of SthK-bPAC to more precisely control cAMP level and thus channel closing.

1.6 Motivation of the study

Optogenetic silencing tools permit the functional removal of selected neurons on a trial-by-trial basis, and benefit exploring signal processing in neural circuits. The existing rhodopsin-based hyperpolarization tools require either high power of light, or may lead to paradoxical effects. CsR has natural robust expression in *Xenopus* oocytes and in plant cells, and is a potentially powerful hyperpolarization tool. It is worthwhile to further improve it and explore new tools based on it. Potassium conductance is the conductance that natively terminate action potentials, and K^+ conductance underlies the resting membrane potential in excitable cells. The existing synthesized light-activated potassium channels either require additional photoswitch, are single-use or not temporally precise, which limited their wide application. A long lasting, high light sensitive, high potassium conducting silencing tool is needed. To achieve this, we designed a synthesized light-activated potassium channel by the combination of a photoactivated adenylyl cyclase (PAC) and cyclic nucleotide-gated potassium channel (CNG). Illumination activates PAC to produce cAMP, elevated cAMP level opens CNG. The slow diffusion of cAMP contributes to long lasting K^+ conductance.

Chapter 2 Method

2.1 Chemicals and reagents

All the primers were ordered from Sigma. SthK, PACs, CyclOps and HsPDE2A Genes were synthesized by GeneArt Strings DNA fragments (Life Technologies, Thermo Fisher Scientific). CsR was a gift from Peter Hegemann of Humboldt University. Phusion® High-Fidelity DNA Polymerase (New England Biolabs) was used for PCR. Restriction enzymes and Ligase enzyme for cloning were purchased from Thermo Fisher Scientific. PCR purification, Gel extraction, and plasmid extraction kits were obtained from QIAGEN. AmpliCap-MaxT7 High Yield Message Maker Kit (Epicentre Biotechnologies) is used for in vitro transcription. All the chemicals were obtained from Sigma (Deisenhofen), Fluka (Neu-Ulm), Applichem and Roth unless otherwise specified.

2.2 Molecular biology

2.2.1 DNA cloning

DNA fragments amplification was achieved by Polymerase chain reaction (Table 2.1). PCR is a method to copy a small amount of DNA in large quantities over a short period of time. Kary Mullis invented this method in 1985 and laurite Nobel prize in Chemistry in 1993. By applying heat, the two strands of DNA molecule are seperated and the DNA building blocks that have been added are bonded to each strand. With the help of the enzyme DNA polymerase, new DNA chains are formed and the process can then be repeated.

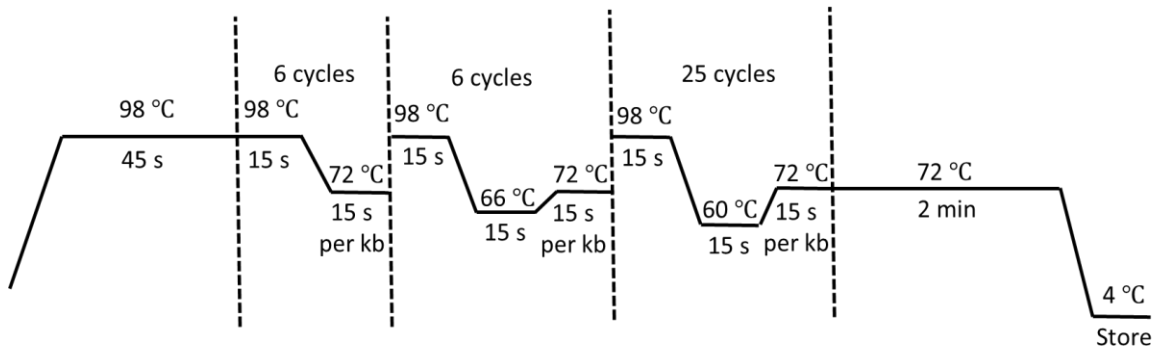

Figure 2.1 A standard touch down PCR program optimized for Phusion DNA polymerase.

A standard touch down PCR program optimized for Phusion DNA polymerase (Fig. 2.1). The PCR products were analysed by DNA electrophoresis. Afterwards, PCR products with correct size on the agarose gel were extracted using the Gel extraction kit from QIAGEN. After

restriction enzyme digestion, purified DNA fragments were inserted into pGEMHE 22 by ligation with T4 ligase.

Table 2.1 The recipe of PCR mix

PCR reaction system	**Total 20μL**
DNA template	1 μL (about 20 ng)
HGD buffer	4.6 μL
Forward primer (10μM)	0.8 μL
Reverse primer (10μM)	0.8 μL
Phusion DNA Polymerase	0.2 μL
dNTP (10mM)	0.8 μL
BSA (100 mg/ml)	0.2 μL
ddH_2O	11.6 μL

2.2.2 Site-directed mutagenesis

Together with Kary Mullis, Micheal Smith received Novel Prize in Chemistry in 1993 for his fundamental contributions to the establishment of oligonucleotide-based, site-directed mutagenesis and its development for protein studies. The QuikChange PCR is an optimized technique that uses a pair of complementary mutagenic primers to amplify the entire plasmid in a thermocycling reaction using a high-fidelity non-strand-displacing DNA polymerase. The methylated template DNA is eliminated by DpnI digestion for 3 hours at 37 ℃ (118).

2.2.3 E. coli transformation

The heat-shock transformation, which is demonstrated by Mandel and Higa in1972, has two steps: $CaCl_2$ treatment und heat shock. DNA molecules can be absorbed on the cell surface with the help of divalent cation Ca2+ and heat shock step make entering DNA into cytosol possible (119) (120). In this study, the ligation or QuikChange products were incubated 20 min with 50 µl *E. coli* MRF strain competent cell on ice. After 60 s 42 ℃ heat-shock, the transformed *E.*

coli MRFs were then plated on the LB agar plates with intended antibiotics (Ampicillin, 50 µg/mL) and incubated at 37 °C overnight.

2.2.4 Cracking of *E. coli* cells

To fast screen the right *E.coli* colonies, colony cracking was performed. This method is reported by Wayne M. Barnes in 1977: plasmid detection an sizing in single colony lysates. He picked bacteria with a toothpick, lysed them with dodecyl sulfate and heat, and placed them directly on an agarose gel for electrophoresis(121). Now, Instead of heat the *E. coli* cells are lysed in an alkaline solution containing detergent and identifying positive clones with electrophoresis based on the electrophoretic mobility difference between the super coiled DNA with and without insert. In this study, the *E. coli* colonies were pipetted into 8 µL sterile water containing tubes, an equal volume of 2x cracking buffer was added (Table 2.2) into the tubes and the mixture was incubated for 10 min at room temperature. After adding the loading buffer, centrifuging at 16,000 g for 2 min, and finally, loaded the mixture in 1% DNA agarose gel to check the size of supercoiled plasmids. 2-4 colonies with correct band size were picked for overnight culture in 5 mL LB medium with antibiotics (Ampicillin, 50 µg/mL).

Table 2.2 Cracking buffer (2x)

0.2 N NaOH
0.5% SDS
20% Sucrose

2.3.6 Plasmids extraction and verification

Qiaprep spin miniprep kit (Qiagen, Hilden, Germany) were used for plasmids extraction. The QIAprep Miniprep procedure is based on alkaline lysis of bacterial cells followed by adsorption of DNA onto silica in the presence of high salt. The procedure consists of 3 basic steps: 1) Preparation and clearing of a bacterial lysate, 2) Adsorption of DNA onto the QIAprep membrane, 3) Washing and elution of plasmid DNA (QIAprep® Miniprep Handbook 03/2020). The extracted plasmids were then verified first by restriction enzyme digestion and then sequencing (GATC Biotech, Constance, Germany). Correct constructs were stored at -20 °C for future use.

2.2.7 In vitro transcription

The cRNA is synthesised by T7 RNA Polymerase, which is an RNA polymerase from the T7 bacteriophage that catalyzes the formation of RNA from DNA in the 5'→ 3' direction, and is high specific for its promoter sequence (122).

The Linearized plasmid DNA (with final concentration above 250 ng/μL) was first prepared by NheI (Thermo fisher) digestion and purification (with PCR purification kit from QIAGEN). The cRNA was *in vitro* generated with the AmpliCap-MaxT7 High Yield Message Maker Kit (Epicentre Biotechnologies), as depicted in Table 2.3, by incubation at 37 °C for 3h. To selectively precipitate RNA, while leaving most of the protein, DNA and unincorporated NTPs in the supernatant, an equal volume 5 M Ammonium acetate (CH_3COONH_4) was added and mixed thoroughly. The mixture was incubated at -20 °C for at least 30 min, and then centrifuged at 4 °C, ~30,000 ×g for 1 h. The pellet was then washed with 50 μL 70% ethanol and dried by twice centrifugation and air dry in a fuming hood. When the white pellet became transparent, add 10-15 μL RNase-free H_2O to dissolve the pellet. The obtained cRNA were then stored at -20 °C.

Table 2.3 *In-vitro* transcription

AmpliCap-Max Cap/NTP PreMix	4 μL
100 mM Dithiothreitol (DTT)	1 μL
10×AmpliCap-Max™T7Transcription Buffer	1 μL
AmpliCap-Max™ T7 Enzyme (5 U/μL)	1 μL
RNase Inhibitor (20 U/μL)	1 μL
Add Linear DNA (~600 ng) to final 10 μL	

2.3 Oocytes preparation

In 1971 Gurdon and colleagues demonstrated that oocytes extracted from the South-African clawed frog *Xenopus laevis* were able to synthesize hemoglobin consequent to injection of the corresponding mRNA(123). Indeed, oocytes are particularly well suited for expression of proteins following mRNA injection, since they contain accumulated stores of enzymes, organelles and proteins that are normally used after fertilization that can be recruited for heterologous proteins.

2.3.1 Surgical oocytes excision

Xenopus laevis surgery for oocytes was under License #70/14 from Landratsamt Würzburg Veterinaeramt. The female Xenopus were anesthetized by immersion in water containing 1 g/L Tricain and increasing amount of ice. The oocytes were surgically removed from theca and follicle layers and were first washed twice in Ca^{2+}-free ND96 buffer (Table 2.4), and digested with 5 mg/mL collagenase for ~1.5 h. After digestion, the oocytes were washed three times by ND96 solution with 1 mM $CaCl_2$. The obtained oocytes were then transferred into a petri dish containing ND96 solution with 1 mM $CaCl_2$ and 50 µg/mL Gentamycin and incubated at 16 ℃ for future use.

Table 2.4 ND96 solution

NaCl	96 mM
KCl	2 mM
$MgCl_2$	1 mM
$CaCl_2$	1 mM
HEPES	5 mM
Adjust pH to 7.4	

2.3.2 Microinjection and maintenance of oocytes

The nano injection machine Nanoject from Drummond Scientific Company was used to inject cRNAs into the Stage V and VI oocytes. The injection capillary (3.511 Drummond #3-000-203- G/X; Drummond Scientific Company) was single pulled by a vertical Puller (PC-10; Narishige) at heat level 55.8, and then the tips were crashed under microfuge with an opening of about 15 µm. The injected oocytes were cultured in ND96 buffer (with 50 µg/mL Gentamycin) at 16 ℃ with (for rhodopsin constructs) or without (for non-rhodopsin constructs) additional 10 µM ATR.

Culture solutions were changed daily to keep the oocytes in good conditions.

2.4 Electrophysiology recording

2.4.1 Two-electrode voltage-clamp

Two-electrode voltage clamp (TEVC) is a conventional electrophysiological technique which is developed by Kennenth Cole and his colleges at the early 20th century to study the

squid giant axon with platinized platinum as electrodes (124). This technique allows to artificially control the membrane potential (V_m) of cells and to study the properties of electrogenic membrane proteins, especially ion channels. It makes use of two intracellular electrodes—a voltage electrode as V_m sensor and a current electrode for current injection to adjust the V_m, thus setting the membrane potential at desired values and recording the membrane current to analyse ion channel activities.

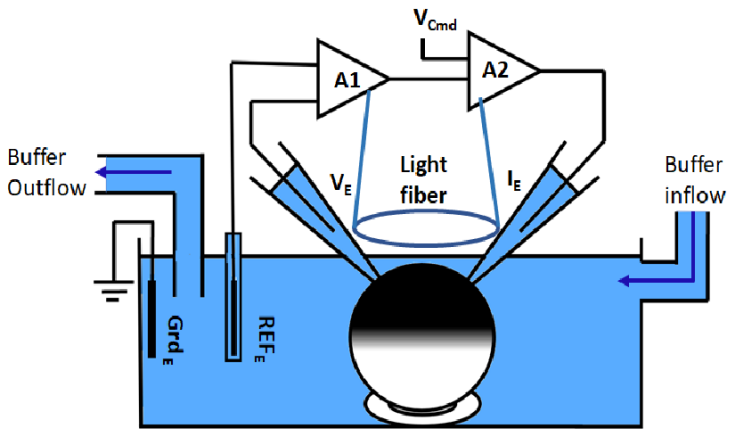

Figure 2.2 Two-electrode voltage clamp (TEVC) on an oocyte. Vm (membrane potential) is monitored by connecting the voltage electrode (V_E) to the input of a voltage follower (A1) with high input impedance. The output potential of A1 is therefore approximately equal to Vm. The clamping amplifier (A2) ensures Vm to approach the voltage command signal (Vcmd) very closely. The current injected by I_E is measured as the membrane current.

As shown in Fig. 2.2, the oocyte is put in a small chamber with constantly flowing buffer in the bath. The voltage electrode (V_E) and current electrode (I_E) were injected into the oocyte. The current injected to the oocyte to maintain the command potential V_c corresponds to the current across the oocyte membrane. TURBO TEC-05 system from npi (npi electronic GmbH, Tamm, Germany) is used in this study.

2.4.1.2 Solution used for oocytes TEVC

All the recordings are obtained in Ori-Standard solution, which contains 115 mM NaCl, 5 mM KCl, 1 mM MgCl2, 2 mM CaCl2, 5 mM HEPES, pH7.6 with NaOH, unless indicated.

2.4.1.3 Electrodes and capillaries for TEVC

The silver wire of the potential, current, reference and grounding electrodes are chlorinated by polishing with sandpaper and immersing in 5% sodium hypochlorite solution for 10 min, to generate the AgCl layer. The Potential and current electrodes capillaries (Φ=1.5 mm, Wall thickness 0.178 mm, Hilgenberg) were made with a two-step heat protocol by a vertical puller (PC-10, Narishige) with an opening of 0.5-1 MOhm, and filled with 3 M KCl.

2.4.2 Inside-out patch clamp

Distinct from the traditional voltage clamp technique, in which the "sharp microelectrodes" are used to puncture cells, the patch clamp electrode is sealed onto the surface of the cell membrane, rather than inserted through it. It allows the recording of macroscopic whole-cell currents or potentials, or microscopic single-channel currents flowing across biological membranes through ion channels or active transporters.

In 1976, Erwin Neher and Bert Sakmann published the single-channel current recordings from a small electrically isolated patch by applying closely the tip of a glass electrode on to the muscle surface and developed the cell-attached patch-clamp technique. In the end of 70s and beginning of 1980s, the seal between glass and membrane was improved by always using fresh glass pipette, fire-polishing the tip of the pipette, filtering the solutions, and applying pressure before seal, and the “Gigaseal” was developed. Electronic amplifiers was also improved by Frederick J. Sigworth and Erwin Neher to match the advances in recording conditions.

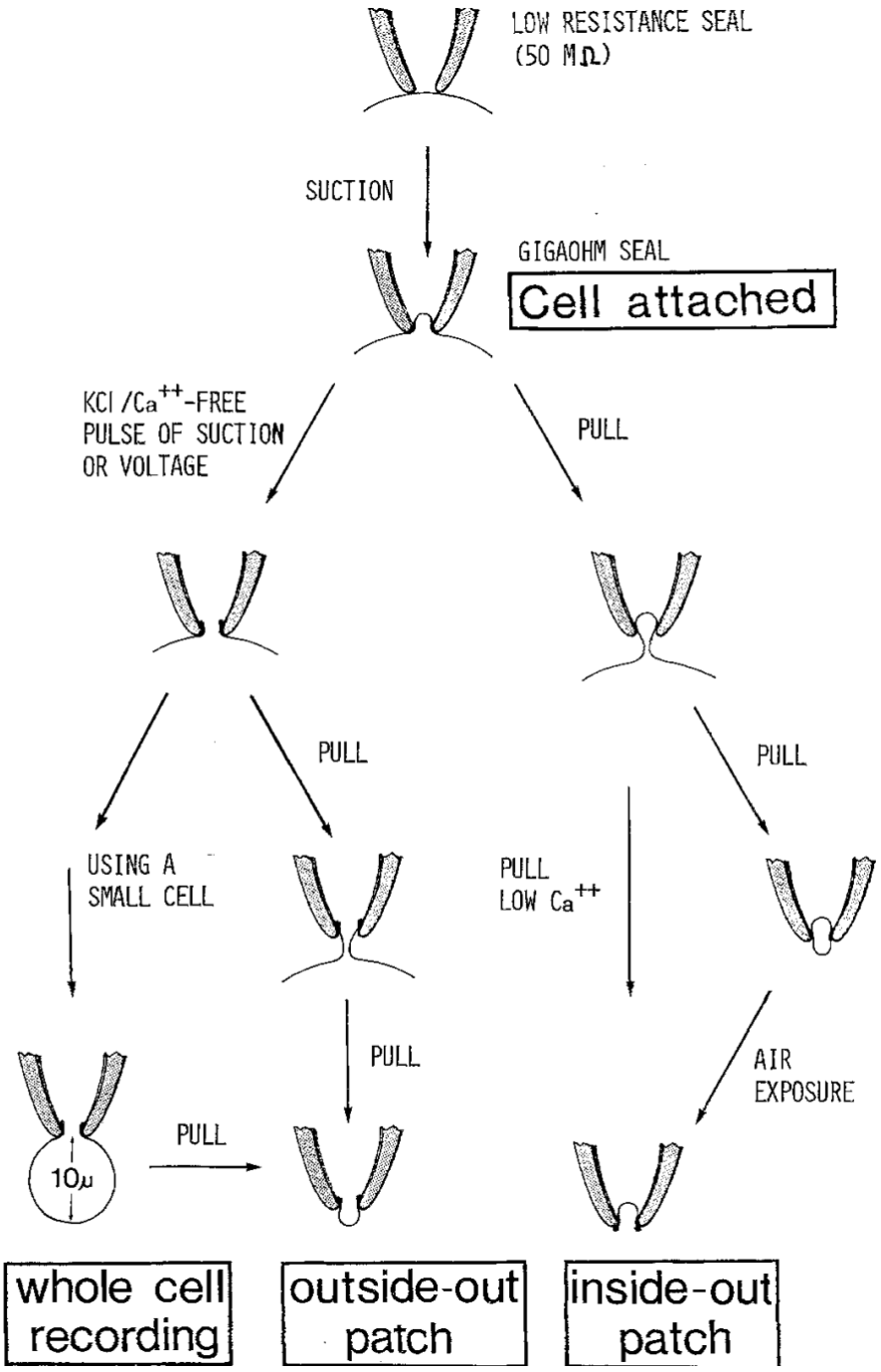

Figure 2.3 Schematic representation of the procedures which lead to recording configurations. The four recording configurations, described in this paper are: "cell-attached", "whole-cell recording", "outside-out patch", and "inside-out patch". Taken from (125).

In 1980 and 1981, Owen Hamill and Bert Sakmann, simultaneously with Horn & Patlak, found that patches could be removed from cells, by simply withdrawing the pipette, and developed the "inside-out patch clamp" configuration. In this configuration, the cytoplasmic membrane face is exposed to the bath solution. Alternatively, after giga-seal formation, the membrane patch can be disrupted keeping the pipette cell-attached. This provides a direct low

resistance access to the cell interior which allows potential recording and voltage clamping of small cells, which is termed “Whole-cell patch clamp”. After whole cell configuration, it can form “outside-out patch clamp” configuration by withdrawing the pipette slowly. In this configuration, the extracellular membrane face exposed to the bath solution. The excised patch configurations enable the recording of currents with superfusion on both sides of the membrane (Fig. 2.3) (125).

The patch-clamp technique is a powerful and versatile to study electrophysiological properties of biological membranes, and revolutionized modern biology, facilitated research, and contributed to the understanding of the cellular mechanisms underlying several diseases, including diabetes and cystic fibrosi s. Neher and Sakmann received the Nobel Prize in Physiology or Medicine in 1991 for this work.

2.4.2.1 Removing the vitelline membrane

The oocytes shrink by incubating in hyperosmotic solution (50 mL ND96 + 2.7g Sorbit) for 3-5 minutes. The vitelline membrane was visible as a transparent layer over the cell, and it was manually removed with two No.5 forceps. The oocytes were washed once in ND96 solution and transfer in recording chamber.

2.4.2.2 Patch clamp electrode fabrication

0.5-2 MΩ glass capillaries (science products) were pulled by a vertical two-step heating puller (Narishgy P-10) and fire-polished under a microfuge (narishgy). Before filling the pipette with an appropriate volume of intracellular solution (135 NaCl, 15 KCl, 5 HEPES, 5 $CaCl_2$, pH7.6 with NaOH) (more volume has lager gravity force and less the capillary effect), dip the pipette into Vitamin E to make better seal.

2.4.2.3 “Gigaseal” formation

A gentle positive pressure (50 mBar) was applied to keep the pipette tip clean. To form a seal, first approach the pipette electrode to the oocyte, and monitor the resistance by applying

5mV squared voltage pulse. Once the resistance increases, release the pressure. In many cases, the gigaseal is already formed. If not, apply a gentle negative pressure.

2.4.2.4 Inside-out patch excision

To excise the patch from oocyte, penetrate the pipette electrode suddenly into the oocyte for several seconds and then withdraw the pipette, at the same time monitor the resistance of the electrode. Move the excised patch near in-flow entrance and start recording (Figure 2.4). Axon geneclamp 500B and USB-6221 NI (national instruments) were used for data acquisition.

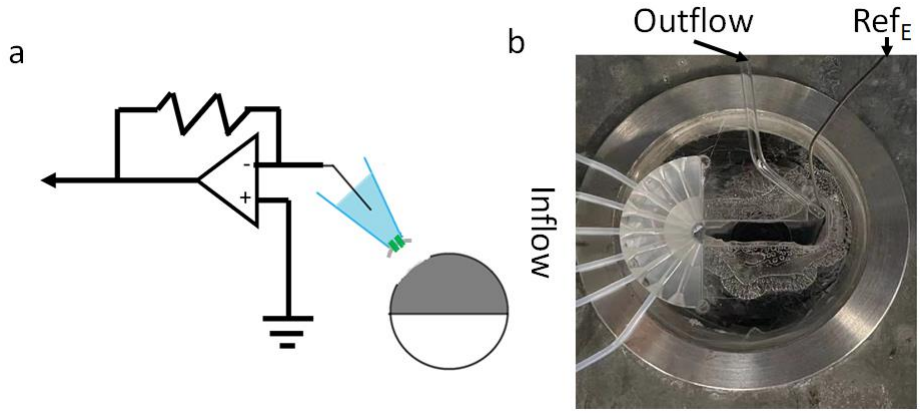

Figure 2.4 (a) Schematic representation of Inside-out patch from an oocyte. (b) Chamber used for recording with gravity perfusion and pumping outflow.

2.4.3 Impalement

2.4.3.1 Leaf discs preparation

Four to Five-week- old *N. benthamiana* were infiltrated with *Agrobacteria tumefaciens* harboring Ret::CsR(Y58AR86h)::YFP plasmid. After two days of expression, Lower epidermises of fresh leaves were peeled off and leaf discs with a diameter of ~0.5 cm were glued upside down on coverslips in chamber with Medical adhesive (ULRICH Swiss). The preparation was incubated in bath solution (0.1 mM KCl, 0.1 mM CaCl2, 1 mM 2-(4-morpholino) ethanesulfonic acid/bis-Tris propane, pH 6.0) overnight at room temperature.

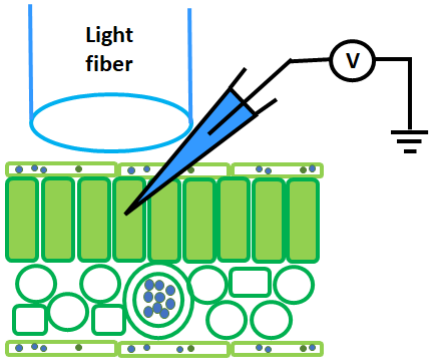

Figure 2.5 Schematic representation of mesophyll membrane potential recording.

2.4.3.2 Impalement electrode fabrication

Microelectrodes for mesophyll cell impalement were pulled by a horizontal laser puller (P2000, Sutter Instrument) from borosilicate glass capillaries (inner diameter 0.58 mm, outer diameter 1.0 mm; Hilgenberg). Single microelectrodes were filled with 300 mM KCl and connected by Ag/AgCl wires to the microelectrode amplifier (Axon geneclamp 500B). Reference electrodes were filled with 300 mM KCl, and plugged with 2% agar in 300 mM KCl. Microelectrodes with resistance of 60–110 MΩ were used for impalement (126).

2.4.3.3 Membrane potential recording

The tip of the light fiber immersed in bath solution and was fixed 1mm above the leaf discs with 45 °. The leaf discs with inhitial membrane potential between -100 to -200 mV were used for membrane potential recording (Fig. 2.5). 10 minutes resting time were give between each recording.

2.4.4 Data analysis

2.4.4.1Software for electrophysiology recordings

WinWCP 5.3.5 (University of Strathclyde) were used for data acquisitions.

2.4.4.2Mathematical fitting of the electrophysiology data

The current decay kinetics of SthK-bPAC were fitted by mono-exponential function to obtain the τ_{off} values.

The photocurrent-light intensity relationship curve of SthK-bPAC and the concentration-activation relationship of SthK-bPAC mutants to cAMP were fitted with Hill equation. K is the concentration of half-maximum activation, n is hill coefficient.

$$y = V_{\max} \frac{x^n}{k^n + x^n}$$

2.5 cAMP/cGMP ELISA assay from whole oocyte lysates

Xenopus oocytes injected with different constructs were incubated at 16◦C for 3 days in ND96. Oocytes were either kept in the dark or illuminated for 20 s with blue light (473 nm, 0.3 mW/mm2). 4–6 oocytes injected with the same construct were homogenized by simply pipetting with a 20–200 µl pipette in Sample Diluent (containing 0.1 N HCl and pH indicator, Arbor Assays). Samples were then centrifuged at 10,000 rpm for 10 min at room temperature. The supernatant was collected for cAMP assays. cAMP concentrations in the prepared samples were determined using DetectX High Sensitivity Direct Cyclic AMP Chemiluminescent Immunoassay Kit (Arbor assays).

2.6 Light source

For oocyte electrophysiology recording, a 635 nm, a 532 nm laser, a 473 nm laser, a 450 nm laser (Changchun New Industries Optoelectronics Tech), a 400 nm LED (ProLight Opto Technology) and a 590 nm LED (WINGER) were used as light sources. The light intensities at different wavelengths were measured with a Laser Check optical power meter (Coherent Inc.).

2.7 Fluorescence imaging

After two to three days expression, fluorescence pictures of *Xenopus* oocytes were obtained either by a Leica DMi8 fluorescence microscope. A confocal laser scanning microscope (LSM

5 Pascal, Carl Zeiss) equipped with a Zeiss Plan-Neofluar 10×/0.5 objective were used for transgenic plant imaging.

2.8 Experimental design and statistical analysis

Data were analyzed using pClamp 10, WinWCP, Microsoft Excel. Statistical analyses were performed using OriginPro 2020. Data were reported as mean ± standard deviation (SD) or mean ± standard error of the mean (SEM). In case of two-sample *t*-tests and unequal group variances, Welch's correction was applied. In case of multiple comparisons, analysis of variance (ANOVA) was used (*post hoc* tests indicated in Results). P values (two-tailed tests) < 0.05 were considered statistically significant.

2.9 Bioinformatics

The Benchling Life Sciences R&D Cloud is used for DNA and Protein sequences editing and normal alignments. Multiple sequence alignments were done by the online portal of Clustal Omega. Protein structure analysis was conducted by using PyMOL Or UCSF Chimera.

3.1 Improving CsR membrane targeting and converting it into a proton channel

3.1.1 Improving the membrane targeting of CsR with LR sequence

The first 20 amino acids of rhodopsin (Rho tag) onto the N-terminus of ORs (Olfactory receptors) enhance OR surface expression for a number of ORs (127). The leucine-rich 17-amino acid cleavable signal peptide (MRPQILLLLALLTLGLA, termed Lucy) is a single-spanning membrane protein in T regulatory cells, where it is essential for proper ER translocation and surface expression. As the signal peptide is cleaved off in the ER, the addition of such a tag would not affect the mature protein function. It is also reported to promote GPCR surface expression in HEK293 cells (128). And when ORs tagged with both Lucy and Rho, the surface expression for all examined ORs were observed. The Lucy-Rho tag is abbreviated as LR (129).

A transmembrane helix (1-105 aa) from the β subunit of the rat gastric H^+, K^+-ATPase is also reported to improve the expression of BR about tenfold (130). Here we abbreviate it as β–linker.

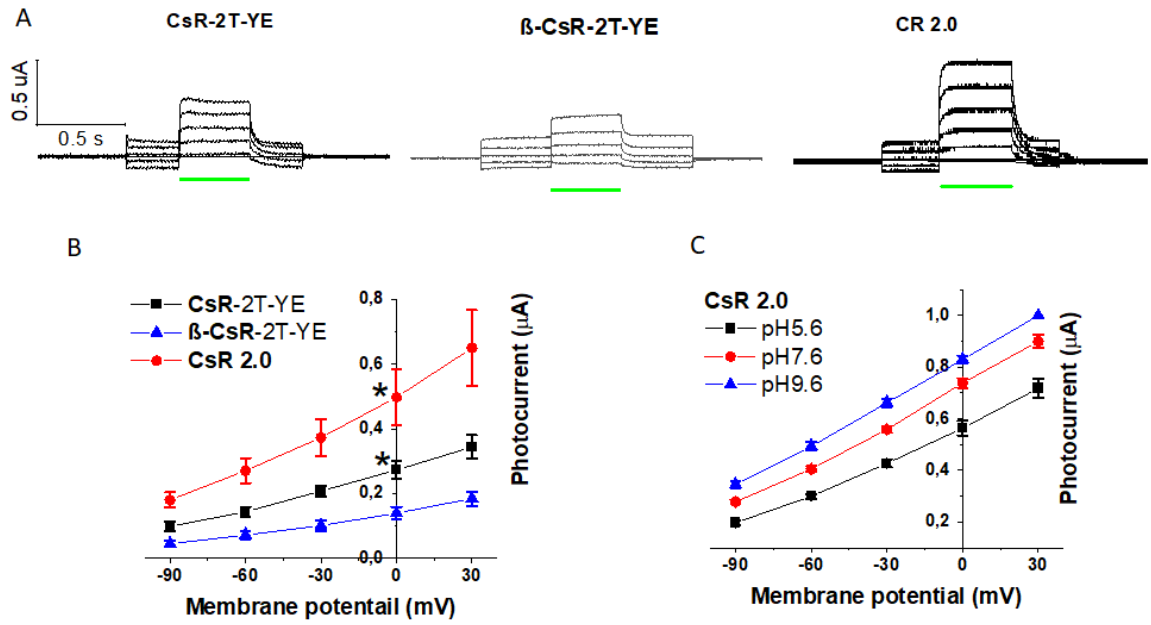

Figure 3.1.1 Enhancing the photocurrent of CsR in Xenopus oocytes. A, Superimposed photocurrent traces of CsR-2T-YE, ß-CsR-2T-YE and CsR2.0 (equal to LR-CsR-2T-YE) expressing oocytes elicited by 0.5 s green light (532nm, LED,10 µW/mm^2) illumination, the membrane potential was clamped from

-90 to +30 mV in 30 mV-steps. B, IV-curve from A. (n = 6-8). C, IV-Curve of CsR2.0 in bath solution with pH5.6, pH7.6 or pH9.6.

In our lab, N-terminal modification with LR or β–linker improved the plasma membrane expression of GtACR1(126) and proton pump rhodopsin *Fragilariopsis cylindru*, respectively (not published data from Shiqiang Gao). To further improve the targeting of CsR, I fused LR or β–linker at the N-terminal of CsR and compare the photocurrent. All three constructs generated outward current during green light illumination within membrane potential from -90 mV to 30 mV and extracellular pH7.6 (Fig. 3.1.1A). While β–linker made smaller photocurrent of CsR, an additional LR sequence enhanced the photocurrent to 1.9 times (at + 30 mV) (Fig. 3.1.1B). Later experiments, I always used LR-CsR-2TYE as a template, and it is termed as CsR2.0 for short.

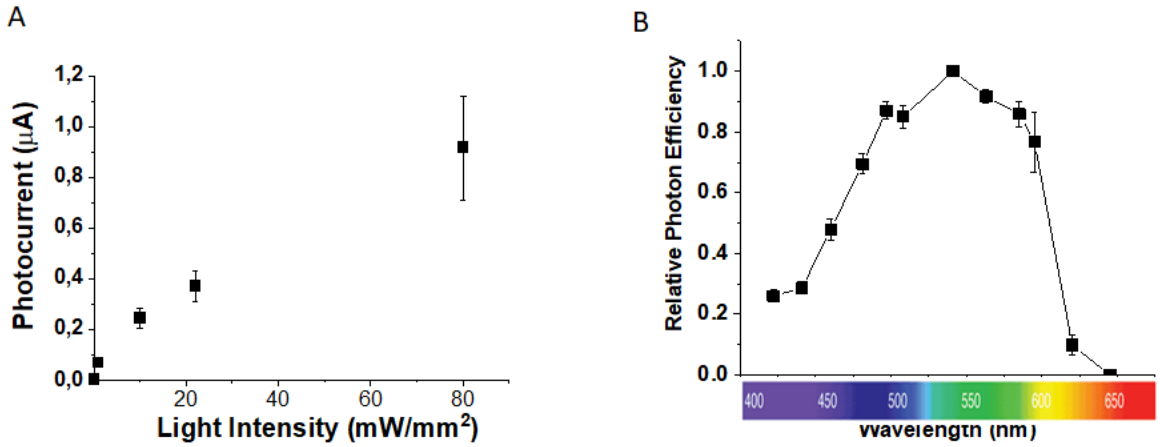

Figure 3.1.2 light sensitivity and action spectrum of CsR2.0. A, Photocurrents-light intensity relationship curve. Photocurrents of series light intensities 0.1, 1, 10, 22, 80 μW/mm^2 green light (532nm, LED,10 μW/mm^2) were recorded from one single oocyte. This was repeated in 6 oocytes. B, Action spectrum of CsR2.0. Relative photon efficiency is the normalization of the quotient of Photocurrent divided by the product of light intensity multiplied by wavelength.

Then I confirmed the proton pump function of CsR2.0 by changing the bath solution pH value. An acidic bath solution led to a smaller photocurrent, and vice versa (Fig. 3.1.1C). The action spectrum of CsR is also not affected by LR with maximum at 540 nm (Fig. 3.2B). Like other pump rhodopsin, the photocurrent is not saturated with increasing light intensity up to 80 μW/mm^2 (Fig. 3.1.2A).

3.1.2 one-point mutation converts CsR2.0 from a proton pump to a proton channel

Previously, our group had identified a light-activated proton pump rhodopsin from *Fragilariopsis cylindru*, which is abbreviated as FR. A point mutation of FR altered the proton

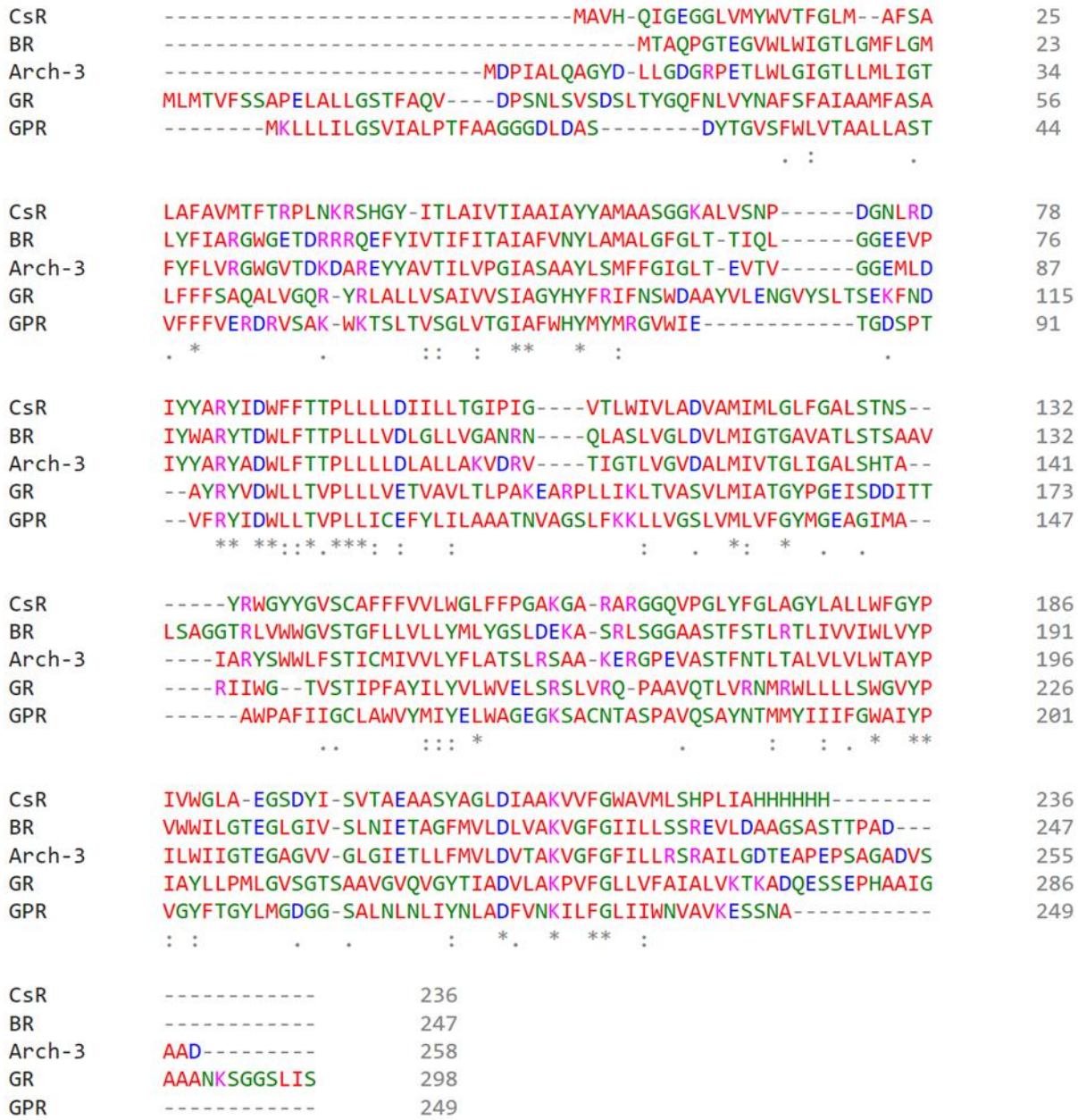

Figure 3.1.3 Amino aicds sequence alignment of CsR, BR, Arch-3, GR, GPR.

pump activity and make it behave like a proton channel (unpublished data from Shiqiang Gao). According to the DNA alignment data, we find the homologous residue Arg 83 and did the same site mutation to His (Fig. 3.1.3). In pH7.6 buffer, this R83H mutant of CsR2.0 evokes an inward current upon illumination at negative membrane potential, while wild type has only

outward current (Fig. 3.1.4A and B). Changing the bath solution from mostly sodium chloride (Ori buffer, pH7.6) to big charged molecular solution (NMG-Asp pH7.6) altered neither the direction nor the amplitude of the photocurrent, indicating the permeability to proton rather than Na^+ or Cl^- (Fig. 3.1.4C). The reversal potential (-14 m V) in Ori pH7.6 buffer is close to proton equilibrium potential -12mV (Fig. 3.4B), when we assume the value of internal oocytes pH is 7.4 (131). As expected, the reverse potential is more negative in alkaline solution (Ori pH9.6) (Fig. 3.1.4C). Taking together, we conclude that CsR (R83H) can bi-directionally transport proton.

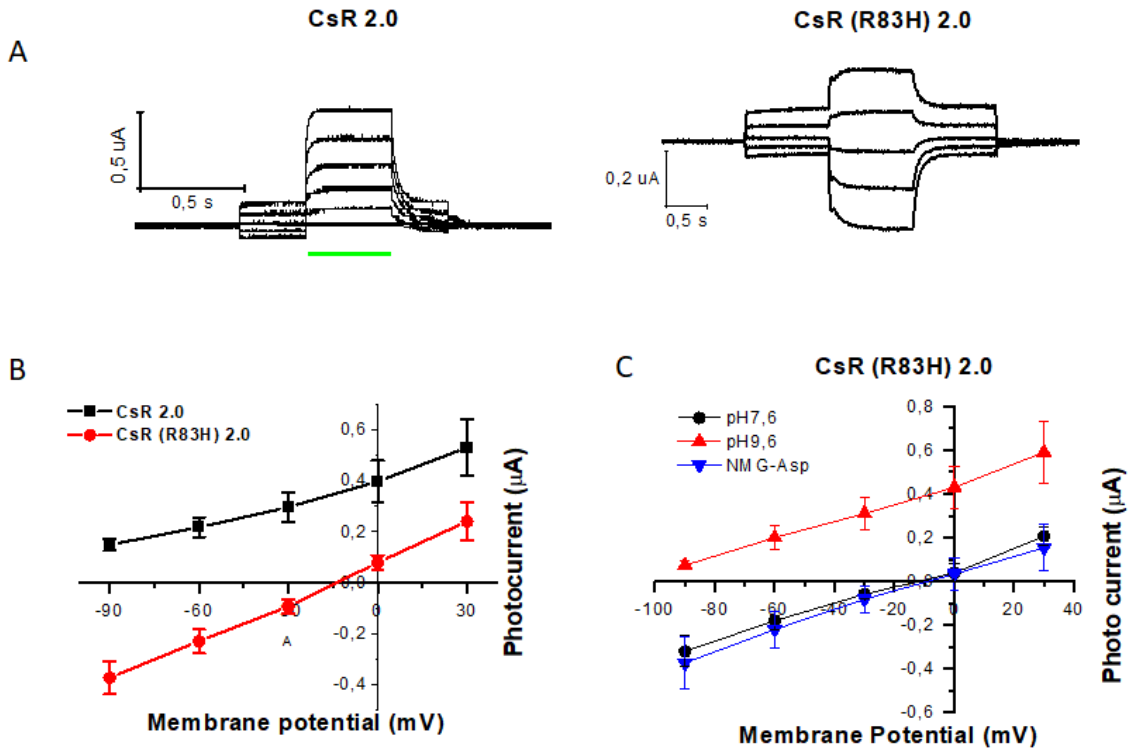

Figure 3.1.4 R83H converts CsR 2.0 from a proton pump to a bi-directional proton channel. A, Representative photocurrent traces of CsR2.0 (left) and CsR (R83H) 2.0 (right). B, IV curves of CsR 2.0 and CsR (R83H) 2.0. C, IV Curve of CsR (R83H) 2.0 in Ori pH7.6, Ori pH9.6 and NMG-Asp Solution (115 mM N-Methyl-D-glucamin, 5 mM KCl, 1 mM MgCl2, 2 mM CaCl2, 5 mM HEPES, pH7.6 with Aspartic acid).

3.1.3 An additional Y58A mutation enhanced the proton channel photocurrent

An additional mutation that mutated Tyr to Ala in FR had enhanced the proton channel photocurrent (unpublished data from Shiqiang Gao). To find the possible homologous residue

Tyr, I used R83H as a template and additionally mutated Tyr57, Tyr 58, or Tyr 207 to Ala. compare the channel photocurrent of 3 double-mutation mutants with R83H, only Y58A had bigger photocurrent, while Y57A, Y207A only had tiny photocurrents (Fig. 3.1.5A).

Even without additional retinal supplement, CsR2.0 can generate nonnegligible photocurrent in *Xenopus* oocyte (Fig. 3.1.5B and C). We assumed that one possible reason why an additional Y58A can enhance the photocurrent would be that Y58A improves the retinal binding efficiency. But it is not the case, since without retinal supply Y58A R83H double mutant generate only tiny photocurrent (Fig. 3.1.5D).

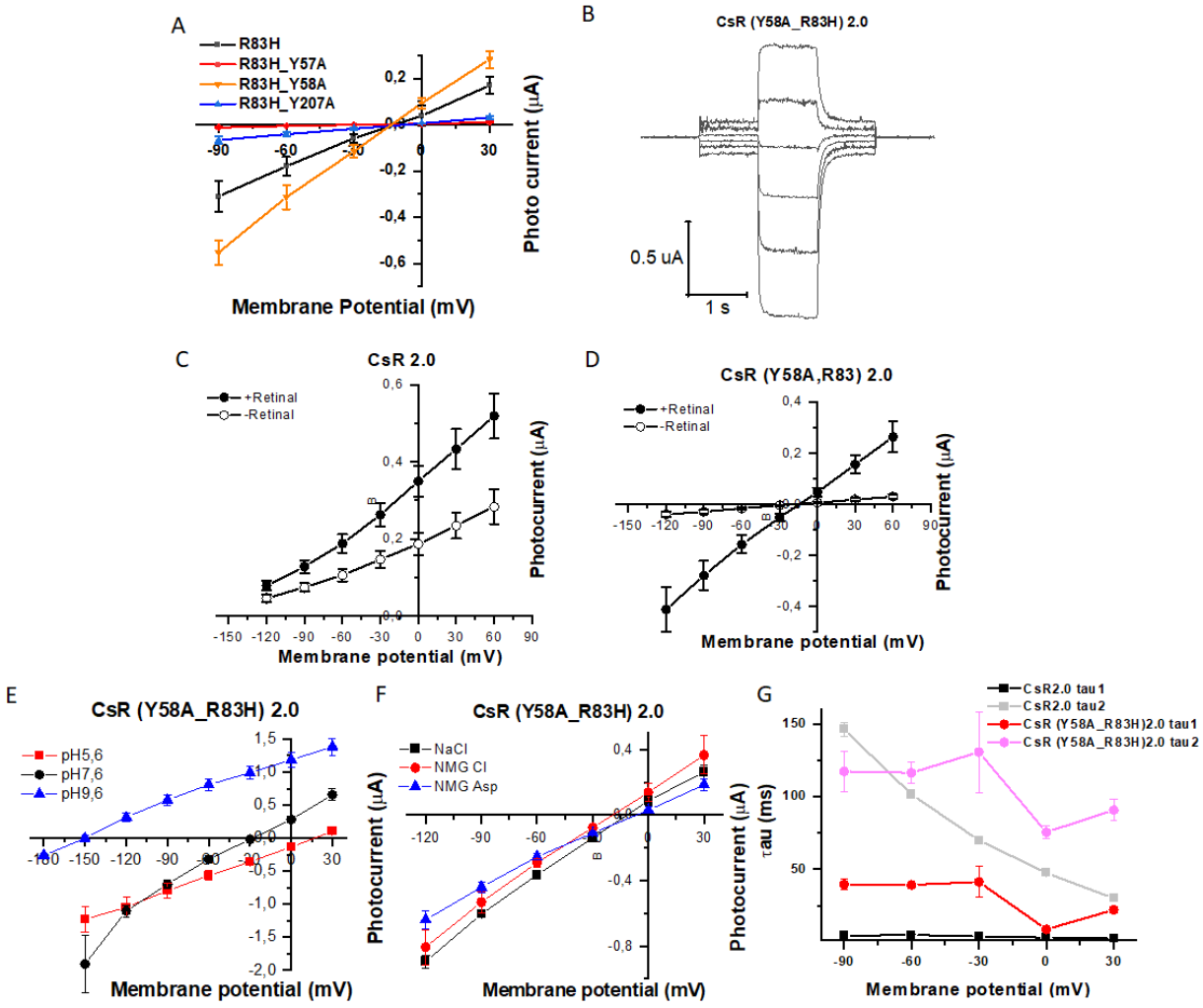

Figure 3.1.5 T58A mutation enhanced the proton channel photocurrent. A, IV-curves of CsR (R83H) 2.0, CsR (Y57A_R83H) 2.0, CsR (Y58A_R83H) 2.0, CsR (Y207A_R83H) 2.0. B, representative trace of CsR (Y58A_R83H) 2.0. C, IV-curves of CsR 2.0 with and without 10 μM retinal supplement. D, IV-curves of CsR (Y58A_R83H) 2.0 with and without 10 μM retinal supplement. E, IV-curves of CsR (Y58A_R83H) 2.0 recorded in Ori pH5.6, Ori pH7.6, Ori pH9.6 solution. F, IV-curves of CsR (Y58A_R83H) 2.0 recorded in Ori pH7.6, NMG-Cl (115 mM N-Methyl-D-glucamin, 5 mM KCl, 1 mM $MgCl_2$, 2 mM $CaCl_2$, 5 mM HEPES, pH7.6 with HCl), NMG-Asp (115 mM N-Methyl-D-

glucamin, 5 mM KCl, 1 mM $MgCl_2$, 2 mM $CaCl_2$, 5 mM HEPES, pH7.6 with Aspartic acid)) solution. G, decay time against membrane potential of CsR 2.0 and CsR (Y58A_R83H) 2.0.

The additional Y58A mutant did not change the proton channel behaver, since replacement of Na^+ with NMG^+ or Cl^- with Aspartic acid in bath solution did not affect the photocurrent (Fig. 3.1.5F). Switching the bath solution pH from 7.6 to 9.6 shifted the reverse potential by -120 mV, indicating almost pure proton-conducting channel within from neutral to alkaline extracellular environment (Fig. 3.1.5E). On the other hand, the reversal potential is not as theoretically expected in lower pH solution (Fig. 3.1.5E).

Besides, the closing dynamic is affected. Unlike the wild type CsR closes faster upon depolarization, the closing of YARH mutant speed up solely at 0 membrane potential (protonation) (Fig. 3.1.5G).

3.1.4 A slow triple mutation mutant

To further enhance the channel photocurrent, I did site-directed mutagenesis to three residues that face to benzene ring of retinal in TM4 and TM5. Side chains of these residues are shortened by mutating Asp116 to Cys, Met 119 to Ala or Cys, Cys 142 to Gly or Leu. Although none of them has a better expression or bigger photocurrent compare to YARH double-mutant (Fig. 3.1.6A and B), surprisingly C142L shows obvious slower kinetics (Fig. 3.1.6 C). At 0 mV membrane potential, the traces are fitting with double-exponential equation and yield a tau value of 280 ms for YARHCL mutant and 70 ms for YARH mutant (Fig. 3.1.6 C).

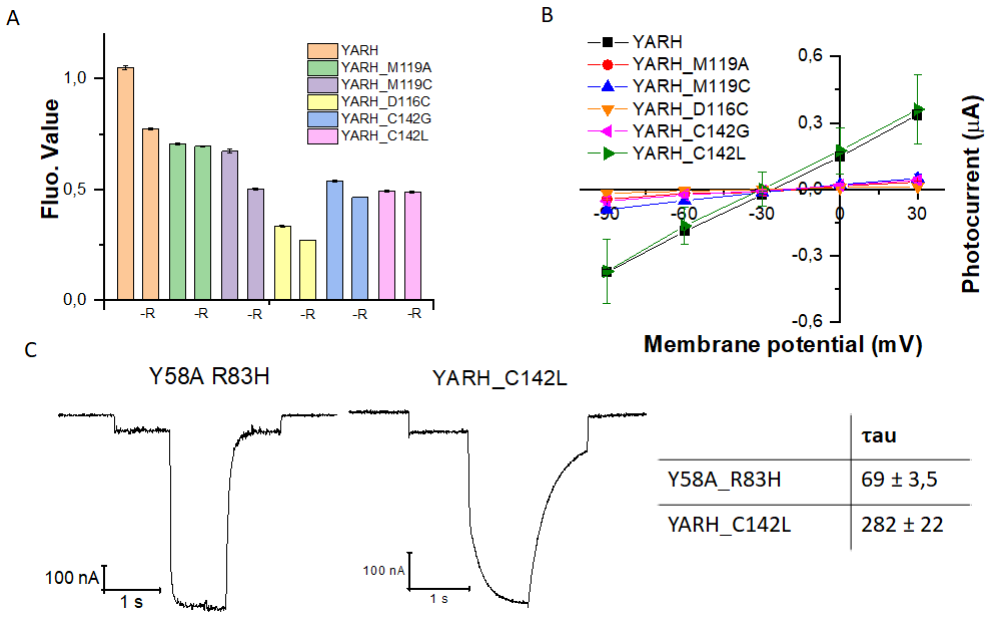

	τau
Y58A_R83H	69 ± 3,5
YARH_C142L	282 ± 22

Figure 3.1.6 A slow triple-mutation mutant. A, expression level comparison of CsR (Y57A_R83H) 2.0 (YARH in short) and 5 triple-mutation mutants. OD values of one oocyte, which is expressing with or without additional 10 µM retinal. B, IV-curves of of CsR 2.0 triple-mutation mutants. C, Representative traces of of CsR (Y57A_R83H) 2.0 and a triple-mutation mutant of CsR (Y57A_R83H_C142L) 2.0. The closing tau values of CsR (Y57A_R83H) 2.0 and CsR (Y57A_R83H_C142L) 2.0 are shown in right.

3.1.5 Comparison of two channel mutants

Hegemann. P group has published several CsR channel mutants, among them Y14E performance the best, in accounting of its big and stable photocurrent (44). Nevertheless, R83H has reverse potential closer to a pure proton channel in a neutral bath solution (Fig. 3.1.7 A and B). A Y14E R83H mutant behavers similarly to R83H single mutant (Fig. 3.1.7 A and B).

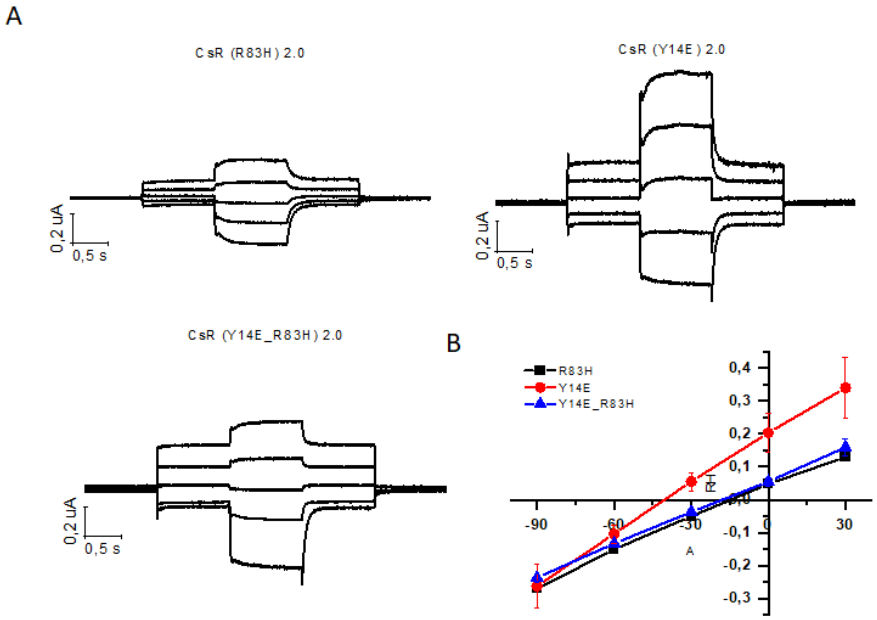

Figure 3.1.7 Comparison of two channel mutants. A representative photocurrent traces of CsR (R83H) 2.0, CsR (Y14E) 2.0 and double mutation mutant CsR (Y14E_R83H) 2.0. B, IV curves of CsR (R83H) 2.0, CsR (Y14E) 2.0 and CsR (Y14E_R83H) 2.0.

3.1.6 CsR2.0 hyperpolarizes mesophyll cells

Due to the poor expression of microbial rhodopsins in plants, the application of optogenetics in plant was complicated. The low concentration of coffector *all-trans* retinal in plant tissues

prevents microbial rhodopsin from expressing. M. Papanatsiou et al reported a non-rhodopsin-based tool, synthesized BLINK 1 that increased the rate of stomata opening and closing in response to light, but without precise temporal control (132). The versatility of microbial rhodopsins, including diverse pumps, ion channels, enzymes with all colour action spectrums make them the favourable optogenetics tools. Our lab successfully introduced retinal producing gene into plants and allow many microbial rhodopsins to be applied (126), including CsR.

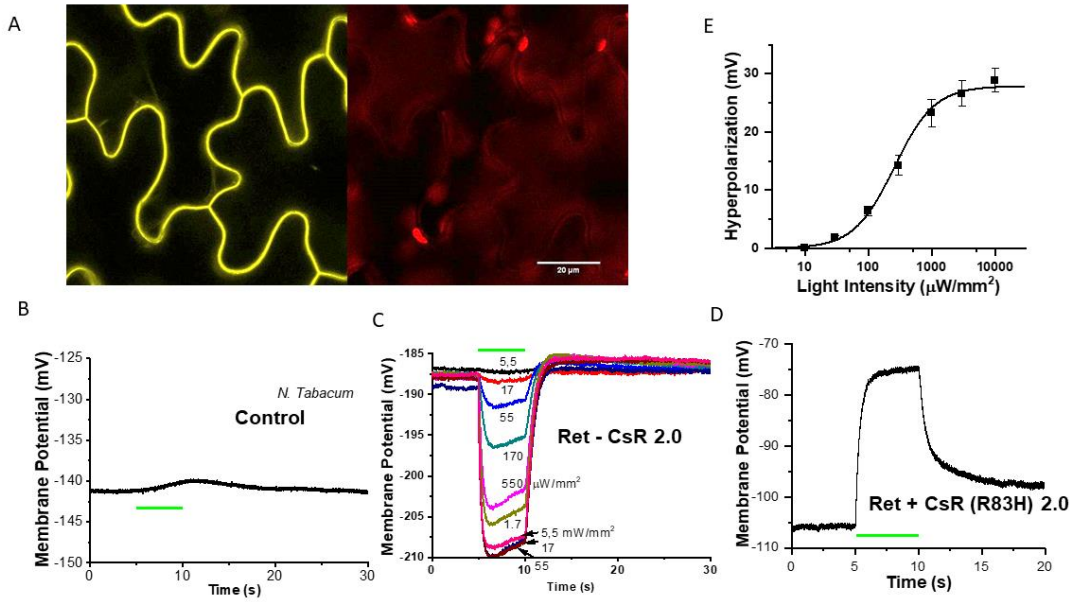

Figure 3.1.8 A, Fluorescent image of Ret-CsR2.0 transgenic N. Tabadum. B, C and D, Representative mesophylls membrane potential recordings of control N.Tabacum plant, Ret-CsR 2.0 transgenic plant and Ret + CsR (R83H) 2.0 transient co-expressing plant. E, Hyperpolarization amplitude against light intensity curve of Ret-CsR2.0 transgenic N. Tabacum.

CsR2.0 has strong expression and clear plasma membrane targeting in epidermis of transgenic *N. tabacum*, when we co-expressed CsR2.0 with retinal producing gene (Ret) (Fig. 3.1.8 A). To exam the function of CsR2.0, I impaled the mesophyll cells of control and transgenic leaves with sharp electrodes (60 to 100 Mohm) and recorded the membrane potential. The resting membrane potential of control tabacum mesophylls is between -150 to -200 mV, a 5s green 500 μW/mm^2 laser flashlight cause a slow 2 mV depolarization of control plant (Fig. 3.1.8 B). The resting membrane potential of CsR2.0 transgenic plants mesophylls is not altered, with between -150 to -200 mV. A 5s green 500 μW/mm^2 laser light flash drives the mesophylls of Ret-CsR2.0 transgenic plants further up to 22 mV hyperpolarization, instead of depolarization (Fig. 3.1.8 C and E). A Fast depolarization is observed in retinal producing gene

(Ret) and proton channel (CsR (R83H) 2.0) transient co-expressing mesophyll upon a 5s green 500 $\mu W/mm^2$ laser illumination (Fig. 3.1.8 C).

3.2 Assemble a light activated-potassium channel

I engineered a light activated-potassium channel by combination of a cyclic nucleotide gated potassium selective channel (CNG channel) and a photoactivated adenylyl cyclase (PAC) or photoactivated guanylyl cyclase. For CNG potassium channel, I have 3 reasons to choose SthK, but not other CNG channels. First, a highly K^+ selective CNG channel is needed, which could already exclude all the eukaryotic CNG and HCN channels, because they are nonselective cation channels or only slightly more permeable to K^+. SthK solo permeate to K^+ with a high single channel conductance of 70 pS (53). Second, the channel should not be very sensitive to cNMP, otherwise the endogenous cNMP level or the low dark activity of PAC or guanylyl-cyclase could already active the channel, which will generate a dark conductance. My college had worked with MlotiK and suffered from dark conductance (data not shown, unpublished from Xiaodong Duan). cAMP is the agonist for SthK with a EC_{50} value of about 4μM, which is higher than oocyte intracellular cAMP concentration. while the other CNG Potassium channel Mlotik has an EC_{50} value of 150 nM (107). Third, the channel is exclusively activated by one cNMP, so that the conductance would not be affected by other factors, which makes the SthK an almost perfect candidate. For PAC, the small size and high light to dark activity ratio (about 1600) of bPAC made it a good candidate (53).

3.2.1 The potassium conductance and cAMP Cyclase function of SthK-bPAC

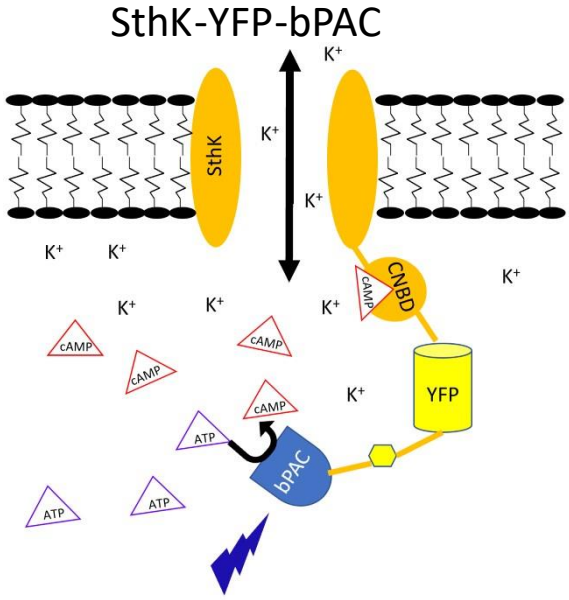

Figure 3.2.1 Cartoon presentation SthK-YFP-bPAC. bPAC is fused to the C-terminal of SthK with a YFP in between. Blue light activates the bPAC to produce cAMP from ATP, the SthK channel opens via the increased cAMP level and conducts potassium ions.

SthK has a C-linker and cyclic nucleotide binding domain at the C-terminal (104). In order not to disturb C-terminal function, we fused bPAC-YFP to the N-terminal of SthK (bPAC-YFP-SthK). Unfortunately, there was no obvious photocurrent in *Xenopus* oocyte in this case. Then I fused bPAC to the C-terminal of SthK with a YFP in between (SthK-YFP-bPAC, SthK-bPAC for short) (Fig. 3.2.1). We observed fluorescence in oocytes expressing SthK-bPAC, but not in control oocytes (Fig. 3.2.2A).

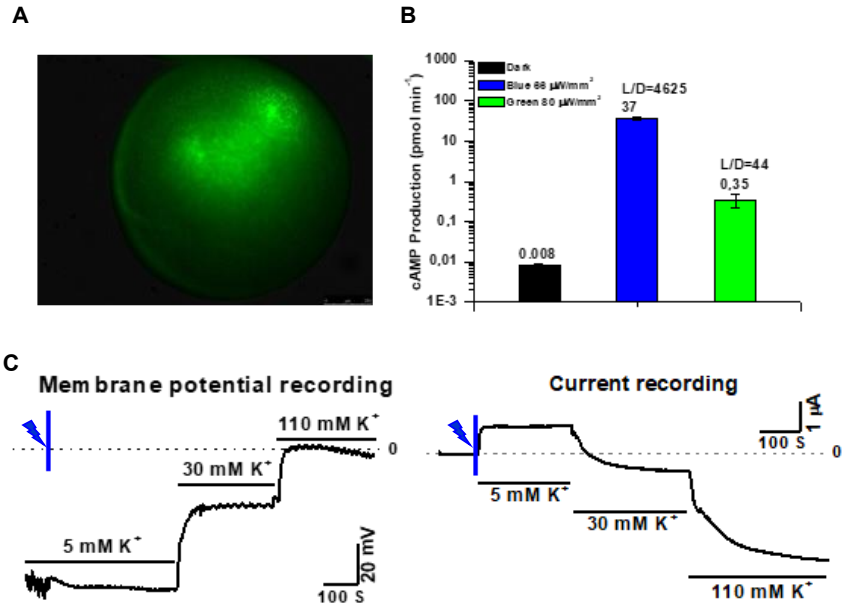

Figure 3.2.2. Validation of SthK-Y-bPAC in *Xenopus* oocytes. A, Fluorescence image of SthK-YFP-bPAC expressing oocytes, injected 2ng cRNA, 3 days after injection. B, cAMP production of SthK-Y-bPAC illumated with blue (473nm 66 µW/mm^2) or green (532nm 80 µW/mm^2) light. C, representative traces of membrane potential recording and current recording (holding at - 40 mV) while switch bath solution from 5 mM to 30 and 110 mM after 5s blue light (473nm, 55 µW/mm^2) illumination.

We hypothesize that light flash actives bPAC to cyclize ATP into cAMP, then the produced cAMP bind to CNBD of SthK, and open the channel. But the channel will keep open until the cAMP level decreases. To confirm the cyclase activity, we extracted the plasma membrane and did the cAMP assay. With 66uW/mm^2 blue light illumination a SthK-bPAC molecular produced 37 pmol cAMP every minute, the light to dark ratio is 4625; with 80 µW/mm^2 green light it produced 0.35 pmol cAMP every minute, the light to dark ratio is 44 (Fig. 3.2.2B). The dark activity of the SthK-bPAC construct is even lower than soluble bPAC (24). To determine channel function, we applied 5s blue light (473nm 550 µW/mm^2) illumination to ensure that the channel will open for a long time, and recorded membrane potential during changing the K^+ concentration of the bath solution, the membrane potential kept close to potassium equillibrium

potential. Then we recorded photocurrent, holding at - 40mV in 5 mM K^+ bath solution it was outward current, in 30 mM K^+ bath solution there was inward current and the amplitude was increased in 110 mM K^+ bath solution, which proved that SthK-bPAC is a photoactivated potassium channel (Fig. 3.2.2C).

3.2.2 SthK-bPAC is activated by cAMP and inhibited by cGMP

While cAMP is the agonist of SthK, cGMP has a higher affinity but extremely small efficiency to SthK, which makes cGMP act as a competitive antagonist to this channel(101, 105). We hypothesized that cGMP could close SthK-bPAC by competing with cAMP. Here we took advantage of another optogenetic tool: BeCyclOp, which is guanylyl cyclase that produce cGMP after green light illumination (27) (Fig. 3.2.3A). We recorded photocurrent of oocytes co-expressing SthK-bPAC and BeCyclOp. Blue light activated bPAC to produce cAMP, therefore generated an outward current, while green light activated BeCyclOP decreased this current (Fig. 3.2.3C). Under green light there are high concentration of cGMP in co-expressed oocytes (Fig. 3.2.3B). These results consist with the character of this channel that cGMP act as an antagonist, it is not able to active the channel and occupied CNBD. These data supported a concept that, optogenetic tools can be turned on and off by two distinct color light.

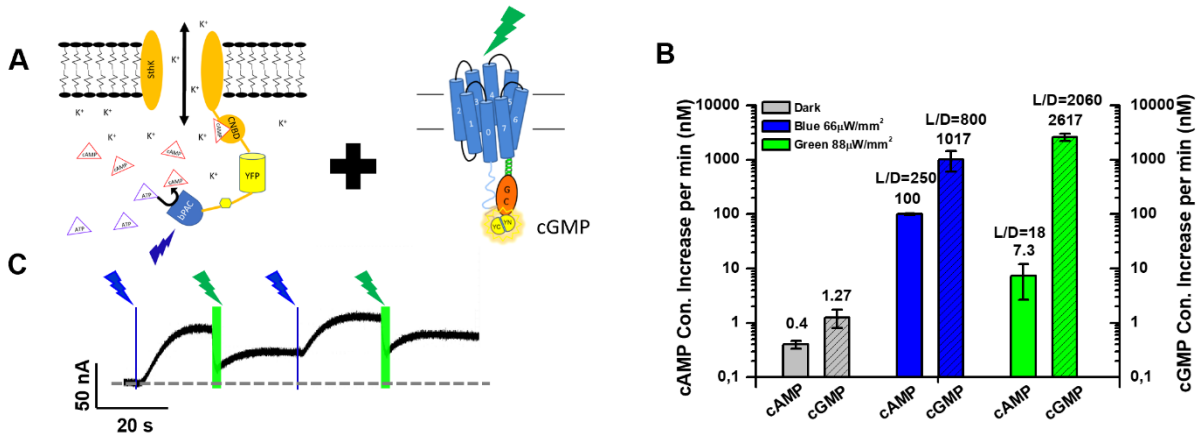

Figure 3.2.3 Co-expression of SthK-YFP-bPAC and Becyclop cRNA in Xenopus oocytes. A, scheme of SthK-bPAC and BeCyclOP. B, cAMP and cGMP production of this co-expressed oocytes by illumating with blue (473nm 66 μW/mm^2) or green (532nm 80 μW/mm^2) light. C, Representitive Photocurrent traces: Current increased by 200 ms blue light (473nm, 550 μW/mm^2) illumination and reduced by 3s green light (532nm 1 μW/mm^2) illumination.

3.2.3 Channel characterization

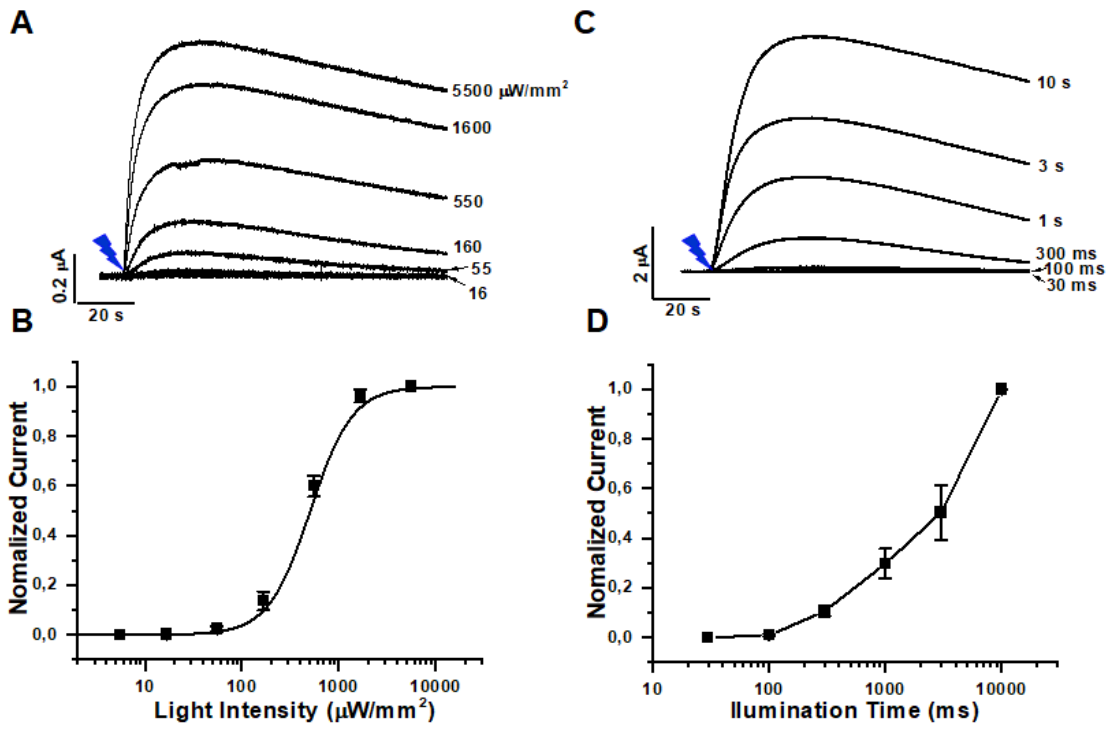

Figure 3.2.4 Light intensity- and illumination time- dependent photocurrent. A, Representitive Photocurrent traces of 2ng SthK-YFP-bPAC cRNA expressed in Xenopus oocytes induced by different intensity of 1 s blue light (473nm). B, Normalized currents against light intensity curve fitted monoexponentially. The half-maximal light intensity value was determined at 500 µW/mm^2. Representative Photocurrent traces of 2ng SthK-YFP-bPAC cRNA expressed in Xenopus oocytes induced by different illumination time of 550 µW/mm^2 blue light (473nm). D, Normalized photocurrents against illumination time.

Through a light intensity-dependent photocurrent test, I determined the half-maximal light intensity value was 500 µW/mm^2 with 1s light flash (Fig. 3.2.4 A&B). With 550 µW/mm^2 blue light, an illumination time test showed that photocurrent appears from 100 ms, and photocurrent increases within longer illumination, did not saturate until 10 s flash (Fig. 3.2.4 C&D).

3.2.4 PDE helps to reduce closing time

Under 1 s 500 µW/mm^2 light illumination, the open time constant of SthK-bPAC is 4 ± 0.6 s, close constant, as we assume should be long, is about 254 ± 50 s (Fig. 3.2.5B) (133). A way to shorten the long closing time of SthK-bPAC is to utilize a phosphodiesterase (PDE) to digest

cAMP, in this way the cAMP level decreases faster than diffusion. I fused a catalytic domain of *Hs*PDE2A to the C-terminal of SthK-bPAC, made a SthK-bPAC-PDE. To confirm the function of PDE, I expressed Cop6 K298A, which is a constant guanylyl cyclase without light regulation, either with or without SthK-YFP-bPAC-PDE in oocytes, and measure cGMP concentration after homogenization. Phosphodiesterase activity preserved in full length catalytic domain of PDE, but lost when only conserved catalytic core exists (Fig. 3.2.5A). photocurrent comparison showed that construct with PDE has fast closing dynamics (Fig. 3.2.5C).

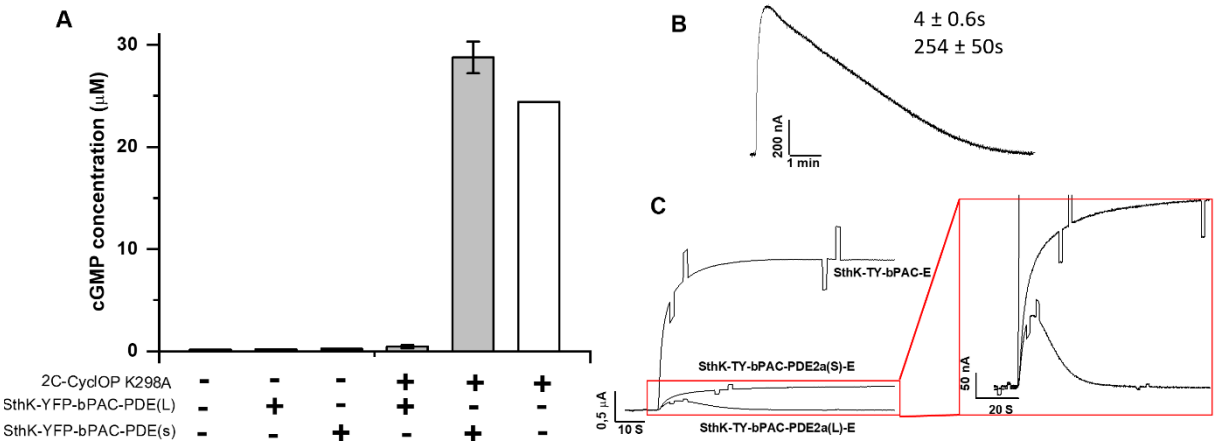

Figure 3.2.5 Validation of the phosphodiesterase function of SthK-YFP-bPAC-PDE. A, cGMP concentration of oocytes expressed of 2C-CyclOP K298A with or without SthK-YFP-bPAC-PDE , either full length catalytic domain (L) or conserved sequence (s) in Xenopus oocytes,. B, On and off kinetics of SthK-bP photocurrents in oocytes with 1s blue light (473nm, 550 µW/mm^2) illumination; n = 4, error bars = SD. C, Representative Photocurrent traces of SthK-YFP-bPAC, SthK-YFP-bPAC-PDE (either L or S), the voltage was Holding at -40 mV with 473nm 1s 550 µW/mm^2 illumination, 5 mM KCl in bath solution).

3.2.5 Screening for low light sensitivity SthK-bPAC variant

Alignment data indicates that SthK shares the common structural motif of the superfamily of voltage-gated K^+ channels. It contains a short N-terminal, 6 putative transmembrane domains, a C-linker and a CNBD (101). To board the application of SthK-bPAC, I attempt to modify the CNBD of SthK to reduce its cAMP sensitivity by mutating key amino acids and truncation. The C-terminal structure of SthK was solved, which gave me the theoretical basis to do modification. The CNBD of SthK is composed of four helices (αA, αB, αP, αC) and eight β-strands. These β-strands are arranged in a so-called β-roll, which is flanked by the A- and B-helices. The cyclic

nucleotide binding cavity is formed by β-roll and C-helix. When SthK binds with cAMP, the phosphoribose group of cAMP is buried into the cavity, and the adenosine ring points outwards (Fig. 3.2.7).

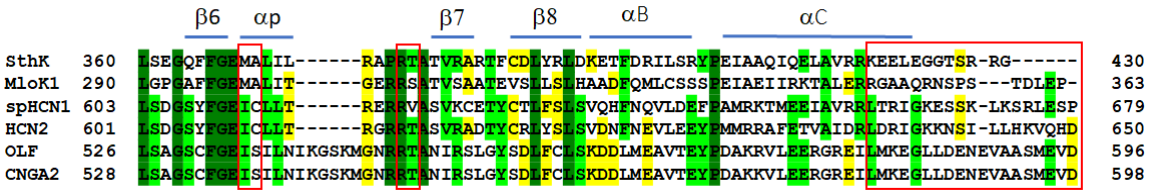

Figure 3.2.6 Amino acids sequence alignment covering the core architecture of CNBD.

I did 3 rounds of mutagenesis or truncation of CNBD in SthK-bPAC, in total 32 constructs, to select the best candidates. The productive avenue towards evaluating their cAMP sensitivity is using TEVC to compare the photocurrent of each mutant expressing oocytes. I injected same amount of RNA (5 ng) for each mutant and let them express 3 days, and I choose oocytes that have similar expression level to do TEVC, so that the molecular amount is assumed to be similar. With the same light condition, the same molecule amount of bPAC should produce the same amount of cAMP, so that the cAMP concentration is also assumed to be the same. Under same illuminate condition, a smaller photocurrent indicates a less sensitive mutant, vice versa.

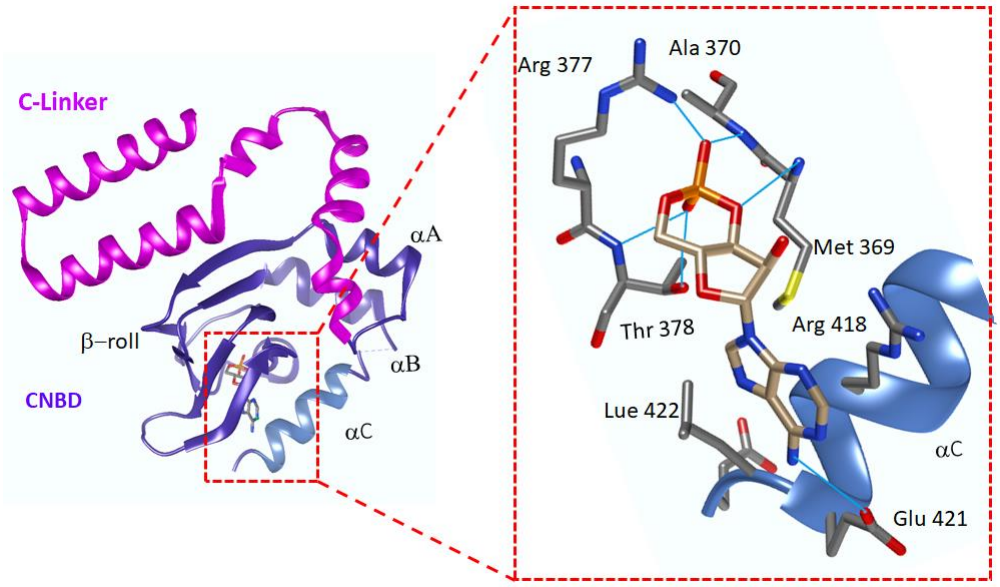

Figure 3.2.7 the structure of SthK-C term and key residues in cyclic nucleotide binding cavity. The C-linker is shown in magenta, the β-roll in purple and the C-helix in light blue. The cAMP molecule in enlarged picture is shown in brown sticks representation. Amino acids lining the binding cavity are shown in grey sticks.

First round, I did single or double mutation among the interface of binding cavity. According to alignment, Met369 and Ala370 in P-helix of SthK are Ile and Cys in spHCN1 and HCN2 channel (Fig. 3.2.6), but this double mutation made a non-light regulation channel (Table 3.1). A Met369 to Leu and Ala370 to Ser single mutation reduced light sensitivity and amplitude, while an Ala370 to Val mutant lose the function. Arg-377 is a highly conserved residue in eukaryotic and prokaryotic CNG channels as well as other cyclic nucleotide dependent proteins, regardless of ligand preference (Fig. 3.2.6). This Arginine is reported to be essential for cNMP binding, the arginine mutated to Glutamate decreased the affinity for cNMP dramatically. I mutated Arg-377 to Alanine, Glutamate, Histidine and Lysine, none of them has photocurrent. Interestingly, R377H T378C double mutant has a reduced light sensitivity. Normally, next to this arginine is a threonine or Serine to provide a hydroxyl group in other CNG channels, which is also conserved in SthK (Thr-378), but spHCN1 has a valline at this very position. When Thr-378 is mutated to alanine, cysteine, serine and tyrosine, the light sensitivity is not changed, while a T378V mutation reduces the light sensitivity and keeps the photocurrent amplitude. At the C-helix, the Arg-417, Arg-418, Lys-419, Glu-421, Leu422, Glu-423 are directly facing to purine ring of cAMP (Fig. 3.2.7). Replacing these long or positive charged R-group with a methane reduced their light sensitivity as well as their photocurrent (R417A, R418A, E421A, L422A, E423A, R428A), while replacing it with another positive residue did not influence the light sensitivity (K419R) (Table 3.1).

cGMP is a competitive antagonist to SthK, as it can bind to SthK but not activate the channel. For other CNG channels, cGMP is bound in its *syn*-conformation and able to active channel. For SthK, cGMP is bound in its *anti*-conformation. The author of SthK C_{-term} Structure suggested that Leu422 prevents cGMP from binding in the *syn*-conformation (Fig. 3.2.7)(104). It is Aspartic acid in this very position in other cGMP-activated CNG channels (Fig. 3.2.5A). L422D did not rescue cGMP from being an antagonist, reduced the light (cAMP) sensitivity and photocurrent (Table 3.1). After the first rounds selection, I chose T378V as a template for further modification.

At the second round, I did truncation at the C-helix of SthK in SthK(T378V)-bPAC. While the 12-aa-deletion reduced the light sensitivity, 9-aa-deletion maintain a big photocurrent.

In MloK1 channel M299C and M299Q mutant have a 3-times and 5-times cAMP EC_{50} value comparing to wild type. According to DNA alignment, I did further mutation to homolog site M369 in SthK in the third rounds selection. Truncated double mutation M369C T378V 418 aa and M369C T378V 421 aa have obvious reduced light sensitivity (Table 1).

Table 3.1 comparison of SthK-bPAC variants

construct	I_{photo} appears (560 μW/mm²)	560 μW/mm² 1 s (μA)	560 μW/mm² 30 s (μA)
First round			
WT	30	2.65 ± 0.27	
M369L	100	0.1 ± 0.04	
A370V	-	-	-
M369I A370C	-	-	-
R377A	-	-	-
R377E	-	-	-
T378A	30	2.53 ± 0.51	
T378C	30	1.13 ± 0.14	
T378S	30	0.56	
T378V	100	1.73 ± 0.12	
T378Y	30	2.75 ± 0.22	
R377A T378V	-	-	0.02
R377H T378C	100	0.43 ± 0.18	
R377H T378V	-	-	0.01
R377K T378V	-	-	0.04
R417A	100	0.2 ± 0.04	
R418A	-	-	-
K419R	30	0.92 ± 0.33	
E421A	100	0.5	
E423A	100	0.89 ± 0.59	
L422A	30	0.86 ± 0.11	
L422D	100	0.24 ± 0.06	
R428A	100	0.64	
Second round			
T378V 418aa	300	0.95 ± 0.33	
T378V 421aa	100	2.3	
T378V 424aa	100	1.01 ± 0.63	
T378V 427aa	100	0.86 ± 0.47	
Third round			
M369C T378V 418aa	1000	0.06 ± 0.04	1.5
M369C T378V 421aa	300	0.27 ± 0.15	
M369K T378V 421aa	-	-	-
M369E T378V 421aa	-	-	-
A370S T378V 421aa	100	0.45	
R418K T378V 421aa	-	-	-

3.2.6 Determine the sensitivities of SthK-bPAC variants to cAMP

The Light sensitivity could not exactly represent the cAMP sensitivity of these channel mutants. In different cell type, endogenous cAMP level, expression level, channel molecular density could all influence their light sensitivity. To provide a referential parameter, I studied the cAMP sensitivities of selected SthK-bPAC variations. As the CNBD is in the cytosol, I did inside-out patch clamp to record current of each mutant expressing oocytes with increasing cAMP concentration. Figure 3.2.8A shows representative traces under 0, 1, 3, 10, 30, 100 μM

cAMP, and Figure 3.2.8B shows the concentration-activation relationship for each mutant. Fitting of my data yielded the cAMP concentration of the half-maximum activation, EC_{50}, of 3.19 ± 0.47 μM, which is proximate to the published value (3.68 ± 0.55 μM)(101). The EC_{50} of SthK-bPAC variations are also calculated: SthK(T378V)-bPAC has a EC_{50} value of 7 ± 0.7 μM, which is about 2 times of wild type; for SthK(T378V 418aa)-bPAC, the value is 10.1 ± 1.4 μM, which is about 3 times of wild type; SthK(M369C 421aa)-bPAC is a much less sensitive mutant with EC50 of 21.2 ± 4.5 μM; an almost 10 times EC_{50}, 29.1 ± 0.6 μM is determined for SthK(M369C T378V 418aa)-bPAC (Fig. 3.2.8B). I have successfully developed 5 variations of light activated potassium channels with various light (cAMP) sensitivity for researcher to choose, according to their cell type and light intensity need.

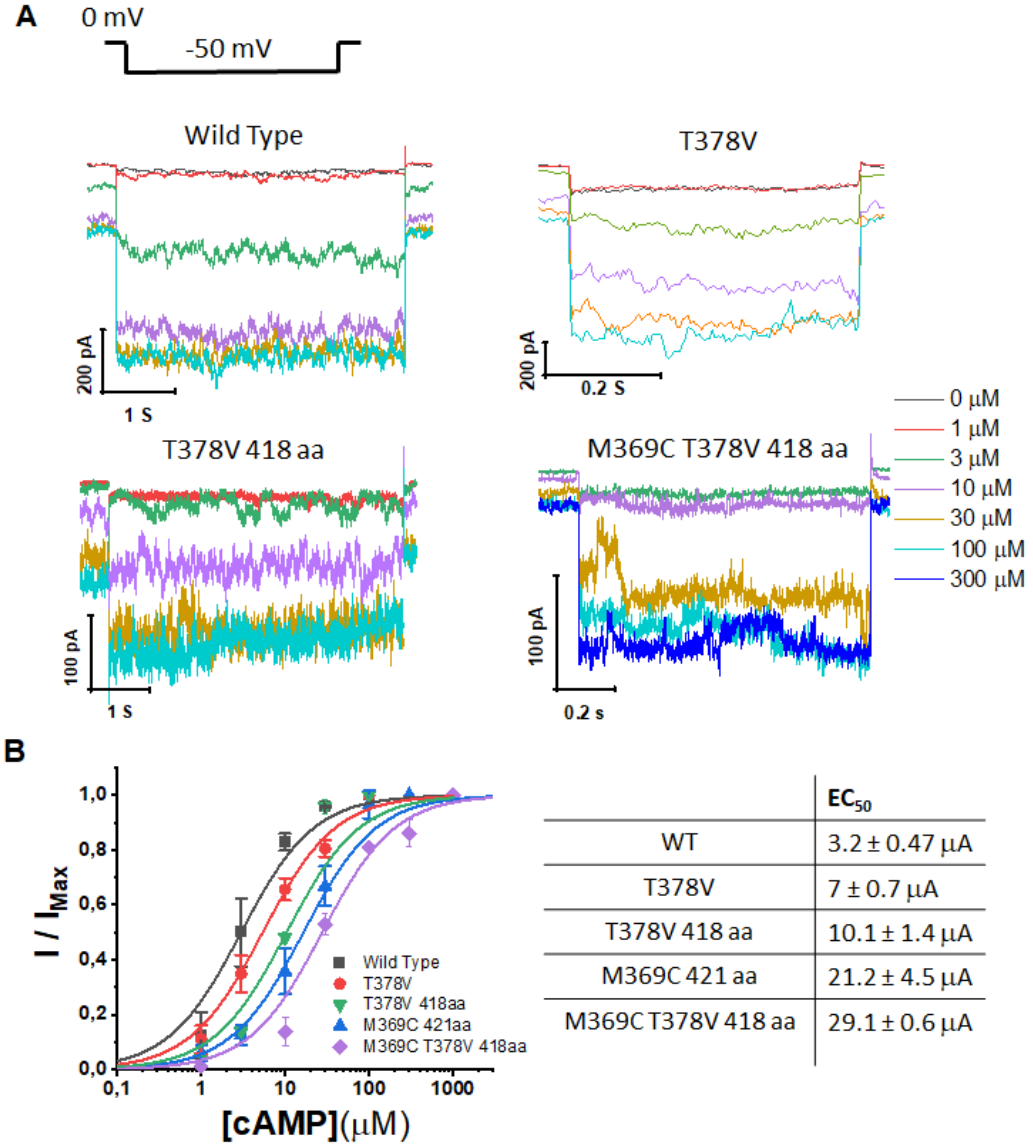

	EC_{50}
WT	3.2 ± 0.47 μA
T378V	7 ± 0.7 μA
T378V 418 aa	10.1 ± 1.4 μA
M369C 421 aa	21.2 ± 4.5 μA
M369C T378V 418 aa	29.1 ± 0.6 μA

Figure 3.2.8 Determination the sensitivities of SthK-bPAC variants to cAMP. A, Supper-imposed current traces of inside-out patch from SthK-bPAC and variants expressing oocyte exposing to solutions

containing 0, 1, 3, 10, 30, 100, 300 µM of cAMP using voltage protocol shown in upper-left pattern. B, Concentration-activation curves with cAMP on SthK-bPAC and variants.

3.2.7 Optimising the targeting of desired location

For different research purpose and different organism, we need our optogenetic tools to have different subcellular location. The SthK-bPAC is expressed only partially in the plasma membrane, also inside the oocytes. In *drosophila* motoneuron, the SthK-bP wild type localizes only to cell body membranes of the ventral nerve cord, and not much to neurites, and is also not detectable in the neuromuscular junction (Fig. 4.2.3A). To overcome this problem, I tried to improve the trafficking by modification of the N-terminal signal peptides and adding transmembrane linker at the C-terminal.

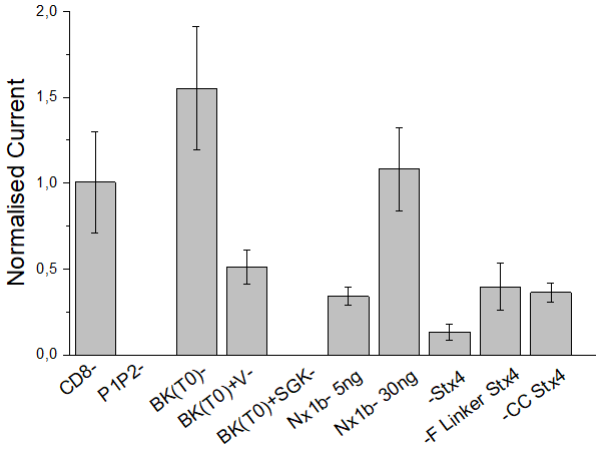

Figure 3.9 Photocurrent of various N-terminal modified SthK-bP constructs.

CD8 is a glycoprotein in T cell, which has 2 transmembrane chains. Adding an additional CD8 (HsCD8) transmembrane chain sequence at the N-terminal of SthK-bPAC did not increase the photocurrent (Fig. 3.2.9).

Adding P1P2 destroyed the light sensitivity (Fig. 3.2.9).

BK channels (big potassium), are large conductance calcium-activated potassium channels). Adding the first transmembrane helix of big potassium channel (BKT0) improved the photocurrent in oocytes (Fig. 3.2.9).

Neurexins are a family of presynaptic cell adhesion proteins that have roles in connecting neurons at the synapse. They are located mostly on the presynaptic membrane and contain a single transmembrane domain. Adding the transmembrane domain of neurexin 1B (Nx1b) to

the N-terminal of SthK-bPAC maintains a relatively good photocurrent in oocytes and helps SthK-bPAC targeting at presynaptic terminals (Fig. 3.2.9 and Fig.4.2.3B) (133).

Syntaxin 4 (Stx4) is a member of t-SNAREs and is involved in vesicle trafficking, such as synaptic vesicle exocytosis. Adding the transmembrane helix of Stx4 reduced the phtocurrent of SthK-bP (Fig. 3.2.9).

Chapter 4 Discussion

4.1 Improve the membrane targeting of CsR and convert it into a proton channel

Light-driven proton pumps are utilized as neural silencers, fluorescence-based voltage sensors (70, 134, 135). Bacteriorhodopsin (BR) is the best-characterized rhodopsin pump. In 1995, Nagel et al has functional expressed BR in *Xenopus* oocyte and identified the voltage dependency of BR(22). However, due to poor heterologous expression of BR in host cells and the small photo current amplitude, a better performed light-driven proton pump is desirable.

4.1.1 Robust heterologous expression

CsR has naturally heterologous robust expression in *Xenopus* oocytes and plant leaves, including *Nicotiana benthamiana, Nicotiana tabacum,* and *Arabidopsis thaliana*. In oocytes, the photocurrent can reach 0.3 μA even without additional retinal supplement (Fig. 3.5B). The N-terminal LR modified version CsR2.0 has 1.9 folds enhanced photocurrent without altering the proton pump function and the action spectrum (Fig. 3.1.1& 3.1.2). In CsR2.0 transgenic *N. tabacum* leaves, whose resting membrane potential is -190 mV, a light flash evokes by up to 20 mV hyperpolarization (Fig. 3.1.8). The robust heterologous expression makes CsR a promising optogenetic tool for hyperpolarization in other organisms.

4.1.2 Rhodopsin proton channel

Arg83 is a highly conserved residue in proton pump rhodopsin. Arg83, together with 6 water molecular forms hydrogen bind network at the extracellular side, prevent passive proton leakage. A single R83H point-mutation converted CsR2.0 into a light-activated proton channel (Fig. 3.1.4).

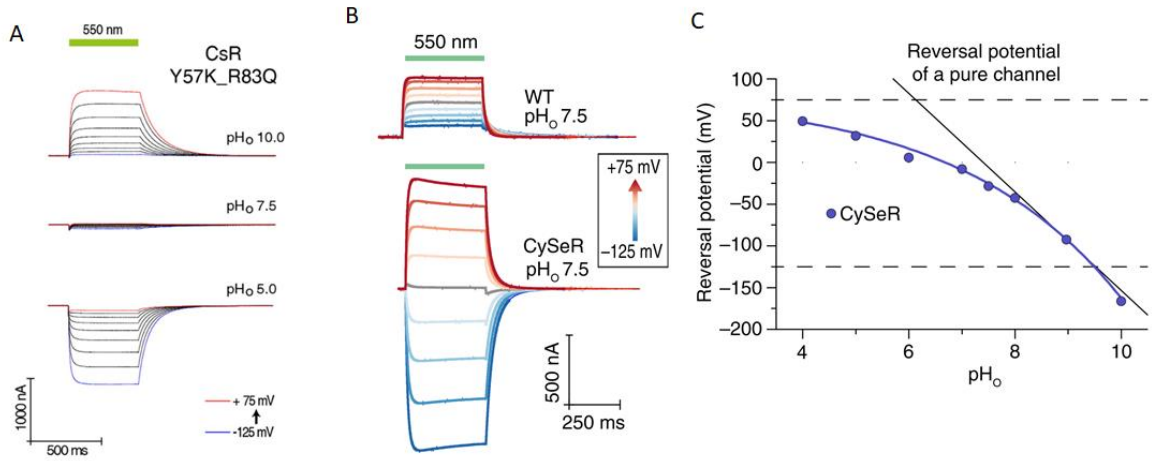

Figure 4.1.1 A, representitave Photocurrent traces of CsR Y57K_R83Q recorded in pH 10, pH 7.5 or pH 5.0 bath solution. B, Representative photocurrents for CsR-WT (top) and CySeR (bottom, which is the CsR Y14E) at an external pH of 7.5 and different holding potentials. Positive currents indicate outward-directed proton flux, whereas negative currents indicate inward-directed proton flux. (C) Reversal potential of CySeR at different pHo values. The black line represents the reversal potential of a pure proton channel according to the Nernst equation.

Previously, Vogt *et al* had studied the function of individual residues along the proton release pathway, and obtained several mutants with bi-direction conductance. The most channel like Y57K R83Q mutant is outward rectified at extracellular pH10, and inward rectified at pH5. On the other hand, the extremely small conductance at pH7.5 hampered the application of Y57K R83Q as a proton channel (Fig. 4.1.1A)(43). Later Fudim and Szczepek *et al* solved the crystal structure of CsR and studied into the determination of ion transport directivity and voltage sensitivity. They designed a mutant Y14E, and named it as CySeR. Unlike Tyr14, the Glu14 in CySeR does not show hydrogen bind interaction with Arg83 in molecular dynamic simulation comparisons. The reversal potential-extracellular pH relationship elucidates that CySeR remains strong pump activity in acidic to neutral extracellular solution (Fig. 4.1.1B)(44). According to my work, the Y14E R83H double mutant rescued the reversal potential, which suggested that Arg83 is more critical in preventing passive leakage than Tyr14. The mutagenesis studies help to understand mechanisms of proton pathway of pump and channel rhodopsins. We expect that the proton channels facilitate modulating the pH in cells or intercellular space (136).

4.2 Design of a Light-gated potassium channel

4.2.1 SthK-bPAC functions as a long-lasting light-activated potassium channel

The fused channel SthK-bPAC possesses both the cyclase activity and potassium conductance. In *Xenopus* oocyte, a short light pulse (1s 0.5 mW/mm^2 473nm) actives SthK-bP and the opening of the channel lasts for more than 4 min.

The property that cGMP acts as an antagonist (or agonist with higher affinity and very low efficiency) to SthK provides a possibility to be controlled by dual-colour. Combined with BeCyclOp, SthK-bP can be opened by blue light, which activates bPAC to produce cAMP, and closed by green light, which activates BeCyclOp to produce cGMP. In reality, the slow decreasing of cAMP and cGMP concentration makes this approach difficult to frequently repeat.

cAMP is a universal second messenger, to prevent inducing physiological changes in host cell, we employed the catalytic domain of *Hs*PDE2A. Fusing an additional PDE to the C-terminal of SthK-bP is able to shorten its closing time. But SthK-bP-PDE has limitations that the large size may hinder its expression in other host cells, and the permanent active PDE may also influence host cells.

4.2.2 Application SthK-bPAC in hippocampal neurons and larvae motoneuron

In SthK expressing rat hippocampal neuron, A single light flash (50ms, 470nm, 1 mW/mm^2) completely blocked action potentials induced by 600ms 1,000pA current injections for around 1min (Fig. 4.2.2)(133). SthK-bP was applied to larvea motoneurons. The larvae expressing SthK-bP in motoneurons were paralyzed upon continuous blue light illumination, with a clear observable body extension (Fig. 4.2.1)(133). These observations fit the known effects of increased K^+ permeability in Drosophila motoneurons: increased K^+ permeability hyperpolarizes motoneurons, synaptic transmission is inhibited and muscles relax. Unfortunately, expression of SthK-bP in motoneurons leads to eclosion failure. This might be due to the activation of the channels by endogenous cAMP. The transgenic *drosophila* of low cAMP-sensitivity version, SthK(TV418)-bP, survives eclosion.

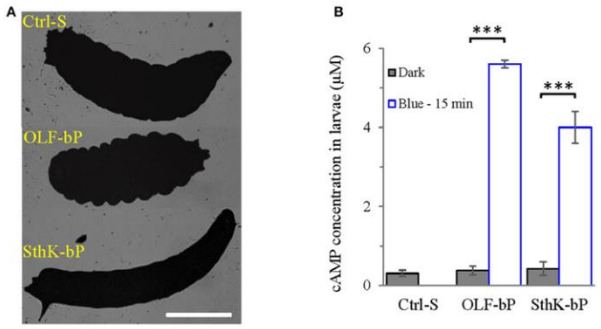

Figure 4.2.1 Functional expression of OLF-bP and SthK-bP in Drosophila larval motoneurons. (A) Expression of OLF-bP and SthK-bP in the larval motoneurons showed different phenotypes upon continuous blue light illumination, Ctrl-S = UAS-SthK-T-YFP-bPAC-Ex/+, Scale bar = 1 mm. (B) Light induced cAMP production in larvae expressing OLF-bP and SthK-bP in motoneurons, blue light (473 nm, 0.3 mW/mm2) n = 3 experiments, each with 6 larvae, error bars = SD. To calculate the final cAMP concentration in larvae, we assumed 1 larva has a volume of 2 µl. Taken from (133).

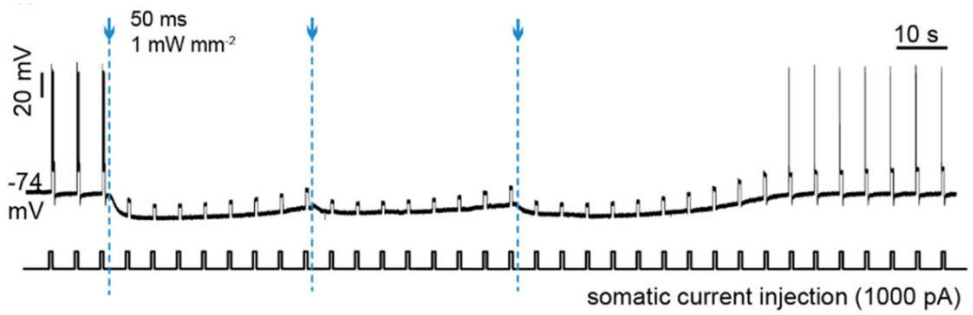

Figure 4.2.2 Action potentials generated by repeated somatic current injection (1,000pA, 600ms, ISI 5s) were blocked for 3min by 3 470nm light flashes at 40 second intervals (50ms at 1 mW/mm^2) in SthK-bPAC expressing hippocampal neuron. Taken from (133).

4.2.3 Strategy to reduce SthK sensitivity to cAMP and optimize the targeting

To widen the application avenue of SthK-bPAC, I screened variants with mutagenesis or truncation among the residues lining the ligand binding cavity of the CNBD of SthK-bPAC. I obtained five variants with cAMP EC_{50} value between 3 and 30 µM. The binding cavity of SthK is unique, because SthK is the only CNG channel that cGMP is able to bind to it, but is not able to efficiently open it (101, 105). The alignment data with eukaryotic CNG channels shows that many key residues in cNMP binding pocket are not conserved. Met-369 and Ala-370 are lining the binding cavity around the phosphoribose group, which are Ile and Cys in eukaryotic HCN channels. Kesters D. argued that the protein-ligand interactions at this location appear to be

backbone interactions, which is wrong as a M369I A370C double mutation made a no function channel. Regardless of ligand preference, an arginine in the CNBD of eukaryotic and prokaryotic CNG channels as well as cNMP-dependent proteins is always conserved, also in SthK, the Arg377, which should not be manipulated. Next to Arginine, a residue provides hydroxyl group (Thr378) is essential for binding both cAMP and cGMP. spHCN channel, which can bind with cAMP and cCMP, cCMP, has a Val at the homologous site (137). This amino acid is manipulatable, replacing it with Ala, Ser, and Tyr enhances the photocurrent, while mutating it to Val reduces the cAMP affinity. The last 12 amino acids are not necessary for gating that the truncated variants maintain channel function. It is also suggested that Leu-422 residue enters the cGMP binding pocket, and prevents cGMP molecule from binding in the syn-conformation, which is equivalent to the Asp residue and has been described to play an important role in cGMP specificity. However, a L422D mutation did not rescue cGMP from efficiently activating the channel. My mutagenesis data provided evidence for the molecular determinants of SthK and cAMP or cGMP binding.

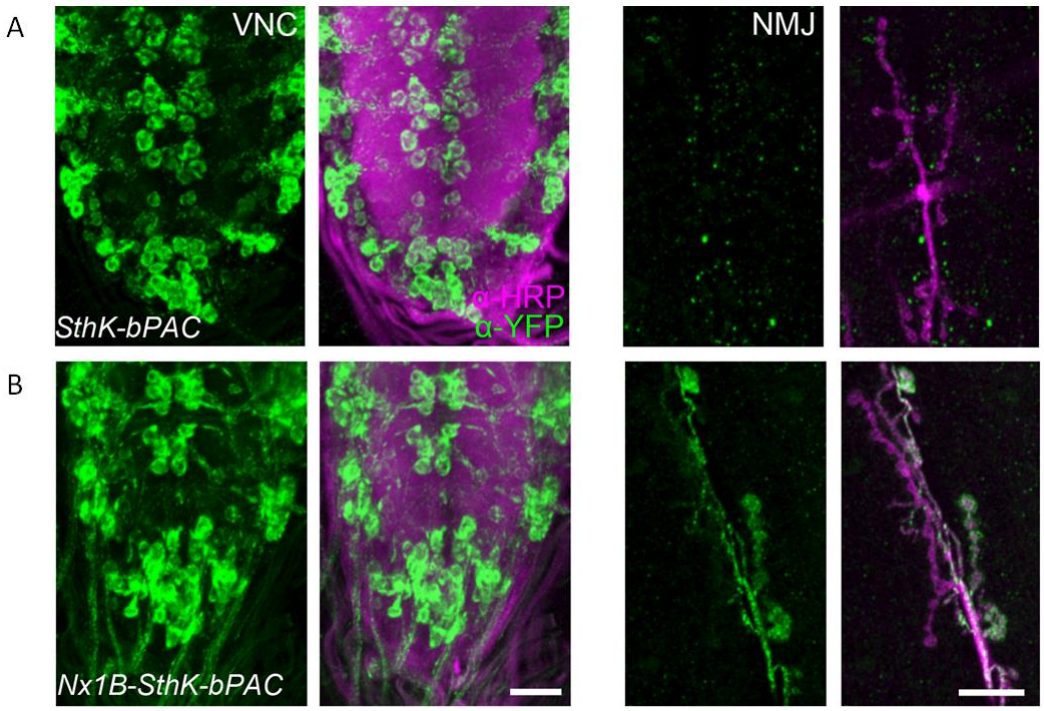

Figure 4.2.3 Expression of SthK-bP and Nx1B-SthK(TV418)-bPAC in larval motoneurons. (A) Staining against YFP (green) reveals that SthK-bP is enriched at cell body membranes in the larval VNC (Left panels) and no signal was detected at the NMJ (Right panels). Anti-HRP (horseradish peroxidase; magenta) was employed to stain neuronal membranes. (Scale bars: 20µm). (B) Nx1B-SthK(TV418)-bPAC localicate in motoneuron cell bodies and also neurites in the VNC (left panels) and at the NMJ. Taken from (138).

In *Drosophila* motoneuron of the ventral nerve cord (VNC), the SthK-bP wild type localizes uniformly to cell body membranes, and very few, if any, to neurites. In neuronal arborizations at the neuromuscular junction (NMJ), the SthK-bP could not be detected (Fig. 4.2.3A)(133, 138). In contrast to wild type, the N-termianl modified variant Nx1B-SthK(TV418)-bPAC localizes to the cell body membranes in the VNC and also at the NMJ, and a stronger signal was also detectable in nerves leaving the VNC comparing to the WT (Fig. 4.2.3B)(138).

4.2.4 SthK(TV418)-bPAC outperforms GtACR2 in low light condition in blocking hippocampal neuron action potential

Different from neuron excitation, neuron inhibition has a low light requirement that avoids tissue heating and damage, especially the inhibition of a widespread neuronal population in vivo. Soma-targeted GtACR2 is a favourable anion channel silencing tool, since it overcome the poor membrane targeting of GtACR2, and requires relatively low light power density for neuronal silencing compared to other inhibitory opsins (76). The fast-closing kinetics of *Gt*ACR2 implies continuous or frequency illumination requirement for long inhibition effect. On the contrary, SthK (TV418)-bP lacks inactivation during prolonged illumination and has post-illumination activity. SthK (TV418)-bP outperforms stGtACR2 in blocking hippocampal neuron action potential with low frequency short light pulses (unpublished data from Oana M. Constantin), which would be propitious to long neuronal inhibition without toxic exposure to prolonged illumination.

4.2.6 SthK(TV418)-bPAC VS KCRs

Recently, Govorunovaa *et al* reported two natural high potassium conducting Channelrhodopsins, *Hc*KCR1 and *Hc*KCR2 (for kalium channelrhodopsins from *Hyphochytrium catenoides*), which have PK/PNa ratios of 23 and 17, respectively. Photoactivation of HcKCR1 was able to inhibit action potentials in neurons of the mouse somatosensory cortex (Fig. 4.2.4) (139).

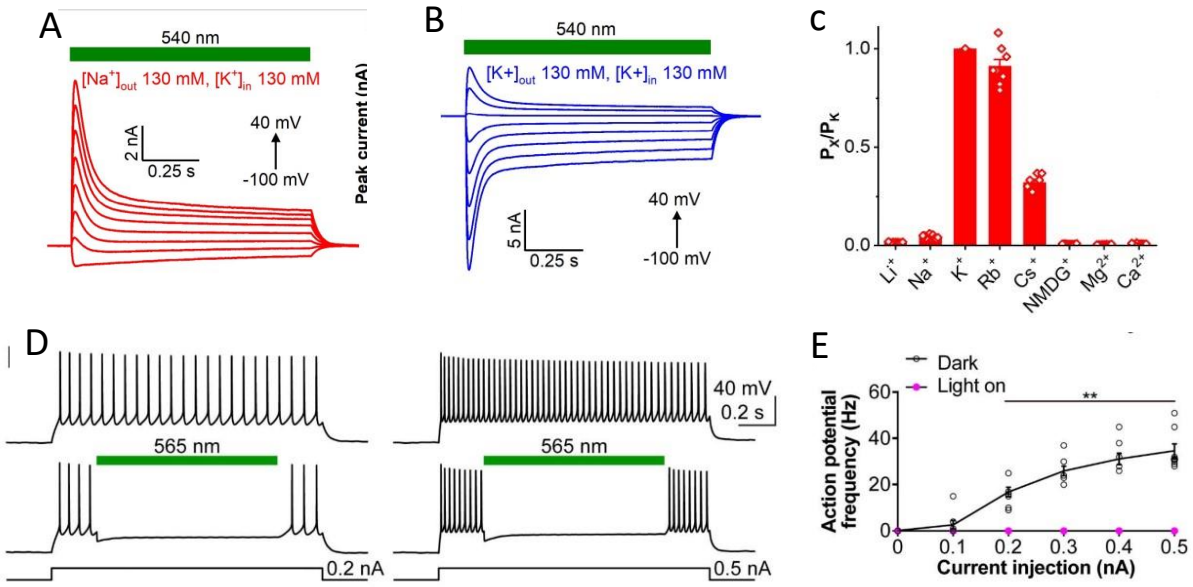

Figure 4.2.4 Photoactivation of HcKCR1 generates robust photocurrents, is highly permeable to K^+ and suppresses neuronal firing. (A and B) Photocurrents traces recorded from HcKCR1 in response to 1-s light pulses upon 20-mV voltage increments. (C) The permeability ratios (PX/PK). (D) Membrane voltage traces of a HcKCR1-expressing layer 2/3 pyramidal neuron of the mouse 5 somatosensory cortex in response to 0.2 (left) and 0.5 nA (right) 10 current injections without (top) and with (bottom) 565 nm light pulses. (E) The frequencies of action potentials evoked by different current injections with (magenta) and without (black) photoactivation. Taken from (139).

*Hc*KCRs and SthK(TV418)-bP are very different in construction, light-driven potassium conducting mechanisms and thus have their own pros and cons.

*Hc*KCRs are single protein complexes, on light illumination, they open and close on the submillisecond or millisecond time scale. While SthK(TV418)-bP is the fusion of two functional proteins, the potassium conductance increases when there is enough cAMP produced by bPAC, and decreases when cAMP level is reduced. It takes seconds and minutes for SthK(TV418)-bP to open and close, respectively. For long-term neuronal silencing, SthK(TV418)-bP is more efficient, since continuous illumination is not necessary. HcKCRs are suitable for precise-temporal inhibition.

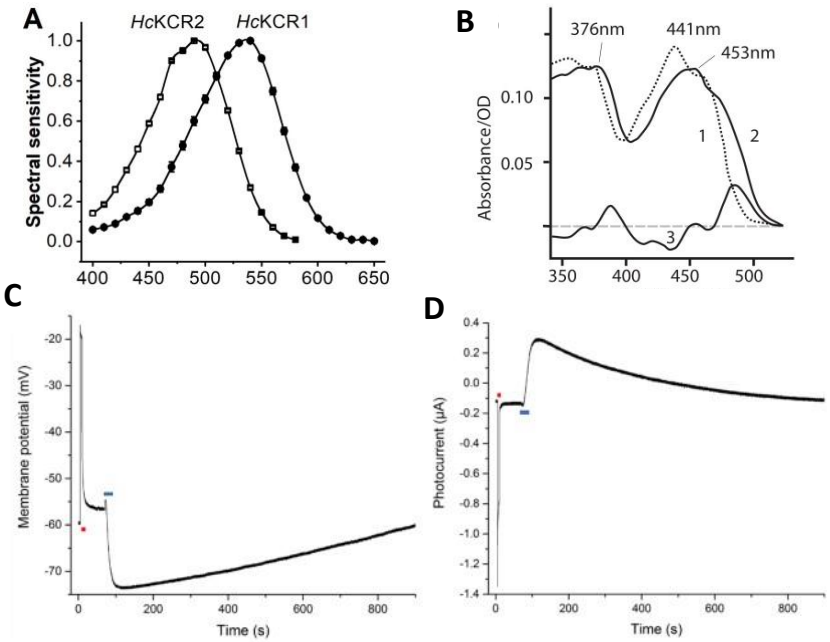

Figure 4.2.5 A, the action spectra of HcKCRs. Taken fom (139). B, absorption spectra of purified bPAC in its dark-adapted (trace 1) and light adapted (trace 2) state. The difference between the two is shown as a line (trace 3). OD, optical density. Taken from (53). C and D, Current-clamp and voltage-clamp measurments of *Xenopus* oocyte expressing vf-Chrimson 2.0 and SthK(TV418)-bP. Unpublishe data from Shang Yang.

Secondly, The intermediate product of SthK(TV418)-bP, cAMP is responsible for signal transductions in many organisms. Depending on cell type and developmental stage, the cAMP may itself induce physiological changes, which need to be taken into consideration when employing such synthetic optogenetic tools. At this point, HcKCR has no complications.

Thirdly, Due to the fundamental property of retinal chromophore, the partial overlap of action spectra of rhodopsins is not avoidable. bPAC absorbs at a more blue-shifted wavelength than HcKCRs.The photocurrent of the more red-shifted HcKCR2 (peak at 490 nm) is nonnegligible with 650 nm illumination, while the light-induced activity of bPAC is not detectable when illuminated with longer than 550 nm light (Fig. 4.2.5A and B). SthK(TV418)-bP enabled the dual-color bi-directional control of cell membrane potential when combining with the red-shifted vf-Chrimson 2.0 (peak at 590 nm) (Fig. 4.2.5C and D). Activating and inactivating genetically targeted neurons with a set of multiple-colour optogenetic tools could contribute to study system-level neuronal processes, like action and thought.

Via molecular engineering, it is promising to mutate KCR into slow closing or blue shifted channels. It is also possible to achieve tightly temporal- and spatial- control of cAMP level, by combining with PDE, in SthK-bP (TV418) construct.

5. references

1. Adamantidis A, Arber S, Bains JS, Bamberg E, Bonci A, Buzsáki G, et al. Optogenetics: 10 years after ChR2 in neurons--views from the community. Nat Neurosci. 2015;18(9):1202-12.

2. Boyden ES. Optogenetics and the future of neuroscience. Nat Neurosci. 2015;18(9):1200-1.

3. Govorunova EG, Sineshchekov OA, Li H, Spudich JL. Microbial Rhodopsins: Diversity, Mechanisms, and Optogenetic Applications. Annu Rev Biochem. 2017;86:845-72.

4. Boyle PM, Karathanos TV, Trayanova NA. Cardiac Optogenetics: 2018. JACC Clin Electrophysiol. 2018;4(2):155-67.

5. Joshi J, Rubart M, Zhu W. Optogenetics: Background, Methodological Advances and Potential Applications for Cardiovascular Research and Medicine. Front Bioeng Biotechnol. 2020;7:466-.

6. Tischer D, Weiner OD. Illuminating cell signalling with optogenetic tools. Nat Rev Mol Cell Biol. 2014;15(8):551-8.

7. Moser T, Dieter A. Towards optogenetic approaches for hearing restoration. Biochem Biophys Res Commun. 2020;527(2):337-42.

8. Garita-Hernandez M, Lampič M, Chaffiol A, Guibbal L, Routet F, Santos-Ferreira T, et al. Restoration of visual function by transplantation of optogenetically engineered photoreceptors. Nat Commun. 2019;10(1):4524.

9. Nagel G, Szellas T, Huhn W, Kateriya S, Adeishvili N, Berthold P, et al. Channelrhodopsin-2, a directly light-gated cation-selective membrane channel. Proceedings of the National Academy of Sciences of the United States of America. 2003;100(24):13940-5.

10. Boyden ES, Zhang F, Bamberg E, Nagel G, Deisseroth K. Millisecond-timescale, genetically targeted optical control of neural activity. Nat Neurosci. 2005;8(9):1263-8.

11. Ishizuka T, Kakuda M, Araki R, Yawo H. Kinetic evaluation of photosensitivity in genetically engineered neurons expressing green algae light-gated channels. Neurosci Res. 2006;54(2):85-94.

12. Li X, Gutierrez DV, Hanson MG, Han J, Mark MD, Chiel H, et al. Fast noninvasive activation and inhibition of neural and network activity by vertebrate rhodopsin and green algae channelrhodopsin. Proc Natl Acad Sci U S A. 2005;102(49):17816-21.

13. Nagel G, Brauner M, Liewald JF, Adeishvili N, Bamberg E, Gottschalk A. Light activation of channelrhodopsin-2 in excitable cells of Caenorhabditis elegans triggers rapid behavioral responses. Curr Biol. 2005;15(24):2279-84.

14. Bi A, Cui J, Ma YP, Olshevskaya E, Pu M, Dizhoor AM, et al. Ectopic expression of a microbial-type rhodopsin restores visual responses in mice with photoreceptor degeneration. Neuron. 2006;50(1):23-33.

15. Schroll C, Riemensperger T, Bucher D, Ehmer J, Voller T, Erbguth K, et al. Light-induced activation of distinct modulatory neurons triggers appetitive or aversive learning in Drosophila larvae. Curr Biol. 2006;16(17):1741-7.
16. Nagel G, Ollig D, Fuhrmann M, Kateriya S, Musti AM, Bamberg E, et al. Channelrhodopsin-1: a light-gated proton channel in green algae. Science. 2002;296(5577):2395-8.
17. Deisseroth K, Feng G, Majewska AK, Miesenböck G, Ting A, Schnitzer MJ. Next-generation optical technologies for illuminating genetically targeted brain circuits. J Neurosci. 2006;26(41):10380-6.
18.Zemelman BV, Lee GA, Ng M, Miesenböck G. Selective photostimulation of genetically chARGed neurons. Neuron. 2002;33(1):15-22.
19. Lima SQ, Miesenböck G. Remote control of behavior through genetically targeted photostimulation of neurons. Cell. 2005;121(1):141-52.
20. Zhou Y, Ding M, Nagel G, Konrad KR, Gao S. Advances and prospects of rhodopsin-based optogenetics in plant research. Plant Physiology. 2021;187(2):572-89.
21. de Mena L, Rizk P, Rincon-Limas DE. Bringing Light to Transcription: The Optogenetics Repertoire. Frontiers in Genetics. 2018;9(518).
22. Nagel G, Möckel B, Büldt G, Bamberg E. Functional expression of bacteriorhodopsin in oocytes allows direct measurement of voltage dependence of light induced H+ pumping. FEBS Lett. 1995;377(2):263-6.
23. Duschl A, Lanyi JK, Zimányi L. Properties and photochemistry of a halorhodopsin from the haloalkalophile, Natronobacterium pharaonis. J Biol Chem. 1990;265(3):1261-7.
24. Yang S, Constantin OM, Sachidanandan D, Hofmann H, Kunz TC, Kozjak-Pavlovic V, et al. PACmn for improved optogenetic control of intracellular cAMP. BMC Biology. 2021;19(1):227.
25. Tian Y, Gao S, von der Heyde EL, Hallmann A, Nagel G. Two-component cyclase opsins of green algae are ATP-dependent and light-inhibited guanylyl cyclases. BMC Biol. 2018;16(1):144.
26. Tian Y, Gao S, Yang S, Nagel G. A novel rhodopsin phosphodiesterase from Salpingoeca rosetta shows light-enhanced substrate affinity. Biochem J. 2018;475(6):1121-8.
27. Gao S, Nagpal J, Schneider MW, Kozjak-Pavlovic V, Nagel G, Gottschalk A. Optogenetic manipulation of cGMP in cells and animals by the tightly light-regulated guanylyl-cyclase opsin CyclOp. Nat Commun. 2015;6:8046.
28. Tang R, Yang S, Nagel G, Gao S. mem-iLID, a fast and economic protein purification method. Biosci Rep. 2021;41(7).
29. John L. Spudich, Chii-Shen Yang, Kwang-Hwan Jung a, Spudich EN. Retinylidene Proteins: Structures and Functions from Archaea to Humans. Annual Review of Cell and Developmental Biology. 2000;16(1):365-92.

30. Luecke H, Schobert B, Richter H-T, Cartailler J-P, Lanyi JK. Structure of bacteriorhodopsin at 1.55 Å resolution 11Edited by D. C. Rees. Journal of Molecular Biology. 1999;291(4):899-911.
31. Palczewski K, Kumasaka T, Hori T, Behnke CA, Motoshima H, Fox BA, et al. Crystal Structure of Rhodopsin: A G Protein-Coupled Receptor. Science. 2000;289(5480):739-45.
32. Shichida Y, Matsuyama T. Evolution of opsins and phototransduction. Philos Trans R Soc Lond B Biol Sci. 2009;364(1531):2881-95.
33. Ernst OP, Lodowski DT, Elstner M, Hegemann P, Brown LS, Kandori H. Microbial and animal rhodopsins: structures, functions, and molecular mechanisms. Chem Rev. 2014;114(1):126-63.
34. Francis SH, Blount MA, Corbin JD. Mammalian cyclic nucleotide phosphodiesterases: molecular mechanisms and physiological functions. Physiol Rev. 2011;91(2):651-90.
35. Haupts U, Tittor J, Bamberg E, Oesterhelt D. General Concept for Ion Translocation by Halobacterial Retinal Proteins: The Isomerization/Switch/Transfer (IST) Model. Biochemistry. 1997;36(1):2-7.
36. Rosenbaum DM, Rasmussen SGF, Kobilka BK. The structure and function of G-protein-coupled receptors. Nature. 2009;459(7245):356-63.
37. Oesterhelt D, Stoeckenius W. Rhodopsin-like protein from the purple membrane of Halobacterium halobium. Nat New Biol. 1971;233(39):149-52.
38. Oesterhelt D, Stoeckenius W. Functions of a new photoreceptor membrane. Proc Natl Acad Sci U S A. 1973;70(10):2853-7.
39. Racker E, Stoeckenius W. Reconstitution of purple membrane vesicles catalyzing light-driven proton uptake and adenosine triphosphate formation. J Biol Chem. 1974;249(2):662-3.
40. Lanyi JK. Bacteriorhodopsin. Annual Review of Physiology. 2004;66(1):665-88.
41. Zhang F, Vierock J, Yizhar O, Fenno LE, Tsunoda S, Kianianmomeni A, et al. The microbial opsin family of optogenetic tools. Cell. 2011;147(7):1446-57.
42. Blanc G, Agarkova I, Grimwood J, Kuo A, Brueggeman A, Dunigan DD, et al. The genome of the polar eukaryotic microalga Coccomyxa subellipsoidea reveals traits of cold adaptation. Genome Biol. 2012;13(5):R39-R.
43. Vogt A, Guo Y, Tsunoda SP, Kateriya S, Elstner M, Hegemann P. Conversion of a light-driven proton pump into a light-gated ion channel. Sci Rep. 2015;5:16450.
44. Fudim R, Szczepek M, Vierock J, Vogt A, Schmidt A, Kleinau G, et al. Design of a light-gated proton channel based on the crystal structure of Coccomyxa rhodopsin. Science Signaling. 2019;12(573):eaav4203.
45. Darienko T, Gustavs L, Eggert A, Wolf W, Pröschold T. Evaluating the Species Boundaries of Green Microalgae (Coccomyxa, Trebouxiophyceae, Chlorophyta) Using Integrative Taxonomy and DNA

Barcoding with Further Implications for the Species Identification in Environmental Samples. PLoS One. 2015;10(6):e0127838.
46. Vieira AL, Camilo CM. Agrobacterium tumefasciens-mediated transformation of the aquatic fungus Blastocladiella emersonii. Fungal Genet Biol. 2011;48(8):806-11.
47. Schroder-Lang S, Schwarzel M, Seifert R, Strunker T, Kateriya S, Looser J, et al. Fast manipulation of cellular cAMP level by light in vivo. Nat Methods. 2007;4(1):39-42.
48. Häder DP, Iseki M. Photomovement in Euglena. Adv Exp Med Biol. 2017;979:207-35.
49. Iseki M, Matsunaga S, Murakami A, Ohno K, Shiga K, Yoshida K, et al. A blue-light-activated adenylyl cyclase mediates photoavoidance in Euglena gracilis. Nature. 2002;415(6875):1047-51.
50. Looser J, Schröder-Lang S, Hegemann P, Nagel G. Mechanistic insights in light-induced cAMP production by photoactivated adenylyl cyclase alpha (PACalpha). Biol Chem. 2009;390(11):1105-11.
51. Nagahama T, Suzuki T, Yoshikawa S, Iseki M. Functional transplant of photoactivated adenylyl cyclase (PAC) into Aplysia sensory neurons. Neurosci Res. 2007;59(1):81-8.
52. Weissenberger S, Schultheis C, Liewald JF, Erbguth K, Nagel G, Gottschalk A. PACalpha--an optogenetic tool for in vivo manipulation of cellular cAMP levels, neurotransmitter release, and behavior in Caenorhabditis elegans. Journal of neurochemistry. 2011;116(4):616-25.
53. Stierl M, Stumpf P, Udwari D, Gueta R, Hagedorn R, Losi A, et al. Light modulation of cellular cAMP by a small bacterial photoactivated adenylyl cyclase, bPAC, of the soil bacterium Beggiatoa. J Biol Chem. 2011;286(2):1181-8.
54. Penzkofer A, Stierl M, Hegemann P, Kateriya S. Photo-dynamics of the BLUF domain containing soluble adenylate cyclase (nPAC) from the amoeboflagellate Naegleria gruberi NEG-M strain. Chem Phys. 2011;387(1-3):25-38.
55. Penzkofer A, Tanwar M, Veetil SK, Kateriya S. Photo-dynamics of photoactivated adenylyl cyclase TpPAC from the spirochete bacterium Turneriella parva strain H-T. J Photoch Photobio B. 2015;153:90-102.
56. Raffelberg S, Wang L, Gao S, Losi A, Gartner W, Nagel G. A LOV-domain-mediated blue-light-activated adenylate (adenylyl) cyclase from the cyanobacterium Microcoleus chthonoplastes PCC 7420. Biochem J. 2013;455(3):359-65.
57. Ohki M, Sugiyama K, Kawai F, Tanaka H, Nihei Y, Unzai S, et al. Structural insight into photoactivation of an adenylate cyclase from a photosynthetic cyanobacterium. P Natl Acad Sci USA. 2016;113(24):6659-64.
58. Blain-Hartung M, Rockwell NC, Moreno MV, Martin SS, Gan F, Bryant DA, et al. Cyanobacteriochrome-based photoswitchable adenylyl cyclases (cPACs) for broad spectrum light regulation of cAMP levels in cells. J Biol Chem. 2018;293(22):8473-83.

59. Stuven B, Stabel R, Ohlendorf R, Beck J, Schubert R, Moglich A. Characterization and engineering of photoactivated adenylyl cyclases. Biol Chem. 2019;400(3):429-41.
60. Ryu MH, Moskvin OV, Siltberg-Liberles J, Gomelsky M. Natural and engineered photoactivated nucleotidyl cyclases for optogenetic applications. J Biol Chem. 2010;285(53):41501-8.
61. Møller MM, Nielsen LP, Jørgensen BB. Oxygen Responses and Mat Formation by Beggiatoa spp. Appl Environ Microbiol. 1985;50(2):373-82.
62. Mills HJ, Martinez RJ, Story S, Sobecky PA. Identification of members of the metabolically active microbial populations associated with Beggiatoa species mat communities from Gulf of Mexico cold-seep sediments. Appl Environ Microbiol. 2004;70(9):5447-58.
63. Jansen V, Alvarez L, Balbach M, Strunker T, Hegemann P, Kaupp UB, et al. Controlling fertilization and cAMP signaling in sperm by optogenetics. Elife. 2015;4.
64. Xiao Y, Tian W, Lopez-Schier H. Optogenetic stimulation of neuronal repair. Curr Biol. 2015;25(22):R1068-9.
65. Costa WS, Yu SC, Liewald JF, Gottschalk A. Fast cAMP Modulation of Neurotransmission via Neuropeptide Signals and Vesicle Loading. Curr Biol. 2017;27(4):495-507.
66. Scholz N, Guan CL, Nieberler M, Grotemeyer A, Maiellaro I, Gao SQ, et al. Mechano-dependent signaling by Latrophilin/CIRL quenches cAMP in proprioceptive neurons. Elife. 2017;6.
67. Zhang K, Cu BX. Optogenetic control of intracellular signaling pathways. Trends Biotechnol. 2015;33(2):92-100.
68. Lindner R, Hartmann E, Tarnawski M, Winkler A, Frey D, Reinstein J, et al. Photoactivation Mechanism of a Bacterial Light-Regulated Adenylyl Cyclase. J Mol Biol. 2017;429(9):1336-51.
69. Wiegert JS, Mahn M, Prigge M, Printz Y, Yizhar O. Silencing Neurons: Tools, Applications, and Experimental Constraints. Neuron. 2017;95(3):504-29.
70. Chow BY, Han X, Dobry AS, Qian X, Chuong AS, Li M, et al. High-performance genetically targetable optical neural silencing by light-driven proton pumps. Nature. 2010;463(7277):98-102.
71. Zhang F, Wang L-P, Brauner M, Liewald JF, Kay K, Watzke N, et al. Multimodal fast optical interrogation of neural circuitry. Nature. 2007;446(7136):633-9.
72. Chuong AS, Miri ML, Busskamp V, Matthews GA, Acker LC, Sørensen AT, et al. Noninvasive optical inhibition with a red-shifted microbial rhodopsin. Nat Neurosci. 2014;17(8):1123-9.
73. Berndt A, Lee SY, Wietek J, Ramakrishnan C, Steinberg EE, Rashid AJ, et al. Structural foundations of optogenetics: Determinants of channelrhodopsin ion selectivity. Proceedings of the National Academy of Sciences. 2016;113(4):822-9.
74. Wietek J, Beltramo R, Scanziani M, Hegemann P, Oertner TG, Wiegert JS. An improved chloride-conducting channelrhodopsin for light-induced inhibition of neuronal activity in vivo. Scientific Reports. 2015;5(1):14807.

75. Govorunova EG, Sineshchekov OA, Janz R, Liu X, Spudich JL. NEUROSCIENCE. Natural light-gated anion channels: A family of microbial rhodopsins for advanced optogenetics. Science. 2015;349(6248):647-50.
76. Mahn M, Gibor L, Patil P, Cohen-Kashi Malina K, Oring S, Printz Y, et al. High-efficiency optogenetic silencing with soma-targeted anion-conducting channelrhodopsins. Nature Communications. 2018;9(1):4125.
77. Sørensen AT, Ledri M, Melis M, Nikitidou Ledri L, Andersson M, Kokaia M. Altered Chloride Homeostasis Decreases the Action Potential Threshold and Increases Hyperexcitability in Hippocampal Neurons. eNeuro. 2018;4(6):ENEURO.0172-17.2017.
78. Raimondo JV, Kay L, Ellender TJ, Akerman CJ. Optogenetic silencing strategies differ in their effects on inhibitory synaptic transmission. Nat Neurosci. 2012;15(8):1102-4.
79. Mahn M, Prigge M, Ron S, Levy R, Yizhar O. Biophysical constraints of optogenetic inhibition at presynaptic terminals. Nat Neurosci. 2016;19(4):554-6.
80. Alfonsa H, Merricks EM, Codadu NK, Cunningham MO, Deisseroth K, Racca C, et al. The contribution of raised intraneuronal chloride to epileptic network activity. J Neurosci. 2015;35(20):7715-26.
81. Banghart M, Borges K, Isacoff E, Trauner D, Kramer RH. Light-activated ion channels for remote control of neuronal firing. Nat Neurosci. 2004;7(12):1381-6.
82. Janovjak H, Szobota S, Wyart C, Trauner D, Isacoff EY. A light-gated, potassium-selective glutamate receptor for the optical inhibition of neuronal firing. Nat Neurosci. 2010;13(8):1027-32.
83. Fortin DL, Dunn TW, Fedorchak A, Allen D, Montpetit R, Banghart MR, et al. Optogenetic photochemical control of designer K+ channels in mammalian neurons. J Neurophysiol. 2011;106(1):488-96.
84. Kang J-Y, Kawaguchi D, Coin I, Xiang Z, O'Leary DDM, Slesinger PA, et al. In vivo expression of a light-activatable potassium channel using unnatural amino acids. Neuron. 2013;80(2):358-70.
85. Schmidt D, Tillberg PW, Chen F, Boyden ES. A fully genetically encoded protein architecture for optical control of peptide ligand concentration. Nature communications. 2014;5:3019-.
86. Alberio L, Locarno A, Saponaro A, Romano E, Bercier V, Albadri S, et al. A light-gated potassium channel for sustained neuronal inhibition. Nature methods. 2018;15(11):969-76.
87. Cosentino C, Alberio L, Gazzarrini S, Aquila M, Romano E, Cermenati S, et al. Engineering of a light-gated potassium channel. Science. 2015;348(6235):707-10.
88. Lin JY, Sann SB, Zhou K, Nabavi S, Proulx CD, Malinow R, et al. Optogenetic inhibition of synaptic release with chromophore-assisted light inactivation (CALI). Neuron. 2013;79(2):241-53.

89. Shu X, Lev-Ram V, Deerinck TJ, Qi Y, Ramko EB, Davidson MW, et al. A genetically encoded tag for correlated light and electron microscopy of intact cells, tissues, and organisms. PLoS Biol. 2011;9(4):e1001041.
90. Masseck OA, Spoida K, Dalkara D, Maejima T, Rubelowski JM, Wallhorn L, et al. Vertebrate cone opsins enable sustained and highly sensitive rapid control of Gi/o signaling in anxiety circuitry. Neuron. 2014;81(6):1263-73.
91. Mahn M, Saraf-Sinik I, Patil P, Pulin M, Bitton E, Karalis N, et al. Efficient optogenetic silencing of neurotransmitter release with a mosquito rhodopsin. Neuron. 2021;109(10):1621-35.e8.
92. Copits BA, Gowrishankar R, O'Neill PR, Li JN, Girven KS, Yoo JJ, et al. A photoswitchable GPCR-based opsin for presynaptic inhibition. Neuron. 2021;109(11):1791-809.e11.
93. Kaupp UB, Seifert R. Cyclic nucleotide-gated ion channels. Physiol Rev. 2002;82(3):769-824.
94. Fesenko EE, Kolesnikov SS, Lyubarsky AL. Induction by cyclic GMP of cationic conductance in plasma membrane of retinal rod outer segment. Nature. 1985;313(6000):310-3.
95. Kaupp UB. The cyclic nucleotide-gated channels of vertebrate photoreceptors and olfactory epithelium. Trends Neurosci. 1991;14(4):150-7.
96. Menini A. Cyclic nucleotide-gated channels in visual and olfactory transduction. Biophys Chem. 1995;55(3):185-96.
97. Kraus-Friedmann N. Cyclic nucleotide-gated channels in non-sensory organs. Cell Calcium. 2000;27(3):127-38.
98. Dryer SE, Henderson D. A cyclic GMP-activated channel in dissociated cells of the chick pineal gland. Nature. 1991;353(6346):756-8.
99. Biel M, Michalakis S. Function and dysfunction of CNG channels: insights from channelopathies and mouse models. Mol Neurobiol. 2007;35(3):266-77.
100. Nimigean CM, Shane T, Miller C. A cyclic nucleotide modulated prokaryotic K+ channel. J Gen Physiol. 2004;124(3):203-10.
101. Brams M, Kusch J, Spurny R, Benndorf K, Ulens C. Family of prokaryote cyclic nucleotide-modulated ion channels. Proc Natl Acad Sci U S A. 2014;111(21):7855-60.
102. James ZM, Borst AJ, Haitin Y, Frenz B, DiMaio F, Zagotta WN, et al. CryoEM structure of a prokaryotic cyclic nucleotide-gated ion channel. Proc Natl Acad Sci U S A. 2017;114(17):4430-5.
103. Mari SA, Pessoa J, Altieri S, Hensen U, Thomas L, Morais-Cabral JH, et al. Gating of the MlotiK1 potassium channel involves large rearrangements of the cyclic nucleotide-binding domains. Proc Natl Acad Sci U S A. 2011;108(51):20802-7.
104. Kesters D, Brams M, Nys M, Wijckmans E, Spurny R, Voets T, et al. Structure of the SthK carboxy-terminal region reveals a gating mechanism for cyclic nucleotide-modulated ion channels. PLoS One. 2015;10(1):e0116369.

105. Schmidpeter PAM, Gao X, Uphadyay V, Rheinberger J, Nimigean CM. Ligand binding and activation properties of the purified bacterial cyclic nucleotide-gated channel SthK. The Journal of general physiology. 2018;150(6):821-34.
106. Wirth R, Ugele M, Wanner G. Motility and Ultrastructure of Spirochaeta thermophila. Frontiers in Microbiology. 2016;7(1609).
107. Pessoa J, Fonseca F, Furini S, Morais-Cabral JH. Determinants of ligand selectivity in a cyclic nucleotide–regulated potassium channel. Journal of General Physiology. 2014;144(1):41-54.
108. Conti M, Beavo J. Biochemistry and physiology of cyclic nucleotide phosphodiesterases: essential components in cyclic nucleotide signaling. Annu Rev Biochem. 2007;76:481-511.
109. Omori K, Kotera J. Overview of PDEs and their regulation. Circ Res. 2007;100(3):309-27.
110. Gomelsky M. cAMP, c-di-GMP, c-di-AMP and now cGMP: bacteria use them all! Mol Microbiol. 2011;79(3):562-5.
111. Houslay MD, Adams DR. PDE4 cAMP phosphodiesterases: modular enzymes that orchestrate signalling cross-talk, desensitization and compartmentalization. Biochem J. 2003;370(Pt 1):1-18.
112. Sette C, Conti M. Phosphorylation and activation of a cAMP-specific phosphodiesterase by the cAMP-dependent protein kinase. Involvement of serine 54 in the enzyme activation. J Biol Chem. 1996;271(28):16526-34.
113. Pandit J, Forman MD, Fennell KF, Dillman KS, Menniti FS. Mechanism for the allosteric regulation of phosphodiesterase 2A deduced from the X-ray structure of a near full-length construct. Proceedings of the National Academy of Sciences of the United States of America. 2009;106(43):18225-30.
114. Martins TJ, Mumby MC, Beavo JA. Purification and characterization of a cyclic GMP-stimulated cyclic nucleotide phosphodiesterase from bovine tissues. J Biol Chem. 1982;257(4):1973-9.
115. Yang X, Kuk J, Moffat K. Crystal structure of Pseudomonas aeruginosa bacteriophytochrome: photoconversion and signal transduction. Proc Natl Acad Sci U S A. 2008;105(38):14715-20.
116. Taylor BL, Zhulin IB. PAS domains: internal sensors of oxygen, redox potential, and light. Microbiol Mol Biol Rev. 1999;63(2):479-506.
117. Gasser C, Taiber S, Yeh CM, Wittig CH, Hegemann P, Ryu S, et al. Engineering of a red-light-activated human cAMP/cGMP-specific phosphodiesterase. Proc Natl Acad Sci U S A. 2014;111(24):8803-8.
118. Braman J, Papworth C, Greener A. Site-directed mutagenesis using double-stranded plasmid DNA templates. Methods Mol Biol. 1996;57:31-44.
119. Mandel M, Higa A. Calcium-dependent bacteriophage DNA infection. J Mol Biol. 1970;53(1):159-62.

120. Cohen SN, Chang AC, Hsu L. Nonchromosomal antibiotic resistance in bacteria: genetic transformation of Escherichia coli by R-factor DNA. Proc Natl Acad Sci U S A. 1972;69(8):2110-4.
121. Barnes W. Plasmid detection and sizing in single colony lysates. Science. 1977;195(4276):393-4.
122. Rong M, He B, McAllister WT, Durbin RK. Promoter specificity determinants of T7 RNA polymerase. Proc Natl Acad Sci U S A. 1998;95(2):515-9.
123. Gurdon JB, Lane CD, Woodland HR, Marbaix G. Use of frog eggs and oocytes for the study of messenger RNA and its translation in living cells. Nature. 1971;233(5316):177-82.
124. Cole KS, Curtis HJ. Electric Impedance of the Squid Giant Axon during Activity. J Gen Physiol. 1939;22(5):649-70.
125. Hamill OP, Marty A, Neher E, Sakmann B, Sigworth FJ. Improved patch-clamp techniques for high-resolution current recording from cells and cell-free membrane patches. Pflugers Arch. 1981;391(2):85-100.
126. Zhou Y, Ding M, Gao S, Yu-Strzelczyk J, Krischke M, Duan X, et al. Optogenetic control of plant growth by a microbial rhodopsin. Nat Plants. 2021;7(2):144-51.
127. Krautwurst D, Yau KW, Reed RR. Identification of ligands for olfactory receptors by functional expression of a receptor library. Cell. 1998;95(7):917-26.
128. Chan DV, Somani A-K, Young AB, Massari JV, Ohtola J, Sugiyama H, et al. Signal peptide cleavage is essential for surface expression of a regulatory T cell surface protein, leucine rich repeat containing 32 (LRRC32). BMC Biochem. 2011;12:27-.
129. Shepard BD, Natarajan N, Protzko RJ, Acres OW, Pluznick JL. A cleavable N-terminal signal peptide promotes widespread olfactory receptor surface expression in HEK293T cells. PloS one. 2013;8(7):e68758-e.
130. Kleinlogel S, Terpitz U, Legrum B, Gökbuget D, Boyden ES, Bamann C, et al. A gene-fusion strategy for stoichiometric and co-localized expression of light-gated membrane proteins. Nature Methods. 2011;8(12):1083-8.
131. Cicirelli MF, Robinson KR, Smith LD. Internal pH of Xenopus oocytes: A study of the mechanism and role of pH changes during meiotic maturation. Developmental Biology. 1983;100(1):133-46.
132. Papanatsiou M, Petersen J, Henderson L, Wang Y, Christie JM, Blatt MR. Optogenetic manipulation of stomatal kinetics improves carbon assimilation, water use, and growth. Science. 2019;363(6434):1456-9.
133. Beck S, Yu-Strzelczyk J, Pauls D, Constantin OM, Gee CE, Ehmann N, et al. Synthetic Light-Activated Ion Channels for Optogenetic Activation and Inhibition. Front Neurosci. 2018;12:643.
134. Maclaurin D, Venkatachalam V, Lee H, Cohen AE. Mechanism of voltage-sensitive fluorescence in a microbial rhodopsin. Proceedings of the National Academy of Sciences of the United States of America. 2013;110(15):5939-44.

135. Gong Y, Li JZ, Schnitzer MJ. Enhanced Archaerhodopsin Fluorescent Protein Voltage Indicators. PLoS One. 2013;8(6):e66959.
136. Rost BR, Schneider F, Grauel MK, Wozny C, Bentz C, Blessing A, et al. Optogenetic acidification of synaptic vesicles and lysosomes. Nat Neurosci. 2015;18(12):1845-52.
137. DeBerg HA, Brzovic PS, Flynn GE, Zagotta WN, Stoll S. Structure and Energetics of Allosteric Regulation of HCN2 Ion Channels by Cyclic Nucleotides. J Biol Chem. 2016;291(1):371-81.
138. Keske M. Characterization of Novel Optogenetic Inhibitors in Drosophila melanogaster. unpublished Bachelor thesis. 2019.
139. Govorunova EG, Gou Y, Sineshchekov OA, Li H, Wang Y, Brown LS, et al. Kalium rhodopsins: Natural light-gated potassium channels. bioRxiv. 2021:2021.09.17.460684.

6. Appendix

6.1 List of primers used for Sthk and CsR clonings.

SthK M369L qcF	cgagCTCgctctgatcctgagagcc
SthK M369L qcR	tcagaGCGAGctcgccgaagaactg
SthK A370V qcF	cgagATGgTCctgatcctgagagcc
SthK A370V qcR	tcagGaCCATctcgccgaagaactg
SthK M369A370IC qcF	tcggcgagatCTGtctgatcctgagagcc
SthK M369A370IC qcR	ggatcagaCAGatctcgccgaagaactg
SthK R377A qcF	ccgccaccgccacagtgcgggcca
SthK R377A qcR	tggcggtggcgggggctctcaggatc
R377E qcF	ctctgatcctgagagcccccgaaaccgccacagtg
R377E qcR	tcgggggctctcaggatcagagccatctcgccgaa
T378A qcF	cagagccgccacagtgcgggcca
T378A qcR	tggcggctctgggggctctcaggatc
T378Y qcF	cagatacgccacagtgcgggcca
T378Y qcR	tggcgtatctgggggctctcaggatc
T378V qcF	tgatcctgagagcccccagagtcgccacagtgcggc
T378V qcR	actctgggggctctcaggatcagagccatctcgcc
R377A T378C qcF	ccgcatgcgccacagtgcgggcca
R377A T378C qcR	tggcgcatgcgggggctctcaggatc
R377H T378C qcF	cccactgcgccacagtgcgggcca
R377H T378C qcR	tggcgcagtgggggctctcaggatc
R377H T378V qcF	cccacgtcgccacagtgcgggcca
R377H T378V qcR	tggcgacgtgggggctctcaggatc
R377K T378V qcF	ccaaggtcgccacagtgcgggcca
R377K T378V qcR	tggcgaccttgggggctctcaggatc
R377H T378V qcF	cccacgtcgccacagtgcgggcca
R377H T378V qcR	tggcgacgtgggggctctcaggatc
SthK R377A qcF	ccgccaccgccacagtgcgggcca
SthK R377A qcR	tggcggtggcgggggctctcaggatc
SthK R417A Xh3R	GCCGctcgaggccccgtctgctggtgccgccttccagttcctctttccgAGCcacagccagttcctg
SthK R418A Xh3R	GCCGctcgaggccccgtctgctggtgccgccttccagttcctctttAGCccgcacagccagttc
SthK K419R Xh3R	GCCGctcgaggccccgtctgctggtgccgccttccagttcctctCtccgccgcacagccag
SthK E421A Xh3R	GCCGctcgaggccccgtctgctggtgccgccttccagtGcctctttccgccgcaca
SthK E423A Xh3R	GCCGctcgaggccccgtctgctggtgccgcctGccagttcctctttccg
SthK R428A Xh3R	GCCGctcgaggccccgtGCgctggtgccgcctt
SthK 427Xh3R	GCCGCTCGAGgctggtgccgccttccagt
SthK 424Xh3R	GCCGCTCGAGgccttccagttcctctttcc
SthK 421Xh3R	GCCGCTCGAGttcctctttccgccgcac
SthK 418Xh3R	GCCGCTCGAGccgccgcacagccagttc
PDEcore240 XbEx2 5F	GCtctagaCGCAGTAGGTTTGTGAAGAAAAGCTACCTGGCGAACGAAATCCTCT GGGCCCCCTACCACAACTGGAT
PDEcore240 Ex1Hd 3R	acccaagcttatgcaacttcattttcatagcaaaaCTCACCGTTGGAGGCCAC
PDE2aCat Sp5F	ggACTAGTAAAAAAGTGAATGAGGCTCAGT
PDE2a Xh3R	ccgCTCGAGGCTTTTGCTCGTACGCTCA
CsR Y14E F	GGTTATGTACTGGGTTACATTTGGCCTGAT
CsR Y14E R	GTAACCCAGTACATAACCAGTCCGCCTTCT
CsR M119A F	GTGGCTATGATTATGCTGGGACTGTTTG
CsR M119A R	GCATAATCATAGCCACATCAGCCAG
CsR D116C F	GCTGGCTGATGTGGCTATGATTATGCT

CsR D116C R	AGCCACATCAGCCAGCACAATCCACA
CsR C142L F	GTGTCCTGCGCTTTTTTCTTTGTGGTGCT
CsR C142L R	GAAAAAAGCGCAGGACACGCCGTAGT

6.2 Abbreviation

AC	domain adenylyl cyclases domain
cAMP	adenosine 3, 5-cyclic monophosphate
ACRs	Anion conductive ChRs
BR	Bacteriorhodopsin
BLINK1	blue-light-induced K(+) channel 1
BLINK2	blue-light-induced K(+) channel 2
BLUF	blue-light using FAD
BSA	bovine serum albumin
bPAC	Photoactivated Adenylyl Cyclase from *Beggiatoa*
CCR	Cation Conductin Channelrhodopsin
CD8	Cluster of differentiation 8
CFTR	Cystic fibrosis transmembrane conductance regulator
ChRs	channelrhodopsins
ChR1	channelrhodpsin-1
ChR2	channelrhodpsin-1
ChloC	chloride conducting ChR
CNBD	C-linker and cyclic nucleotide-binding domain
cNMP,	cyclic nucleotide monophosphates
cRNA	complementary RNA
CsR,	*Coccomyxa subellipsoidea*
CvRh,	a proton-pumping rhodopsin from Chlorella vulgaris
CNG	cyclic nucleotide-gated channel
CyclOp	Cyclase Opsin
DNA,	Deoxyribonucleic acid
dNTP	desoxynucleoside triphosphate
DTT	dithiothreitol
E	endoplasmic reticulum export signal
ER	endoplasmic reticulum
EuPAC,	Photoactivated Adenylyl Cyclase from *Euglene gracilis*
FAD	flavin adenine dinucleotide ()

GIRK	G-protein-coupled inwardly rectifying K^+
GPCRs	G-protein-coupled receptors ()
cGMP	guanosine 3,5- cyclic monophosphate
HCN	hyperpolarization-activated and cyclic nucleotide-gated
InSynC	Inhibition of Synapses with CALI)
KCR	potassium Conducting Channelrhodopisn
LB	lysogeny broth
LED	light emitting diode
LliK ,	*Leptospira licerasiae*
MlotiK1	*Mesorhizobium loti*
PTL	photoswitched tethered ligands) channels
PIRK	photoinducible inwardly rectifying potassium
PCR	polymerase chain reaction
PDE	Phosphodiesterase
$RSBH^+$	protonated retinal Schiff base
SthK,	Potassium channel from *Spirochaeta thermophila*
SPARK	synthezed photoisomerizable azobenzene-regulated K^+
T	trafficking signal
GAF domains	terminal cGMP PDE/adenylyl cyclase/FhlA
TEVC	two-electrode voltage-clamp
TM	transmembrane
wt	wild-type
YFP	yellow fluorescent protein

7. Acknowledgement

I feel really lucky that I have the opportunity to do my doctoral study under the supervision of Prof. Georg Nagel. I would like to express my gratitude and appreciation for his supervision, discussion and 6 years long financial support. I have learned electrophysiology, scientific and critical thinking from him, which inspires me to do research. Thanks to my thesis committee: Prof. Dr. Robert J. Kittel and Prof. Dr. Tobias Langenhan for their kind supports and helpful suggestions on my start-up report, progress report and thesis. I would like to thank Prof. Manfred Heckmann for imparting his expertise in electrophysiology.

Thanks to Dr. Shiqiang Gao for his instructions. Dr. Shiqiang guided me in focusing on scientific questions, design experiments, and scientific writing. Not only in research but also in daily life, Dr. Shiqiang Gao helped me a lot, like a big brother. Thanks to Dr. Shang Yang for the experimental discussions and advice in my thesis. Thanks to my colleagues, Dr. Yuehui Tian, Dr. Xiaodong Duan, Dr. Sebastian Beck, Dr. Ruijing Tang, Dr. Yang Zhou, Meiqi Ding, Dr. Kunkun Li, Chong Zhang, Yundan Wang, Dr. med. Maximilian Pitsch, and Elfriede Reisberg for offering me help whenever I needed.

Thanks to our collaborators: Dr. Markus Bender and Yujing Zhang in University hospital Würzburg, Dr. Kai Konrad in Botany I, Dr. Christine Gee and Oana Constantin in Hamburg.

Thanks to my Parents, Guiyun Du, Hongbin Yu, who always support me and respect my decision, and let their only daughter study abroad. I would like to thank Prof. Georg Nagel one more time for offering me the opportunity to study in Würzburg, where I started a family. Thanks to my husband Damian Strzelczyk for his support and for helping me to filter the bath solution and take care of our son. Also, thanks to my son Hugo Strzelczyk, who always accompanies me, in my belly when I was patching cell, and on my lap when I was writing my thesis.

This work is funded by TRR166 ReceptorLight and TR240 Platelets.

Eidesstattliche Erklärung

Hiermit erkläre ich an Eides statt, die Dissertation: “Generierung und Charakterisierung neuartiger Proteine für Licht-aktivierte Hyperpolarisation von Zellmembranen”, eigenständig, d. h. insbesondere selbständig und ohne Hilfe eines kommerziellen Promotionsberaters, angefertigt und keine anderen, als die von mir angegebenen Quellen und Hilfsmittel verwendet zu haben.

Ich erkläre außerdem, dass die Dissertation weder in gleicher noch in ähnlicher Form bereits in einem anderen Prüfungsverfahren vorgelegen hat.

Weiterhin erkläre ich, dass bei allen Abbildungen und Texten bei denen die Verwertungsrechte (Copyright) nicht bei mir liegen, diese von den Rechtsinhabern eingeholt wurden und die Textstellen bzw. Abbildungen entsprechend den rechtlichen Vorgaben gekennzeichnet sind sowie bei Abbbildungen, die dem Internet entnommen wurden, der entsprechende Hypertextlink angegeben wurde.

Affidavit

I hereby declare that my thesis entitled: “ Generation and Characterization of novel proteins for light-activated hyperpolarization of cell membranes” is the result of my own work. I did not receive any help or support from commercial consultants. All sources and / or materials applied are listed and specified in the thesis.

Furthermore, I verify that the thesis has not been submitted as part of another examination process neither in identical nor in similar form.

Besides I declare that if I do not hold the copyright for figures and paragraphs, I obtained it from the rights holder and that paragraphs and figures have been marked according to law or for figures taken from the internet the hyperlink has been added accordingly.

Würzburg, den_____

_____

Signature PhD-student